Swarm and Evolutionary Computation 65 (2021) 100907

Contents lists available at ScienceDirect

Swarm and Evolutionary Computation

journal homepage: www.elsevier.com/locate/swevo

An opposition equilibrium optimizer for context-sensitive entropy dependency based multilevel thresholding of remote sensing images

Manoj Kumar Naik [a], Rutuparna Panda [b,*], Ajith Abraham [c]

[a] Faculty of Engineering and Technology, Siksha O Anusandhan, Bhubaneswar, Odisha, 751030, India
[b] Dept. of Electronics and Telecommunication Engineering, Veer Surendra Sai University of Technology, Burla, Odisha, 768018, India
[c] Machine Intelligence Research Labs, Scientific Network for Innovation and Research Excellence, WA 98071-2259, USA

ARTICLE INFO

Keywords:
Evolutionary computation
Computational intelligence
Multilevel thresholding
Remote sensing image thresholding

ABSTRACT

Earlier 1D histogram-based entropic methods for multilevel image thresholding suffer from the lack of contextual information. Subsequently, the idea was extended for 2D histogram-based methods, where neighbourhood pixels were considered to retain the contextual information. Nevertheless, 2D histogram-based entropic methods are computationally intensive. Moreover, these methods are based on the maximization of entropic functions using an optimizer, leading to less accuracy. To address these issues, we propose a context-sensitive entropy dependency (CSED) based multilevel thresholding method. A new optimizer called opposition equilibrium optimizer (OEO) is introduced. The opposition based learning and escaping strategy are incorporated to enhance exploration capability. Here, 31 test functions including 8 from standard testbed IEEE CEC 2014 are used for validation. The merits are – i) reduced complexity, ii) improved accuracy, iii) better stability and scalability, iv) enhanced exploration capability, v) well suited to random problems with changing dimensions, etc. The search history, trajectory, and average fitness history of the OEO are explicitly discussed. The Box plots and the convergence curves are presented to confirm its stability and faster convergence. Friedman's mean rank test, Bonferroni-Dunn test, and Holm's test are also carried out to ensure OEO superiority over others. Encouraging thresholding results on high dimensional colour satellite images from the *Landsat image gallery* are shown based on the suggested method (CSED-OEO). The quantitative measures (Peak Signal to Noise Ratio, Feature Similarity Index, and Structure Similarity Index) are used for validation. The CSED-OEO is compared with state-of-the-art methods and found better. It means, realistically, the method may be useful for segmentation-based analysis of colour images.

1. Introduction

Image segmentation is one of the primary requirements in machine vision. The thresholding-based approach is a more popular methodology in image segmentation. The thresholding-based approach either uses the gray-scale image or the colour image, as a target source, to get the segmented image for further processing. In earlier days, gray-scale images are a more preferred way of target images for the image segmentation problem, which consists of the intensity information of a true image. However, the colour image contains extra information called hue and saturation along with the intensity. Hence, the colour image has more information content than the gray-scale image [1]. This is the reason, nowadays, for which the researchers are moving towards the colour image thresholding. The colour image thresholding has special importance for a geographic information system (GIS), which captures the remote sensing images. It stores, checks, and displays the data related to the earth surface. The remote sensing images are used to locate the objects and the boundary for further processing to generate potential information like landscape, kind of soil, roads and forest fires, etc [2]. The colour image thresholding played a major role in GIS to analyse the remote sensing image for easy analysis, simple interpretation with exposed features, and reduced storage through compression of data [3–6].

Based on the survey of thresholding techniques [7–9], the thresholding methods are classified as bi-level and multilevel thresholding depending on the number of thresholds used to segment the images. The bi-level (global) thresholding approach uses only one threshold. The image is segmented into two areas – object and background. This method is known as the binarization of the image. However, in real life, the binarization of the image using bi-level thresholding does not provide sufficient information for further analysis. So, the researchers move towards the multilevel thresholding approach, which uses two or more threshold values to segment the image simultaneously for multiple objects from an image based on some criterion to be optimized. Some of the popular, recently developed (maximization/minimization criterion-based)

* Corresponding author.
E-mail addresses: rpanda_etc@vssut.ac.in (R. Panda), ajith.abraham@ieee.org (A. Abraham).

https://doi.org/10.1016/j.swevo.2021.100907
Received 2 September 2020; Received in revised form 20 April 2021; Accepted 8 May 2021
Available online 16 May 2021
2210-6502/

one dimensional (1D) thresholding methods are Otsu's method [10], Tsallis entropy [11], Kapur's entropy [12], Masi entropy [13], Rényi entropy [14], minimum cross entropy [15] and interdependence based approach [16]. All these methods use the 1D gray-level histogram of the image to obtain the optimal threshold values. The search complexity for the 1D thresholding method based on the 1D histogram for 'd' threshold values with L distinct gray levels is $O(L^d)$ for the gray-scale image while $O(3L^d)$ for the colour (RGB) image. The results of 1D thresholding methods are encouraging, with some drawbacks of not considering spatial correlation among the neighbourhood pixels. Therefore, these methods are called context-free methods. To overcome the drawbacks, Abutaleb proposed two-dimensional entropy in [17], an extension to Kapur's entropy [12] using a novel 2D histogram. The 2D histogram is formed using the information of a 1D histogram together with the local averaging information of its neighbourhood pixels (gray-level values). Some of the prominent works on the 2D thresholding approach that used a 2D histogram are proposed using Otsu's method in [18], Rényi entropy [19], Tsallis-Havrda-Charvát entropy [20], and Masi entropy [21], which show improved performance over 1D thresholding methods. However, as the 2D thresholding approach uses a 2D histogram, the search complexity for the gray-scale image is $O(L^{2d})$ while for the colour (RBG) image is $O(3L^{2d})$ for 'd' threshold values. Nevertheless, the complexity increases by a factor L^d. To reduce the complexity, researcher proposed 2D gray gradient based thresholding approach in [22,23] that used a modified 2D histogram with the gradient information. The gray gradient approach used row wise quadrants instead of the diagonal quadrants in the 2D histogram. However, this still requires a search complexity of $O(L^{(d+1)})$ for the gray-scale image while $O(3L^{(d+1)})$ for the colour images. Nonetheless, here also the complexity increases by a factor 'L'. In summary, these 2D thresholding methods suffer from high computational complexity. Higher is the number of threshold values 'd', more is the complexity.

To overcome the problem, the energy curve [24] is used instead of a histogram. The energy curve is computed at each gray level by considering the spatial contextual information of an image. It is more like a 1D histogram, which consists of several valleys and hills. From this knowledge, different regions are identified and segmented. The search complexity of the thresholding method is now – $O(L^d)$ for gray-scale image and $O(3L^d)$ for colour (RGB) image. So, the threshold section using the energy curve has two advantages. Firstly, the spatial contextual information is incorporated in the threshold selection process. Hence, the thresholding performance is improved. Secondly, the computational demand is reduced. This has motivated the authors to use the energy curve instead of a 2D histogram.

Moreover, for the multilevel thresholding, the nature-inspired optimization algorithms are used to reduce the computational complexity when the number of threshold levels 'd' increases. Therefore, a suitable optimizer is needed for this purpose. Some of the energy curve based multilevel thresholding using nature-inspired optimization algorithms are discussed here. The energy curve based multilevel thresholding was first used by Patra et al. in [24]. They used entropy based objective function to obtain the optimal thresholds. A genetic algorithm (GA) was used for optimization. The experiment was carried out in a gray-scale image. Pare et al in [25,26] came up with the colour image multilevel thresholding using the Cuckoo search (CS) algorithm and energy curve to obtain the optimal threshold values using Otsu's method, Kapur's entropy and Tsallis entropy based objective functions. A breast thermogram analysis based on the multilevel thresholding approach is presented in [27]. The authors used the energy curve in place of the histogram. The Otsu' method and Kapur's entropy were considered as the objective functions. The dragonfly algorithm (DA) was used as an optimizer. Recently, the CS is used as an optimizer for the energy curve based Otsu's method in [28], which shows better thresholding performance compared to the gray-level co-occurrence matrix (GLCM) and Rényi entropy. This prompts us to use the energy curve instead of a histogram for the multilevel thresholding followed by a good optimizer.

Recently, Faramarzi et al. proposed an equilibrium optimizer (EO) [29] inspired by the behaviour of dynamic and equilibrium state in a controlled mass volume model. Its exploration capability is limited because the particle position updating rule only depends on the best candidate. Although it shows better performance than some well-known optimization algorithms, there is still scope for its enhanced exploration. This had encouraged Wunnava et al. [16] to come up with an adaptive equilibrium optimizer (AEO) using an adaptive decision for dispersal of the non-performer particles. However, the adaptive decision depends on the fitness value of the particle; the search trajectory strictly follows the best solutions (obtained so far). Hence, there is likely to miss other possible solutions on the opposite (or near to the opposite) side. As a result, the search is limited. To overcome the problem, an opposition equilibrium optimizer (OEO) is proposed in this work. An effort is made to increase the exploration capability using the escaping strategy. Further, an idea of the opposition based learning (OBL) [30,31] search strategy is incorporated. The novel escaping strategy helps the OEO not to be trapped in the local optimal solution. Moreover, it ensures exploration from the opposite side of the search space. The performance of the OEO is evaluated using 23 well-known classical diversified test functions selected from the literature [32,33] together with 8 composition test functions from the IEEE CEC 2014 standard testbed [34]. The performance of the suggested OEO is also compared with some well-known and recently developed optimization algorithms – differential algorithm (DE) [35], particle swarm optimization (PSO) [35], equilibrium optimizer (EO) [29], Harris hawks optimizer (HHO) [36], sailfish optimizer (SFO) [37], whale optimization algorithm (WOA) [38], gray wolf optimizer (GWO) [39] and high-performance optimizer such as Success-History based Adaptive DE with Linear Population Size Reduction (L-SHADE) [40]. The qualitative and quantitative results are quite impressive and exhibit superiority over other optimization algorithms. For a detailed statistical analysis, both Friedman's mean rank test [41], Bonferroni-Dunn test [42], Holm's test [43] Wilcoxon's signed ranked tests [41] are emphasized. The performance of the suggested OEO warrants us to use it for the multilevel thresholding of remote sensing images.

A minimization of entropic objective function based multilevel thresholding method is proposed in Wunnava et al. [16], which uses a 1D histogram as an input to obtain the threshold values for the gray-scale image. The information regarding the neighbourhood pixels is ignored. As a result, there is some loss in the contextual information. On the other hand, the energy curve has contextual information, which can be used for thresholding purposes in place of the 1D histogram. This has inspired us to propose a context-sensitive entropy dependency (CSED) based multilevel thresholding method. A CSED objective function is introduced to enhance the performance, with reduced computational complexity. Optimal threshold values are obtained by minimizing the objective function using the OEO. Need to mention here that the present problem is a minimization problem, which leads to reduced computations. The proposal is coined as CSED-OEO based multilevel thresholding method. The proposed CSED-OEO based multilevel thresholding technique is evaluated using high dimensional remote sensing images from the *Landsat image gallery* [44]. The quantitative analysis is carried out based on some well-known metrics like Peak Signal to Noise Ratio (PSNR) [45], Feature Similarity (FSIM) [46], Structure Similarity (SSIM) [47], optimal threshold values, and mean gray level. For the qualitative analysis, we present the thresholded images for some sample images. Further, a statistical test is also carried out with the help of Friedman's mean rank test, which shows the overall performance of the CSED-OEO method. Results are discussed in a detailed manner in the results and discussion section.

The rest of this piece of work is as follows. Section 2 briefly describes the minimum entropy dependency based multilevel thresholding; the energy curve; and the equilibrium optimizer (EO). Section 3 proposes an opposition equilibrium optimizer (OEO) to enhance the exploration capability of the EO. This section also presents a comparative performance analysis. Section 4 describes the proposed CSED-OEO based multilevel thresholding. The results and discussion on the proposed multilevel thresholding using high dimensional remote sensing images are presented in Section 5. Finally, the concluding remarks are drawn in Section 6.

2. Preliminaries

2.1. Minimum entropy dependency based Multilevel Thresholding

The multilevel thresholding uses a set of thresholds $\tau = (\tau_1, \tau_2, \cdots, \tau_d)$ to classify the image into $(d+1)$ classes C_i, where $i = 1, 2, \cdots, d+1$. An individual class is represented as:

$$\begin{aligned} \langle 0, \tau_1 - 1\rangle &\in C_1 \\ \langle \tau_1, \tau_2 - 1\rangle &\in C_2 \\ &\vdots \\ \langle \tau_d, L - 1\rangle &\in C_{d+1} \end{aligned} \tag{1}$$

where $\tau_1, \tau_2, \cdots, \tau_d$ are the threshold gray level values and L is the maximum gray level in an image I. The C_1 and C_{d+1} are the foreground and background classes or vice versa, whereas C_i with $i = 2, 3, \cdots, d$ are the intermediate classes.

Recently, multilevel thresholding using the minimum interdependency is proposed in [16], which is an extension of the idea of bi-level thresholding proposed in [44]. The optimal threshold values $\tau^* = (\tau_1^*, \tau_2^*, \cdots, \tau_d^*)$ are obtained by minimizing the interdependency function:

$$\begin{aligned} \tau^* = \left(\tau_1^*, \tau_2^*, \cdots, \tau_d^*\right) = \arg \min_{0<\tau_1^*<\tau_2^*<\cdots<\tau_d^*<L-1} &\{\psi_1(C_1) + \cdots + \psi_i(C_i) \\ &+ \cdots + \psi_{d+1}(C_{d+1})\}. \end{aligned} \tag{2}$$

where entropic information ψ_i of the ith class $C_i(for\ i = 1, 2, \cdots, d+1)$ is evaluated using Eq. (3).

$$\begin{aligned} \psi_1(C_1) &= \log_e\left(\sum_{i=0}^{\tau_1} p_i\right) - \frac{1}{\sum_{i=0}^{\tau_1} p_i}\left[\left(\sum_{i=0}^{\tau_1-1} p_i\right)\log_e\left(\sum_{i=0}^{\tau_1-1} p_i\right) + p_{\tau_1}\log_e p_{\tau_1}\right] \\ &\vdots \\ \psi_i(C_i) &= \log_e\left(\sum_{i=\tau_{i-1}}^{\tau_i} p_i\right) - \frac{1}{\sum_{i=\tau_{i-1}}^{\tau_i} p_i}\left[p_{\tau_{i-1}}\log_e p_{\tau_{i-1}} + \left(\sum_{i=\tau_{i-1}+1}^{\tau_i-1} p_i\right)\log_e\left(\sum_{i=\tau_{i-1}+1}^{\tau_i-1} p_i\right) + p_{\tau_i}\log_e p_{\tau_i}\right] \\ &\vdots \\ \psi_{d+1}(C_{d+1}) &= \log_e\left(\sum_{i=\tau_d}^{L} p_i\right) - \frac{1}{\sum_{i=\tau_d}^{L} p_i}\left[p_{\tau_d}\log_e p_{\tau_d} + \left(\sum_{i=\tau_d+1}^{L} p_i\right)\log_e\left(\sum_{i=\tau_d+1}^{L} p_i\right)\right] \end{aligned} \tag{3}$$

The probability distribution $p = \{p_0, p_1, \cdots, p_l\}$ of all possible individual gray level in the image I of dimension, $m \times n$ is described as:

$$p_l = \frac{c_l}{M \times N}, \ \forall l \in [0, L] \tag{4}$$

where c_l is the occurrence of the gray level l in the image I, $\sum c_l = m \times n$ and $0 \le p_l \le 1$.

2.2. Energy curve and its application to multilevel thresholding

The histogram of an image does not contain contextual information. Hence, the histogram-based thresholding approach may not provide an optimal threshold value. To overcome this, an energy curve is introduced in [24], that can preserve the contextual information with the similar characteristics of a histogram.

Let us take an image $I = \{z_{ij}, 1 \le i \le m, 1 \le j \le n\}$ of size $\times n$, where z_{ij} is the intensity values at coordinates (i, j). The neighborhood system [48] N of order D for a spatial coordinate (i, j) can be defined as:

$$N_{ij}^D = \left\{(i+u, j+v), (u, v) \in N^D\right\} \tag{5}$$

In the thresholding application, we require the second order ($D = 2$) neighborhood system, i.e., $(u, v) \in \{(\pm 1, 0), (0, \pm 1), (1, \pm 1), (-1, \pm 1)\}$, shown in Fig. 1.

Let us generate a two-dimensional binary matrix $B_l = \{b_{ij}, 1 \le i \le m, 1 \le j \le n\}$ for intensity values $l (0 \le l \le L)$ using Eq. (6) and a two-dimensional constant matrix $C = \{c_{ij}, 1 \le i \le m, 1 \le j \le n\}$ using the Eq.(7).

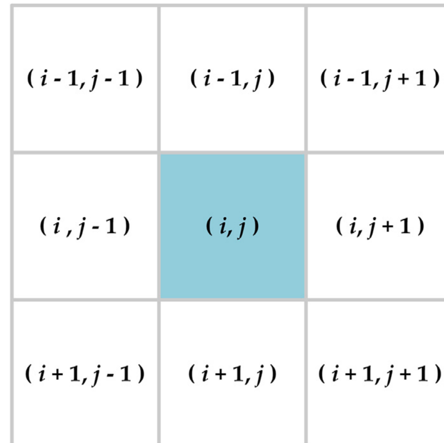

Fig. 1. Spatial coordinate representation of a pixel (i, j) in N^2 neighborhood.

$$b_{ij} = \begin{cases} 1, & z_{ij} > l \\ -1, & z_{ij} \le l \end{cases}, \ \forall i \in [1, m] \text{ and } \forall j \in [1, n] \tag{6}$$

$$c_{ij} = 1, \ \forall i \in [1, m] \text{ and } \forall j \in [1, n]. \tag{7}$$

The energy curve is defined as $= \{E_0, E_1, \cdots, E_L\}$, where E_l is the energy value of the image at intensity values l and is defined as:

$$E_l = -\sum_{i=1}^{m}\sum_{j=1}^{n}\sum_{pq \in N_{ij}^2} b_{ij} \cdot b_{pq} + \sum_{i=1}^{m}\sum_{j=1}^{n}\sum_{pq \in N_{ij}^2} c_{ij} \cdot c_{pq}. \tag{8}$$

The $\sum_{i=1}^{m}\sum_{j=1}^{n}\sum_{pq \in N_{ij}^2} c_{ij} \cdot c_{pq}$ term of Eq. (6) is a constant term. This ensures that the energy value is always a positive quantity. The energy value E_l for a gray level l is zero, only when all the elements of B_l are either 1 or - 1. Otherwise, E_l is always positive. The energy curve retains the contextual information, which is more like a histogram. So, the energy curve can be used instead of a histogram. We get an additional advantage of smoothness in a curve and a more prominent discriminatory property of classes.

2.3. Equilibrium optimizer (EO)

The equilibrium optimizer (EO) [29] is inspired by the mass balance model of dynamics and equilibrium states. The approach is based on the mass conservation within a control volume, a physics principle. Let X_i be the ith particle concentration from a population of N particle in d dimensional search space is initialized within the upper search boundary (UB) and the lower search boundary (LB) using Eq. (9).

$$X_i = LB + rand_i(1, d) \cdot (UB - LB), \ \forall i \in [1, N] \tag{9}$$

Then, the particle concentration X and the fitness value $f(X)$ for N particles are:

$$X = \begin{bmatrix} X_1 \\ X_2 \\ \vdots \\ X_i \\ \vdots \\ X_N \end{bmatrix} = \begin{bmatrix} x_1^1 & x_1^2 & \cdots & x_1^j & \cdots & x_1^d \\ x_2^1 & x_2^2 & \cdots & x_2^j & \cdots & x_2^d \\ \cdots & \cdots & \cdots & \cdots & \cdots & \cdots \\ x_i^1 & x_i^2 & \cdots & x_i^j & \cdots & x_i^d \\ \cdots & \cdots & \cdots & \cdots & \cdots & \cdots \\ x_N^1 & x_N^2 & \cdots & x_N^j & \cdots & x_N^d \end{bmatrix} \tag{10}$$

and

$$f(X) = \left[f(X_1), f(X_2), \cdots, f(X_i), \cdots, f(X_N)\right]' \tag{11}$$

Further, in the subsequent generation, the particle concentration X_i for ith particle is updated as:

$$X_i = X_{eq} + \left(X_i - X_{eq}\right) \cdot F_i + \frac{G_i}{\lambda V} \cdot (1 - F_i), \ \forall i \in [1, N] \tag{12}$$

where X_{eq} is a randomly pooled candidate from an equilibrium pool $X_{eq,pool}$, F_i is the exponential factor, G_i is the generation rate, V is the control volume taken a fixed value equal to 1 and λ_i is a random vector in the range $[0,1]$.

The equilibrium pool $X_{eq,pool}$ is formed using the particle concentration of the four best candidates $X_{eq(1)}$, $X_{eq(2)}$, $X_{eq(3)}$, $X_{eq(4)}$ based on the fitness value $f(X)$ and the average concentration among them $X_{eq(ave)}$, which is represented as:

$$X_{eq,pool} = \{X_{eq(1)}, X_{eq(2)}, X_{eq(3)}, X_{eq(4)}, X_{eq(ave)}\} \tag{13}$$

For a minimization problem, the selection of $X_{eq(1)}$, $X_{eq(2)}$, $X_{eq(3)}$, $X_{eq(4)}$ is based on a condition $f(X_{eq(1)}) \le f(X_{eq(2)}) \le f(X_{eq(3)}) \le f(X_{eq(4)})$. The average concentration $X_{eq(ave)}$ is evaluated as:

$$X_{eq(ave)} = \frac{X_{eq(1)} + X_{eq(2)} + X_{eq(3)} + X_{eq(4)}}{4} \tag{14}$$

The exponential factor F_i is used to make a balance between the exploitation and the exploration, which is generated as:

$$F_i = a_1 sign(r_1 - 0.5)\left[e^{-\lambda_i\left(1-\frac{t}{T}\right)^{\left(a_2 t/T\right)}} - 1\right],\ \forall i \in [1, N] \tag{15}$$

where r_1 and λ_i are the random vectors of size $1 \times d$ within the range $[0,1]$, which keep balance in the direction of the exploitation and exploration, a_1 and a_2 are taken as fixed values of 2 and 1 in [29]. The t represents the current iteration and T represents the maximum iteration allowed to reach the optimal equilibrium points.

The generation rate G_i help to extract the optimal solution by improvising exploration phase and for the ith particle is evaluated as:

$$G_i = GCP_i\left(X_{eq} - \lambda_i X_i\right)F_i \tag{16}$$

$$GCP_i = \begin{cases} 0.5 r_2, & r_2 \ge 0.5 \\ 0, & r_2 < 0.5 \end{cases} \tag{17}$$

where GCP_i is the generation rate control parameter and r_2 is a random number in the range of $[0,1]$.

2.4. Opposition based learning (OBL)

The opposition based learning (OBL) was proposed by Tizahoos in 2005 [30]. The technique is based on its current solution X and its opposite estimate $\hat{X}$ of the current solution. Generally, the population X of an optimization algorithm are initialized in a random d dimensional search space. If the random solution space is nearer to the optimal solution space, the algorithm converges with a lesser function evolution. On the other way, if the random solution space is far away from the optimal solution space, then the algorithm may fall in the local optimal solution or takes a long time to converge. To overcome this problem, one can take an estimate $\hat{X}$ in the opposite direction of X and compare it to update the solution for the next generation.

Definition 1: Let x be a real number defined within the interval $[lw, up]$, then the opposite number $\hat{x}$ is described as:

$$\hat{x} = lw + up - x \tag{18}$$

If $l = 0$ and $u = 1$, then

$$\hat{x} = 1 - x \tag{19}$$

Similarly, one can estimate the opposite number for higher dimensional problem.

Definition 2: Let us define a d-dimensional point $X = \{x^1, x^2, \cdots, x^d\}$ in a coordinate system where $x^1, x^2, \cdots, x^d$ are real numbers and the interval for each x^j lies between $[lw^j, up^j]$. Then, the d-dimensional opposite number $\hat{X} = \{\hat{x}^1, \hat{x}^2, \cdots, \hat{x}^d\}$ is defined as:

$$\hat{x}^j = lw^j + up^j - x^j,\ \forall j \in [1, d] \tag{20}$$

Let $f(X)$ is the fitness value of the d-dimensional point $X = \{x^1, x^2, \cdots, x^d\}$ and $f(\hat{X})$ is the fitness value of the estimated n-dimensional opposite point $\hat{X} = \{\hat{x}^1, \hat{x}^2, \cdots, \hat{x}^d\}$. The solution space updating equation, based on the opposition based learning, is described as:

$$X_{new} = \begin{cases} X, & f(X) \ge f(\hat{X}) \\ \hat{X}, & Otherwise \end{cases} \tag{21}$$

3. The proposed Opposition Equilibrium Optimizer (OEO)

This section proposes an opposition equilibrium optimizer (OEO), an efficient algorithm supplemented with opposition based learning and a novel escaping strategy. The particle position updating rule in EO mainly depends on the position of the particles from the equilibrium pool $X_{eq,pool}$, that are formed using the best candidates $X_{eq(1)}$, $X_{eq(2)}$, $X_{eq(3)}$, $X_{eq(4)}$ and they are average $X_{eq(ave)}$. Therefore, the search is primarily guided by the best solutions. This may lead to the local optimal solution, because all four best solutions may be found in a particular area of the search space. Especially, it reduces the chances of getting global optimal or near-global optimal solutions. This encourages us to incorporate a novel escaping strategy to elude such a situation. This proposal inherits an escaping strategy, one-third of the particles are randomly escaping from the local trap after the equilibrium is achieved. Even more interesting is its search capability throughout the entire search space. Thus, the suggested OEO is competent to explore better than the EO. Besides, the emphasis is also given on opposition based learning. The opposition based learning is established on the simultaneous evaluation of a particle on its position and its opposite points referred to as anti-particle. To explore the entire search space, the search trajectory should move in both directions – zone around the best solutions obtained so far, and the anti-particle concentration region. This warrants us to include opposition based learning in the OEO. This kind of learning strategy further enhances exploration capability.

Escaping strategy: Let us assume that a particle suddenly escapes from the current search space to a randomly new location with an escaping probability P_e, which is described as:

$$X_i = \begin{cases} X_i \cdot \left(2 \cdot r_3 - 1\right), & r_4 < P_e \\ X_i, & r_4 \ge P_e \end{cases},\ \forall i \in [1, N] \tag{22}$$

where r_3 is a random vector of size $1 \times d$ and r_4 is a random number in the interval $[0,1]$. This novel updating rule helps the OEO search trajectory to avoid the local optimal solution.

Opposition based learning: Let us extend the solution space for the particle along with the corresponding anti-particle using OBL, which helps to explore the search space from both directions. The anti-particle concentration $\hat{X}_i^j$ for ith particle in jth dimension is generated as:

$$\hat{X}_i^j = \min\left(X_i\right) + \max\left(X_i\right) - X_i^j,\ \forall i \in [1, N] \text{ and } \forall j \in [1, d] \tag{23}$$

Finally, the selection-based updating rule of the OEO is described as:

$$X_i = \begin{cases} X_i, & f\left(X_i\right) \ge f\left(\hat{X}_i\right) \\ \hat{X}_i, & Otherwise \end{cases},\ \forall i \in [1, N] \tag{24}$$

where $f(X_i)$ and $f(\hat{X}_i)$ are the fitness value of ith particle X_i and anti-particle $\hat{X}$.

3.1. Pseudocode of the OEO

In the beginning, determine the number of particles $\boldsymbol{N}$ to involve in the search process, the dimension of the problem $\boldsymbol{d}$, search boundary interval $[\boldsymbol{LB}, \boldsymbol{UB}]$, maximum allowable generation $\boldsymbol{T}$ of the particle to reach the optimal equilibrium point, escaping probability $\boldsymbol{P_e}$ and a fitness function $\boldsymbol{f}(\cdot)$ for a problem statement. Also, assign free parameters $a_1 = 2$, $a_1 = 1$ and $V = 1$.

Begin:
Input:
N, d, LB,UB, T, P_e, a_1, a_2, V and $f(\cdot)$
Initialization:
Initialize current iteration $t = 1$
Generate the particle concentration X using the Eq. (9-10)
Update the fitness vector $f(X)$ using Eq. (11)
while $(t \le T)$
Update the equilibrium candidates $X_{eq(1)}$, $X_{eq(2)}$, $X_{eq(3)}$, $X_{eq(4)}$, $X_{eq(ave)}$ and construct the equilibrium pool $X_{eq,pool}$ using Eq. (13-14)
for $(i = 1\ to\ N)$
Generate the random vector r_1, r_3, λ_i of size $(1\ \times d)$ and random numbers r_2, r_4 in the interval $[0, 1]$
Construct the F_i using the Eq. (15)
Update the G_i using the Eq. (16)
Update the particle concentration X_i using Eq. (12)
if $(r_4 < P_e)$// *Escaping strategy*
Update the particle concentration X_i using Eq. (22)
end
Estimate the $\hat{X}_i$ using the Eq. (23) // *Generation of anti-particle*
Evaluate the fitness value $f(X_i)$ and $f(\hat{X}_i)$.
Selection of next iteration X_i using the Eq. (24). //*Opposition based learning*
Update the fitness vector $f(X)$ for ith particle concentration X_i .
end (for)
Next iteration $t = t + 1$
end (while)
Output: $C_{eq(1)}$

3.2. Performance evaluation of OEO

3.2.1. Test functions, experimental setup, and evaluated algorithms

In this section, we evaluate the performance of the OEO using 23 well-known classical diversified test functions [32,33] together with 8 composition test functions from the IEEE CEC 2014 test suite [34]. Note that these 31 test functions are classified into four categories such as unimodal test functions ($f_1 - f_7$), scalable multimodal test functions ($f_8 - f_{13}$), fixed multimodal test functions ($f_{14} - f_{23}$)and composition test functions ($f_{24(CEC-14-F23)} - f_{31(CEC-14-F30)}$). The unimodal test functions have unique minima that demonstrate the exploration capability, whereas multimodal test functions are used to demonstrate the exploitation capability, avoiding many local minima to reach the global minima. The composition test functions have many local minima with variations of shapes of the functions in different regions within a search space. These functions are composed of shifted, rotated, hybrid, expanded versions of the unimodal and multimodal test functions.

The performance of the OEO is compared with some recently developed and well-recognized optimization algorithms such as EO [29], HHO [36], SFO [37], WOA [38], GWO [39], PSO [35], DE [35] and L-SHADE [40]. A qualitative analysis [49] of the results of the OEO is carried out through the search history, trajectory, and average fitness history. Also, a qualitative comparison of the OEO with other optimization algorithms is done using Boxplots, convergence curves, and scalability curves. A quantitative analysis, based on the statistical results of fitness evaluation is carried out in terms of the average result ('Ave') and standard deviation ('Std') metric obtained from the fitness value of 51 independent runs of each optimization algorithm. Further, Friedman's mean rank test and Wilcoxon signed-rank test with a 5% degree of significance are used to demonstrating the significant differences between the other optimization algorithms. The Wilcoxon signed-rank test is evaluated based on p-value compared with OEO vs. other optimization algorithms for 51 independent optimal results, and assign '+' for p-value significantly better than 5% degree of significance, '−' for p-value significantly inferior to 5% degree of significance, and '≈' for p-value with no significant difference. To provide a fair comparison, all test functions are evaluated with 30 particles through 500 iterations with a maximum of 15000 function evaluations. The control parameters for the OEO, EO [29], HHO [36], SFO [37], WOA [38], GWO [39], PSO [35], DE [35] and L-SHADE [40] are presented in Table 1. The optimization algorithms are implemented in MATLAB R2018b in the Windows 10 environment of the Intel Core i3 processor with 8GB RAM.

Table 1
The control parameters of various optimization algorithms.

Algorithms	Control parameters
OEO	Constant $a_1 = 2$, $a_2 = 1$, $V = 1$ and escaping probability $P_e =$ 0.33
EO	Constant $a_1 = 2$, $a_2 = 1$ and $V = 1$
SFO	Power attack control coefficient $A = 4$ and $\varepsilon = 0.001$
WOA	Logarithmic spiral constant $b = 1$
GWO	Convergence constant $a = [2, 0]$
PSO	Inertia factor = 0.3, cognitive and social constant $(C_1, C_2) = (2, 2)$
DE	Scaling factor $F = 0.5$ and crossover probability $Cr = 0.5$
L-SHADE	$p = 0.11$, Arc rate = 2.6 and $H = 6$.

3.2.2. Qualitative results of OEO

The qualitative results of the OEO during the iteration progress for one test function from each category are presented in Fig. 2. The well-known metrics such as search history, trajectory, and average fitness history are used. The search history diagram of Fig. 2 presents the positions (only the first two dimensions) of each particle during the initial iteration to the maximum iterations. From the search history diagram, one can visualize that the OEO utilizes the whole search space to find the optimal solution. A higher concentration of points is aggregated nearer to the optimal solutions points. The trajectory of the best particle among N particles of the OEO is demonstrated in the *3*rd and *4*th columns of Fig. 2. The *3*rd column of Fig. 2 demonstrates the trajectory of the best particle in *1*st dimension. It reveals that, with the search progress, the concentration (position) reaches optimal or near-optimal solution space, although the initial search space is widely dispersed. Further, the trajectory of the best particle in d-dimension of the OEO is demonstrated in the *4*th column of Fig. 2. It clearly shows how the OEO converges to an optimal solution space from a randomly distributed search space, as the iteration progresses. The last column of Fig. 2 displays the average fitness history based on Eq. (25) to demonstrate the collaborative behaviour of all N particles to reach the optimal or near-optimal solutions. A decreasing trend in the average fitness history shows the collaborative behaviour of the particle to reach an optimal solution. As the iterations progress, the newly updated solutions are better than the previous solutions. All these qualitative metrics help us to understand that the OEO has a well-balanced exploration and exploitation, to reach an optimal or near-optimal solution.

$$f_{ave}(t) = \frac{1}{N}\sum_{i=1}^{N} f\left(X_i\right),\ \forall t = [1, T] \tag{25}$$

3.2.3. Quantitative results comparison of OEO with other optimization algorithms

The comparison results (of optimization algorithms) on the test functions ($f_1 - f_{31}$) are presented in Table 2. The unimodal ($f_1 - f_7$), scalable multimodal ($f_8 - f_{13}$) and composition ($f_{24} - f_{31}$) test functions are evaluated for d=30 for the statistical results presented in Table 2. The unimodal test functions $f_1 - f_4$ results on the OEO are improved significantly than other optimization algorithms. However, for the unimodal test function f_5, the OEO behaves the same way as the EO, behind the HHO and L-SHADE to reach the optimal solution. The performance of the test function f_6 the OEO behind the L-SHADE, and for test function f_7 the OEO behind the HHO. The performance of the OEO on the scalable multimodal test function f_8 has improved over the EO and lags the HHO. The OEO obtain the same optimal results as the HHO for the test functions $f_9 - f_{11}$. The OEO also achieve similar results with EO for the test function f_9, however, OEO lags L-SHADE for the test functions f_{12}, f_{13}. The performance of the OEO on fixed multimodal test functions $f_{14} - f_{23}$ show mixed responses of a similar result with EO, L-SHADE, and DE, however, it shows quite improved performance over EO for f_{15}, $f_{20} - f_{23}$. The performance of the OEO on composition test

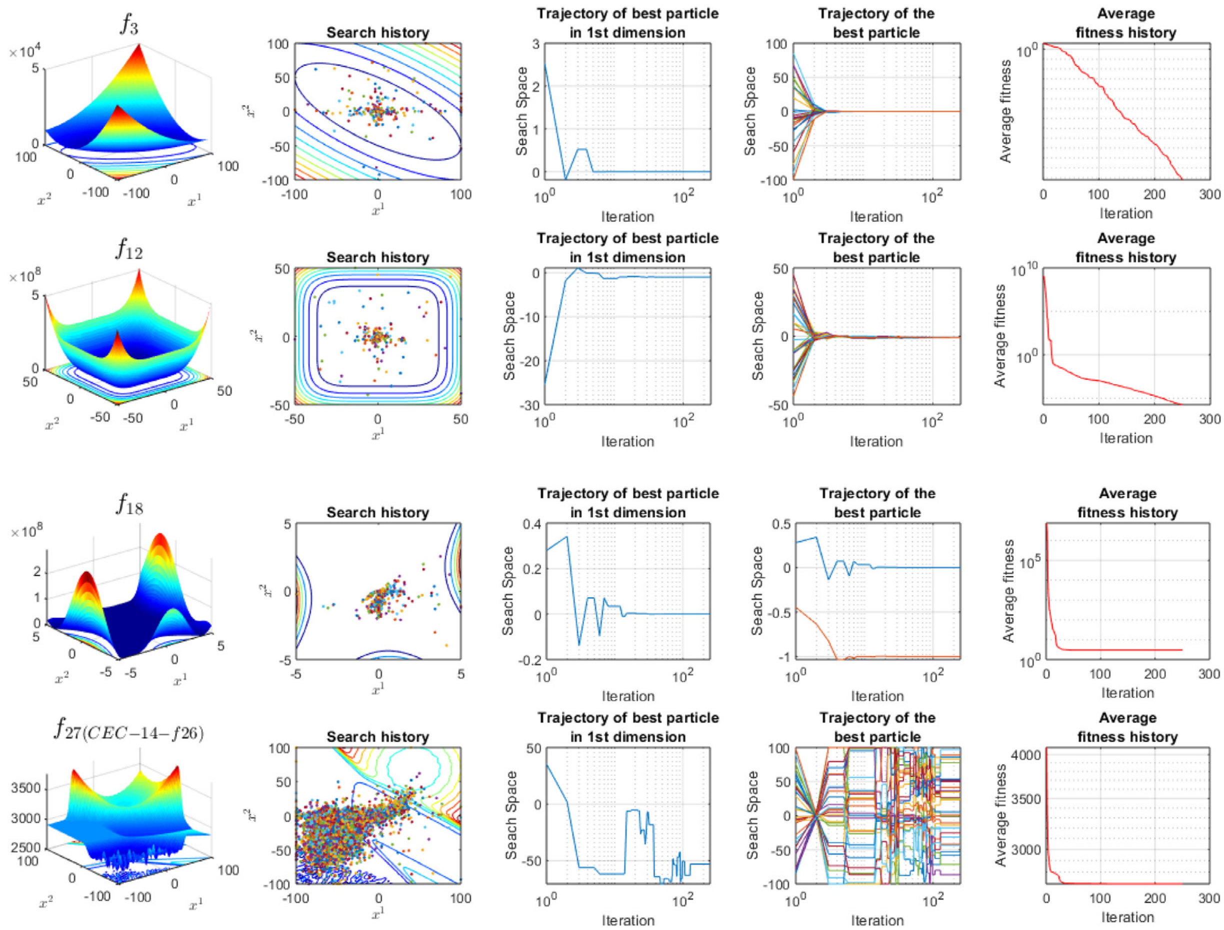

Fig. 2. Qualitative results (search history, trajectory, and average fitness history) of OEO.

functions $f_{24} - f_{31}$ from CEC 2014 shows better optimal solutions than other optimization algorithms. In most of the test functions, the OEO performs statistically better. However, in some cases, it lags from other optimization algorithms – HHO, DE, and L-SHADE.

To analyse the statistical performance of the OEO, an statistical analysis based on the Friedman test [50] is first considered. Friedman's mean rank is analysed on all 51-independent run of 31 test functions ($f_1 - f_{31}$) for various optimization algorithms and reported in Table 2. Based on the Friedman mean rank reported in Table 2 the null hypothesis is rejected, which shows a significant difference in the performance of various optimizers. Interestingly, based on the Friedman mean rank OEO ranked first.

Further, to demonstrate the significant difference of OEO performance with another optimization algorithm, Bonferroni-Dunn [42] post hoc statistical analysis is carried out. The Bonferroni-Dunn test help to demonstrate the two algorithms are significantly different if the difference in the average ranking of the algorithms is larger than the critical distance (CD) [50]. Fig. 3 shows the average rank of the optimizer with a threshold line based on CD and OEO as control algorithms. The OEO shows better performance than EO, SFO, WOA, GWO, PSO, and DE at significance level $\alpha = 0.05$. The OEO outperformed all other optimizers and ranked first based on the lowest average rank of 2.355.

The disadvantage of the Bonferroni-Dunn test is, it cannot differentiate the methods which are below (e.g., HHO and L-SHADE) or close (e.g., EO) to the critical line. So further a sequential rejective multiple test procedure Holm's test [43] is carried out to identify which algorithm is superior/inferior to OEO. The Holm test is based on the sorted p-value and a comparison with them $\frac{\alpha}{k-m+1}$, where α is the target significance level, k is the degree of freedom and m is the rank. The Holm

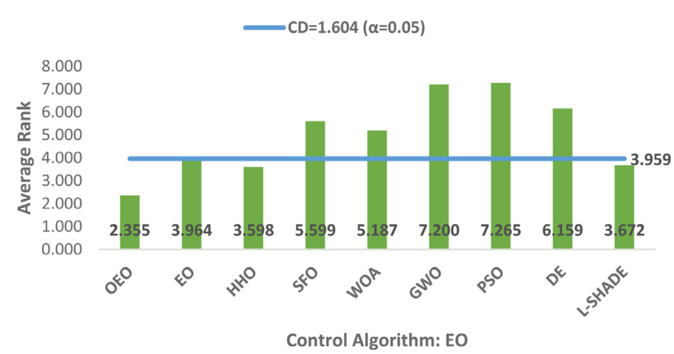

Fig. 3. Bonferroni-Dunn test for the various algorithms with $\alpha = 0.05$.

test begins by comparing with p-value with corresponding $\frac{\alpha}{k-m+1}$ and reject the null hypothesis whenever it founds $p_i < \frac{\alpha}{k-m+1}$. The results of Holm's test using OEO as the control algorithm is shown in Table 3, which show OEO outperformed the PSO, GWO, EO, DE, WOA and SFO by rejecting the null hypothesis. However, OEO statistically likes HHO, and L-SHADE by accepting the null hypothesis.

Further, another statistical test called Wilcoxon's signed ranked test is also carried out in this work. The p-values are reported in Table 4 based on non-parametric Wilcoxon's signed ranked test with a 5% degree of significance. Wilcoxon's signed ranked test is carried out with the help of optimal fitness values obtained from the 51 independent runs of different optimizers taking OEO as a control algorithm. From Table 4, the p-value of the OEO vs. other optimization algorithms

Table 2
Comparison of optimization algorithms results (Best results are shown boldface).

	Function	Metric	OEO	EO	HHO	SFO	WOA	GWO	PSO	DE	L-SHADE
Unimodal test function	f_1	**Ave**	**5.523E-207**	4.570E-41	4.997E-96	3.631E-15	1.953E-18	6.561E-08	5.424E-02	1.370E+01	1.100E-27
		Std	0	1.282E-40	2.787E-95	9.113E-15	2.194E-18	1.623E-07	1.384E-02	5.357E+01	1.771E-27
	f_2	**Ave**	**6.425E-103**	7.562E-24	2.039E-48	1.324E-07	3.569E-11	3.350E-05	1.064E+00	2.084E-02	3.329E-14
		Std	4.567E-102	1.696E-23	1.351E-47	1.541E-07	2.864E-11	3.923E-05	1.273E-01	7.083E-02	2.349E-14
	f_3	**Ave**	**6.012E-186**	1.135E-08	6.503E-71	9.542E-13	9.966E-05	3.290E-01	5.063E-01	6.363E+02	1.945E-13
		Std	0	3.659E-08	4.636E-70	3.113E-12	4.367E-04	4.205E-01	1.390E-01	3.461E+02	3.157E-13
	f_4	**Ave**	**1.524E-99**	5.044E-10	3.428E-48	9.667E-09	8.443E-05	1.448E-01	1.439E-01	2.322E+01	2.324E-06
		Std	4.496E-99	1.569E-09	1.861E-47	1.107E-08	1.318E-04	1.268E-01	2.191E-02	6.204E+00	1.823E-06
	f_5	**Ave**	2.628E+01	2.533E+01	**9.670E-03**	7.742E-02	2.771E+01	2.881E+01	3.373E+01	5.731E+03	1.393E+01
		Std	2.265E-01	2.238E-01	1.205E-02	1.500E-01	7.679E+00	3.220E-01	1.508E+00	1.749E+04	6.097E-01
	f_6	**Ave**	5.150E-08	9.598E-06	1.200E-04	2.727E+00	8.402E-01	3.537E+00	5.883E-02	6.935E+00	**2.679E-27**
		Std	2.304E-07	7.948E-06	2.000E-04	1.640E+00	3.683E-01	5.972E-01	1.484E-02	1.840E+01	4.641E-27
	f_7	**Ave**	2.291E-04	1.149E-03	**1.658E-04**	3.180E-04	6.920E-03	4.986E-03	1.415E-01	6.388E-02	1.341E-03
		Std	1.970E-04	6.636E-04	1.876E-04	2.774E-04	4.147E-03	2.843E-03	4.149E-02	1.540E-02	4.446E-04
Scalable Multimodal test function	f_8	**Ave**	-8185.573	-9089.599	**-12550.462**	-74188.123	-8022.479	-39.591	-157.831	-7034.625	-3321.327
		Std	863.616	931.345	131.793	386258.112	483.637	6.098	26.090	1225.383	406.600
	f_9	**Ave**	**0**	**0**	**0**	3.533E-13	2.009E+01	2.595E+01	1.730E+01	1.509E+02	6.253E+00
		Std	0	0	0	7.058E-13	1.563E+01	1.876E+01	4.684E+00	3.458E+01	1.596E+00
	f_{10}	**Ave**	**8.882E-16**	8.551E-15	**8.882E-16**	2.071E-08	5.265E-10	5.442E-05	3.881E-01	2.232E+00	4.185E-14
		Std	0	2.056E-15	0	2.536E-08	4.429E-10	6.420E-05	2.851E-01	2.721E+00	1.946E-14
	f_{11}	**Ave**	**0**	1.611E-14	**0**	9.578E-17	3.483E-17	1.816E-09	3.262E-03	3.562E-01	0
		Std	0	1.151E-13	0	2.483E-16	6.470E-17	3.368E-09	8.851E-04	7.322E-01	0
	f_{12}	**Ave**	2.225E-07	6.108E-07	8.003E-06	5.043E-01	3.286E-02	2.936E-01	8.009E-04	2.499E+04	**2.972E-16**
		Std	5.720E-07	6.594E-07	1.675E-05	2.835E-01	1.800E-02	8.748E-02	2.369E-04	1.720E+05	1.701E-16
	f_{13}	**Ave**	8.584E-06	2.570E-02	1.020E-04	5.678E-03	7.026E-01	2.072E+00	1.722E-02	3.337E+04	**1.063E-14**
		Std	5.892E-05	4.568E-02	1.818E-04	7.025E-03	2.476E-01	2.674E-01	7.522E-03	1.143E+05	5.958E-15
Fixed Multimodal test function	f_{14}	**Ave**	**0.998**	**0.998**	1.521	6.983	**0.998**	12.671	12.671	1.134	7.868
		Std	3.024E-16	1.22E-16	1.3432087	4.17565175	1.14E-12	1.22E-10	1.42E-12	0.73908425	2.711E+00
	f_{15}	**Ave**	3.080E-04	3.552E-03	**3.489E-04**	5.440E-04	4.153E-04	1.006E-03	3.892E-04	1.817E-03	3.075E-04
		Std	6.374E-07	7.329E-03	3.577E-05	8.806E-04	2.213E-04	1.379E-03	1.884E-04	4.701E-03	2.954E-19
	f_{16}	**Ave**	**-1.032**	**-1.032**	**-1.032**	-1.031	**-1.032**	-1.026	**-1.032**	**-1.032**	-1.032
		Std	3.807E-16	3.124E-16	1.606E-09	4.858E-03	1.441E-10	1.137E-02	5.381E-07	2.243E-16	2.243E-16
	f_{17}	**Ave**	**0.398**	**0.398**	**0.398**	0.419	0.489	0.797	**0.398**	**0.398**	0.758
		Std	1.020E-14	3.924E-16	9.396E-06	1.032E-01	6.500E-01	1.275E+00	3.543E-07	3.924E-16	2.637E-01
	f_{18}	**Ave**	**3.000**	**3.000**	**3.000**	7.786	**3.000**	4.602	**3.000**	**3.000**	**3.000**
		Std	2.695E-15	1.390E-15	1.547E-06	1.398E+01	3.661E-08	6.413E+00	2.905E-05	3.436E-15	2.262E-15
	f_{19}	**Ave**	**-3.863**	-3.862	-3.861	-3.800	-3.858	-3.744	-3.857	**-3.863**	**-3.863**
		Std	2.735E-15	1.545E-03	2.719E-03	7.293E-02	3.848E-03	5.597E-01	3.120E-03	3.140E-15	3.140E-15
	f_{20}	**Ave**	-3.269	-3.233	-3.092	-2.939	-2.843	-2.490	-3.075	-3.238	**-3.287**
		Std	6.188E-02	6.796E-02	1.127E-01	2.598E-01	5.116E-01	8.329E-01	2.279E-01	6.946E-02	5.471E-02
	f_{21}	**Ave**	-9.001	-8.667	-5.346	-5.080	-4.973	-4.971	-5.055	**-9.316**	-5.055
		Std	2.1570E-14	2.629E+00	1.189E+00	4.006E-01	5.845E-01	5.842E-01	2.539E-04	2.166E+00	5.305E-07
	f_{22}	**Ave**	-9.107	-8.982	-5.243	-5.174	-5.006	-4.833	-5.087	**-9.841**	-5.088
		Std	1.042E+00	2.631E+00	1.084E+00	6.839E-01	5.848E-01	1.024E+00	4.285E-04	1.949E+00	1.399E-06
	f_{23}	**Ave**	-9.903	-9.459	-5.569	-5.157	-5.046	-4.380	-5.128	**-10.123**	-5.151
		Std	1.060E+00	2.568E+00	1.564E+00	9.784E-01	5.855E-01	1.627E+00	4.846E-04	1.672E+00	1.374E-01
Composition test function form CEC 2014	f_{24} (CEC−14−F23)	**Ave**	**2500**	2615.299	**2500**	**2500**	**2500**	2500.003	2506.188	2616.419	2500
		Std	0	6.665E-02	0	8.983E-07	1.925E-08	4.641E-03	7.047E-01	2.720E+00	1.896E-12
	f_{25} (CEC−14−F24)	**Ave**	**2600**	2600.021	2600.000	2600.000	2600.283	2601.650	2601.238	2640.234	2600.001
		Std	0	8.418E-03	1.123E-03	3.539E-04	1.050E-01	8.980E-01	1.613E-01	7.037E+00	4.671E-04
	f_{26} (CEC−14−F25)	**Ave**	**2700**	2701.900	**2700**	**2700**	**2700**	2700.000	2700.099	2705.821	**2700**
		Std	0	4.009E+00	0	1.254E-08	4.029E-10	1.172E-04	1.225E-02	1.703E+00	4.898E-13
	f_{27} (CEC−14−F26)	**Ave**	2772.681	2721.840	2778.546	2778.481	**2702.754**	2800.000	2800.002	2706.461	2752.289
		Std	4.485E+01	4.141E+01	4.132E+01	3.919E+01	1.389E+01	8.879E-04	4.335E-04	2.375E+01	3.630E+01
	f_{28} (CEC−14−F27)	**Ave**	**2900**	3270.823	**2900**	**2900**	**2900**	2900.001	2903.891	3261.551	3127.305
		Std	0	1.077E+02	0	2.538E-07	5.116E-09	7.726E-04	9.040E-01	6.765E+01	3.762E+02
	f_{29} (CEC−14−F28)	**Ave**	**3000**	3821.335	**3000**	**3000**	**3000**	3000.002	3005.701	3889.015	3000
		Std	0	1.926E+02	0	4.326E-07	1.080E-08	2.425E-03	1.434E+00	2.205E+02	3.829E-09
	f_{30} (CEC−14−F29)	**Ave**	3199.917	2102159.186	497669.946	62394.447	3100.035	8377.328	7197592.705	1455346.004	**3100.000**
		Std	4.051E+02	4.077E+06	3.509E+06	1.501E+05	4.464E-02	5.600E+03	9.846E+05	3.212E+06	1.096E-05
	f_{31} (CEC−14−F30)	**Ave**	6195.672	9365.528	251365.972	3200.078	17865.186	3531.487	498303.710	10852.880	**3200.002**
		Std	3.573E+03	3.869E+03	3.760E+05	7.683E-02	1.213E+04	3.670E+02	5.818E+04	1.333E+04	6.220E-04
Friedman mean rank			**2.355**	3.964	3.598	5.599	5.187	7.200	7.265	6.159	3.672
Rank			**1**	4	2	6	5	8	9	7	3

shows statistically significant, which are summarised as OEO vs. EO ('+' 83.9%, '≈' 9.6%, '−' 6.5%), OEO vs. HHO ('+' 74.2%, '≈' 22.6%, '−' 3.2%), OEO vs. SFO ('+' 90.3%, '≈' 3.2%,'−' 6.5%), OEO vs. WOA ('+' 96.8%, '−' 3.2%), OEO vs. GWO ('+' 96.8%, '≈' 3.2%), OEO vs. PSO ('+' 100%), OEO vs. DE ('+' 93.6%, '≈' 3.2%,'−' 3.2%) and OEO vs. L-SHADE ('+' 90.3%, '≈' 6.5%,'−' 3.2%). From these statistical values, it is observed that the OEO has significant improvement over other optimization algorithms. Based on the statistical results presented in Tables 2-4, it is believed that the OEO is good enough for function optimization. It ensures us a better trade-off between the exploration and the exploitation to find optimal solutions.

3.2.4. Qualitative results comparison of OEO with other optimization algorithms

This section presents a qualitative comparison of the OEO with other optimization algorithms using Boxplots and convergence curves. The

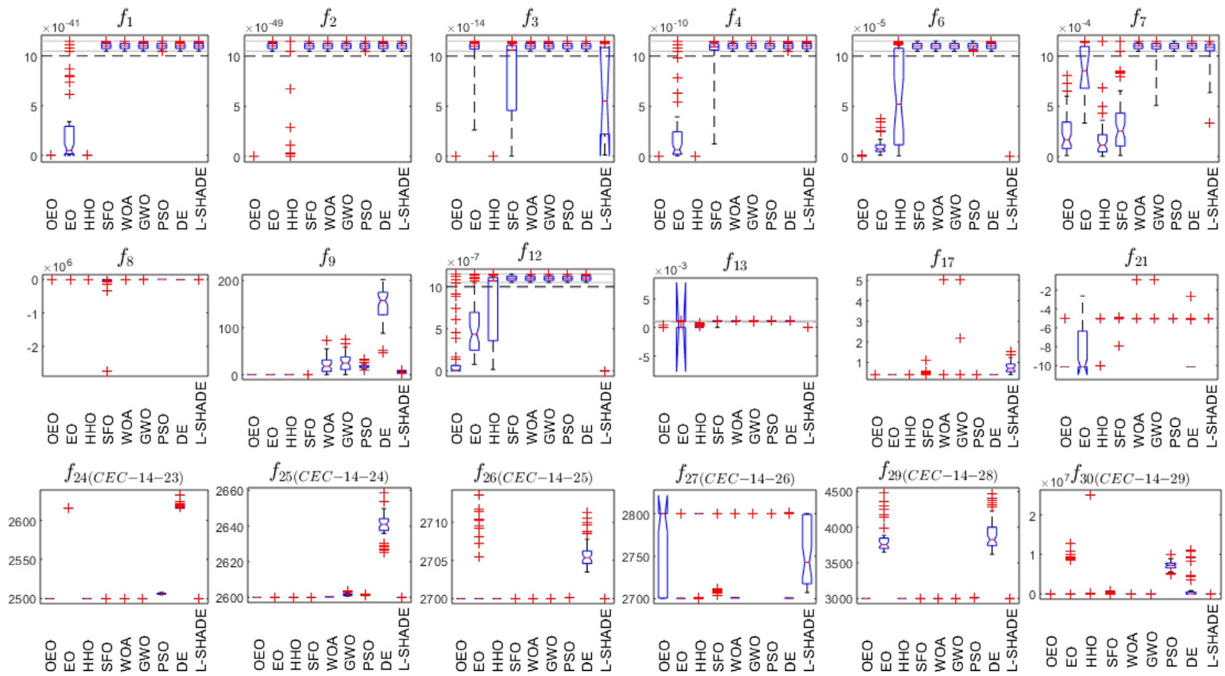

Fig. 4. Boxplot comparison of 18 test functions $f_1 - f_4$, $f_6 - f_9$, f_{12}, f_{13}, f_{17}, f_{21}, $f_{24} - f_{27}$, f_{29} and f_{30}.

Table 3
Holm's test using OEO as the control algorithm.

Method	Rank	z-value	p-value	$\alpha/i(0.05)$
PSO	7.2650	7.6833	1.5543E-14	0.00625
GWO	7.2002	4.4517	8.5165E-06	0.00714
EO	3.9643	3.3094	9.3490E-04	0.00833
WOA	5.1866	3.1150	1.8391E-03	0.01
DE	6.1588	3.1145	1.8422E-03	0.0125
SFO	5.5599	2.6410	8.2652E-03	0.01667
HHO	3.5980	1.4844	0.1376	0.025
L-SHADE	3.6724	0.9379	0.3482	0.05

Boxplot shows the potential of the optimization algorithm. From these plots, one can get an idea of how consistently or frequently the optimal solutions are obtained. The Boxplots of 18 test functions for fitness value using the optimal solutions obtained during 51 independent runs are presented in Fig. 4. Interestingly, the OEO has shown satisfactory results among all optimization algorithms. Further, convergence curves are also compared. A comparison of the OEO with other optimization methods for 12 test functions are performed based on the iteration count and presented in Fig. 5. From Fig. 5, it can be critically analysed that the OEO's performances on unimodal and scalable multimodal test functions are improved a lot than other optimization schemes. However, for the fixed multimodal and composition test functions, it shows a comparative result with other optimization algorithms such as EO, HHO, and DE. The qualitative analysis using Boxplots and convergence curves ensures the readers regarding the use of the OEO to solve complex optimization problems.

3.2.5. *Scalability analysis of scalable test functions* $f_1 - f_{13}$

This section presents the comparison results of the optimal fitness values of scalable unimodal and multimodal test functions $f_1 - f_{13}$ for low to high dimensions. For the scalability analysis, we use $N = 30$ numbers of particles, $T = 500$ (15000 maximum function evaluations) as the maximum iteration count with 51 independent runs for OEO, EO, HHO, SFO, WOA, GWO, PSO, and DE, to validate low to high dimensions test cases for $d = 10$, 30, 50, 100 and 300. The L-SHADE is excluded for scalability test due to a large search agents' requirement $N = 18D$. The scalability analysis of various optimization algorithms is presented in Fig. 6, which reveals the following facts:

1 The OEO consistently obtains the global optimum solutions for test functions $f_9 - f_{11}$.
2 The OEO obtains near-optimal solutions for test functions $f_1 - f_4$.
3 The OEO optimal solutions on test functions f_6, f_7, f_{12} and f_{13} are improved from its predecessors EO.
4 The OEO performances on test functions f_5 and f_8 lags HHO and SFO while a similar result like EO.

The scalability analysis reveals that the OEO can be used to obtain the optimal solution effectively for a set of random dimensional problems. Noteworthy differences are found for which it seems to be attractive for solving real-world engineering problems.

3.2.6. *Discussions on results of OEO*

For completeness, both the statistical and scalability analysis is presented. To enhance the search process of the OEO, the opposition-based learning and the escaping strategy are incorporated. From the statistical analysis based on Friedman's mean rank test, Bonferroni-Dunn test, Holm's test and p-value of Wilcoxon's signed ranked test, presented in Tables 2-4 and Fig. 3, it is revealed that the OEO becomes rank one among some recently developed and well-known optimizers – EO, HHO, SFO, WOA, GWO, PSO, DE, and L-SHADE. The Boxplot in Fig. 4 shows that the OEO has shown consistent performance among other optimization methods in most of the test cases. The OEO also enhances its convergence ability with iteration counts, which is reflected in Fig. 5. The OEO has shown better results in the scalability analysis, which is revealed from Fig. 6. Profound differences are marked in the study. Exemplary solutions are shown to demonstrate the ability of our proposed OEO. As opposed to the existing methods, our algorithm inherently includes certain mechanisms to handle different situations under uncertain dimensions. To figure out, the merits of our algorithm are – i) improved exploration, ii) better accuracy, iii) convergence in terms of iteration count, iv) easy to handle random problems with uncertain dimensions, etc. The reason for advanced technology may be due to the inbuilt escaping strategy and the opposition based learning scheme.

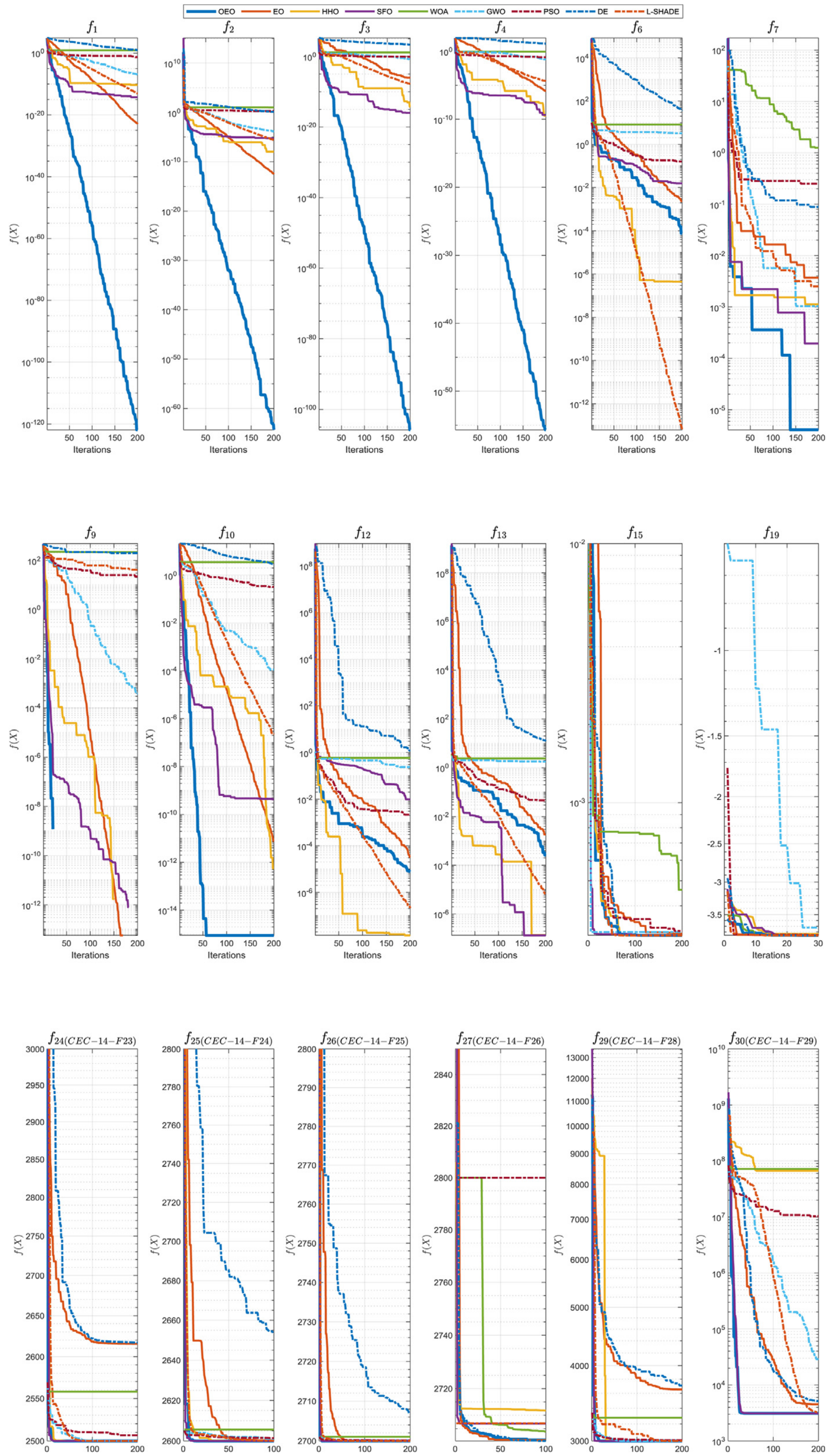

Fig. 5. Convergence curve comparisons of 12 test functions $f_1 - f_4$, f_6, f_7, f_9, f_{12}, f_{15}, f_{19}, f_{24} and f_{29}.

4. The proposed context-sensitive entropy dependency based multilevel thresholding using opposition equilibrium optimizer

In this section, we propose a novel context-sensitive entropy dependency based multilevel thresholding technique using the opposition equilibrium optimizer (CSED-OEO) for colour images. The focus of the contribution is to retain contextual information without increasing the computation load. The idea of the energy curve (discussed in Section 2.2) is used under one-dimensional setting. Therefore, a higher speed in the computation of entropy values is enforced while minimizing

Table 4
p-value of Wilcoxon's signed ranked test with a 5% degree of significance (p-value $\geq$ 0.05 are shown in boldface). '+' for better, '−' for inferior, and '≈' for identical.

Test functions	OEO vs. EO	OEO vs. HHO	OEO vs. SFO	OEO vs. WOA	OEO vs. GWO	OEO vs. PSO	OEO vs. DE	OEO vs. L-SHADE
f_1	8.88E-16	8.88E-16	8.88E-16	8.88E-16	8.88E-16	8.88E-16	8.88E-16	8.88E-16
f_2	8.88E-16	8.88E-16	8.88E-16	8.88E-16	8.88E-16	8.88E-16	8.88E-16	8.88E-16
f_3	8.88E-16	8.88E-16	8.88E-16	8.88E-16	8.88E-16	8.88E-16	8.88E-16	8.88E-16
f_4	8.88E-16	8.88E-16	8.88E-16	8.88E-16	8.88E-16	8.88E-16	8.88E-16	8.88E-16
f_5	8.88E-16	8.88E-16	8.88E-16	**5.76E-01**	8.88E-16	8.88E-16	8.88E-16	8.88E-16
f_6	8.88E-16	4.62E-14	8.88E-16	8.88E-16	8.88E-16	8.88E-16	8.88E-16	8.88E-16
f_7	8.88E-16	4.89E-02	**1.61E-01**	8.88E-16	8.88E-16	8.88E-16	8.88E-16	8.88E-16
f_8	1.21E-07	8.88E-16	**7.80E-01**	4.89E-02	8.88E-16	8.88E-16	1.98E-04	8.88E-16
f_9	**1.00E+00**	**1.00E+00**	7.45E-09	8.88E-16	8.88E-16	8.88E-16	8.88E-16	8.88E-16
f_{10}	8.88E-16	1.00E+00	8.88E-16	8.88E-16	8.88E-16	8.88E-16	8.88E-16	8.88E-16
f_{11}	**1.00E+00**	**1.00E+00**	6.10E-05	2.44E-04	8.88E-16	8.88E-16	8.88E-16	**1.00E+00**
f_{12}	1.47E-05	1.97E-11	8.88E-16	8.88E-16	8.88E-16	8.88E-16	8.88E-16	4.62E-14
f_{13}	4.62E-14	4.62E-14	8.88E-16	8.88E-16	8.88E-16	8.88E-16	8.88E-16	8.88E-16
f_{14}	1.60E-11	8.88E-16	8.88E-16	8.88E-16	8.88E-16	8.88E-16	8.36E-12	8.88E-16
f_{15}	6.87E-07	4.62E-14	4.62E-14	1.98E-04	8.88E-16	4.62E-14	1.98E-04	8.88E-16
f_{16}	5.22E-03	8.88E-16	8.88E-16	8.88E-16	8.88E-16	8.88E-16	4.66E-10	4.66E-10
f_{17}	**1.00E+00**	3.55E-15	8.88E-16	8.88E-16	8.88E-16	8.88E-16	**1.00E+00**	8.88E-16
f_{18}	5.54E-06	8.88E-16	8.88E-16	8.88E-16	8.88E-16	8.88E-16	5.68E-14	2.54E-05
f_{19}	5.08E-04	8.88E-16	8.88E-16	8.88E-16	8.88E-16	8.88E-16	2.27E-13	2.27E-13
f_{20}	**4.01E-01**	1.18E-12	4.62E-14	1.97E-11	1.18E-12	3.39E-06	**1.61E-01**	6.87E-07
f_{21}	**5.76E-01**	8.88E-16	8.88E-16	8.88E-16	8.88E-16	8.88E-16	1.83E-08	8.88E-16
f_{22}	1.18E-12	8.88E-16	8.88E-16	8.88E-16	8.88E-16	8.88E-16	1.18E-12	8.88E-16
f_{23}	1.98E-04	8.88E-16	8.88E-16	8.88E-16	8.88E-16	8.88E-16	1.97E-11	8.88E-16
f_{24} (CEC−14−F23)	8.88E-16	**1.00E+00**	8.88E-16	8.88E-16	8.88E-16	8.88E-16	8.88E-16	8.88E-16
f_{25} (CEC−14−F24)	8.88E-16	3.64E-12	8.88E-16	8.88E-16	8.88E-16	8.88E-16	8.88E-16	8.88E-16
f_{26} (CEC−14−F25)	8.88E-16	**1.00E+00**	8.88E-16	8.88E-16	8.88E-16	8.88E-16	8.88E-16	8.88E-16
f_{27} (CEC−14−F26)	1.98E-04	**2.86E-01**	6.87E-07	6.21E-04	8.88E-16	8.88E-16	1.47E-05	**7.80E-01**
f_{28} (CEC−14−F27)	8.88E-16	**1.00E+00**	8.88E-16	8.88E-16	8.88E-16	8.88E-16	8.88E-16	8.88E-16
f_{29} (CEC−14−F28)	8.88E-16	**1.00E+00**	8.88E-16	8.88E-16	8.88E-16	8.88E-16	8.88E-16	8.88E-16
f_{30} (CEC−14−F29)	4.62E-14	**1.00E+00**	1.97E-11	1.97E-11	4.62E-14	8.88E-16	8.88E-16	1.97E-11
f_{31} (CEC−14−F30)	1.10E-02	3.66E-03	**1.00E+00**	2.33E-09	**1.00E+00**	8.88E-16	4.89E-02	**1.00E+00**
+ / ≈ / −	26 / 3 / 2	23 / 7 / 1	28 / 1 / 2	30 / 0 / 1	30 / 1 / 0	31 / 0 / 0	29 / 1 / 1	28 / 2 / 1

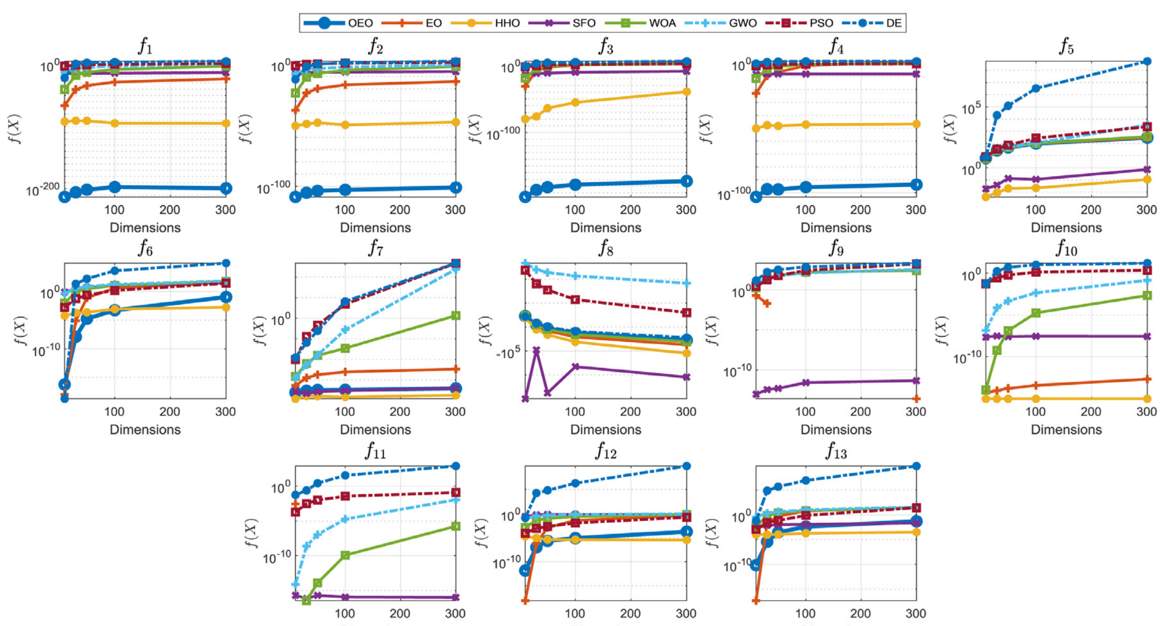

Fig. 6. Scalability analysis for scalable test functions $f_1 - f_{13}$.

the objective function. As opposed to the earlier techniques, our method is based on a minimization approach. All these aspects are enshrined in the present development.

The multilevel thresholding using the CSED-OEO for a colour image is formulated here. The energy curve based minimum entropy dependency objective function for a multilevel thresholding problem is investigated and presented in this section.

Let us define an RGB colour image I for size $m \times n \times 3$ as:

$$I(x, y) = \left[I^R(x, y), I^G(x, y), I^B(x, y)\right],\ 1 \leq x \leq m \text{ and } 1 \leq y \leq n \tag{26}$$

where $I^R(x, y)$ represents the red, $I^G(x, y)$ represents the green and $I^B(x, y)$ represents the blue plane of the image $I(x, y)$, which are mixed to display a true colour image. The arbitrary individual colour plane $I^p(x, y)$, $\forall p \in (R, G, B)$ is of size $m \times n$ pixel. So, each colour pixel is a

Table 5
The Optimal and Average segmentation metric results (PSNR, SSIM, and FSIM) ('↑' as superior result count and '↔' as similar results count).

Test Images	*d*	Metric	OEO	EO	HHO	SFO	WOA	GWO	PSO	DE	L-SHADE
TI1	4	$PSNR_{OPT}$	**26.7311**	26.1953	26.1127	25.9647	25.4479	26.5932	26.3408	24.7168	26.2182
		$FSIM_{OPT}$	**0.9649**	0.9638	0.9630	0.9641	0.9473	0.9665	0.9590	0.9249	0.9506
		$SSIM_{OPT}$	**0.9190**	0.9046	0.9059	0.9048	0.8977	0.9132	0.9136	0.8836	0.9134
		$PSNR_{AVE}$	**26.1839**	25.3158	24.7267	25.1581	24.9962	26.0320	25.7419	24.7999	25.1801
		$FSIM_{AVE}$	**0.9514**	0.9406	0.9216	0.9383	0.9327	0.9572	0.9529	0.9250	0.9313
		$SSIM_{AVE}$	**0.9089**	0.8938	0.8810	0.8929	0.8905	0.9059	0.9020	0.8873	0.8943
	8	$PSNR_{OPT}$	**30.8012**	30.7627	28.8841	29.5309	30.7044	30.6911	29.0388	30.0894	29.2234
		$FSIM_{OPT}$	0.9889	**0.9890**	0.9761	0.9829	0.9868	0.9908	0.9730	0.9866	0.9883
		$SSIM_{OPT}$	**0.9649**	**0.9649**	0.9474	0.9606	0.9655	0.9645	0.9550	0.9569	0.9444
		$PSNR_{AVE}$	30.0965	**30.3724**	28.2630	27.4707	29.9722	29.6723	27.1042	29.1146	29.3374
		$FSIM_{AVE}$	0.9853	**0.9876**	0.9751	0.9684	0.9843	0.9851	0.9657	0.9807	0.9829
		$SSIM_{AVE}$	0.9591	**0.9618**	0.9377	0.9270	0.9573	0.9548	0.9310	0.9490	0.9494
	12	$PSNR_{OPT}$	**33.2166**	33.0970	31.9839	32.1160	33.1312	32.5839	30.9013	31.8378	32.5145
		$FSIM_{OPT}$	0.9947	**0.9952**	0.9931	0.9916	0.9924	0.9949	0.9879	0.9901	0.9929
		$SSIM_{OPT}$	**0.9794**	0.9780	0.9757	0.9765	0.9813	0.9776	0.9671	0.9735	0.9760
		$PSNR_{AVE}$	**32.9053**	32.8811	31.3138	29.4059	32.8995	31.4762	29.5991	31.3018	31.6175
		$FSIM_{AVE}$	0.9938	**0.9946**	0.9901	0.9829	0.9938	0.9886	0.9800	0.9898	0.9920
		$SSIM_{AVE}$	**0.9783**	0.9776	0.9708	0.9466	0.9793	0.9715	0.9518	0.9678	0.9709
TI2	4	$PSNR_{OPT}$	**27.8899**	**27.8899**	27.8790	27.6226	27.5376	27.8717	27.4064	27.8863	27.7021
		$FSIM_{OPT}$	0.9318	0.9318	0.9343	**0.9358**	0.9287	0.9337	0.9310	0.9320	0.9223
		$SSIM_{OPT}$	0.9293	0.9293	0.9299	0.9246	0.9235	0.9259	**0.9307**	0.9278	0.9261
		$PSNR_{AVE}$	**27.7489**	27.7208	27.4155	27.2930	27.6932	27.6973	25.4512	27.6669	27.4911
		$FSIM_{AVE}$	**0.9321**	0.9318	0.9287	0.9322	0.9317	0.9298	0.9152	0.9319	0.9282
		$SSIM_{AVE}$	**0.9258**	0.9254	0.9230	0.9217	0.9243	0.9251	0.8957	0.9242	0.9226
	8	$PSNR_{OPT}$	**31.7228**	31.3243	30.9772	31.5871	31.0988	31.3695	29.5724	30.9483	30.8796
		$FSIM_{OPT}$	0.9647	0.9646	0.9674	0.9606	0.9552	**0.9677**	0.9571	0.9534	0.9526
		$SSIM_{OPT}$	**0.9658**	0.9622	0.9593	0.9648	0.9636	0.9606	0.9390	0.9612	0.9616
		$PSNR_{AVE}$	30.5086	**30.9935**	29.6352	30.5262	30.8446	30.7281	28.9036	30.8518	30.3196
		$FSIM_{AVE}$	0.9577	0.9572	0.9557	**0.9602**	0.9546	0.9575	0.9432	0.9543	0.9516
		$SSIM_{AVE}$	0.9561	0.9608	0.9485	0.9577	0.9609	0.9606	0.9375	**0.9617**	0.9558
	12	$PSNR_{OPT}$	**34.1794**	33.8659	33.1145	32.1654	33.8241	33.1776	32.6510	32.6501	32.4470
		$FSIM_{OPT}$	**0.9765**	0.9730	0.9689	0.9657	0.9743	0.9732	0.9724	0.9590	0.9743
		$SSIM_{OPT}$	**0.9761**	0.9759	**0.9761**	0.9712	0.9778	0.9727	0.9673	0.9706	0.9654
		$PSNR_{AVE}$	**33.7585**	33.2947	31.7067	30.9414	33.3345	32.4432	31.3180	32.1503	32.3080
		$FSIM_{AVE}$	**0.9725**	0.9694	0.9679	0.9578	0.9705	0.9692	0.9646	0.9649	0.9677
		$SSIM_{AVE}$	**0.9775**	0.9754	0.9647	0.9633	0.9752	0.9693	0.9632	0.9703	0.9696
TI3	4	$PSNR_{OPT}$	**25.7751**	25.6857	25.6718	25.5586	25.6738	25.7174	24.9349	25.6742	25.6064
		$FSIM_{OPT}$	**0.9717**	0.9712	0.9704	0.9658	0.9711	0.9713	0.9712	0.9707	0.9707
		$SSIM_{OPT}$	**0.8299**	0.8265	0.8283	0.8222	0.8276	0.8264	0.8175	0.8247	0.8274
		$PSNR_{AVE}$	25.6355	**25.6760**	25.3764	25.3733	25.6738	25.6531	23.5348	25.6617	25.4628
		$FSIM_{AVE}$	**0.9719**	0.9712	0.9668	0.9674	0.9711	0.9696	0.9486	0.9706	0.9696
		$SSIM_{AVE}$	**0.8283**	0.8269	0.8232	0.8208	0.8276	0.8243	0.7490	0.8249	0.8208
	8	$PSNR_{OPT}$	**30.7479**	30.4709	29.9327	30.1617	30.7149	30.3299	28.0452	30.3325	30.2803
		$FSIM_{OPT}$	0.9920	0.9920	0.9905	0.9895	0.9929	**0.9941**	0.9758	0.9923	0.9917
		$SSIM_{OPT}$	0.9105	0.9074	0.9014	0.9089	**0.9165**	0.9139	0.8535	0.9063	0.9202
		$PSNR_{AVE}$	**30.3700**	30.2062	29.6941	29.4834	30.2463	29.8101	27.6049	29.9206	29.9452
		$FSIM_{AVE}$	0.9922	0.9919	0.9917	0.9904	0.9923	**0.9927**	0.9840	0.9918	0.9904
		$SSIM_{AVE}$	0.9069	0.9047	0.9017	0.9045	**0.9073**	0.9004	0.8692	0.9022	0.9068
	12	$PSNR_{OPT}$	**33.0760**	33.0612	31.8935	31.8043	33.1517	31.6193	30.7159	32.2235	32.4433
		$FSIM_{OPT}$	0.9965	**0.9973**	0.9956	0.9964	0.9971	0.9941	0.9820	0.9969	0.9964
		$SSIM_{OPT}$	0.9373	0.9396	0.9354	0.9279	**0.9381**	0.9230	0.8991	0.9276	0.9360
		$PSNR_{AVE}$	32.9308	32.8262	31.7439	31.1283	**33.0178**	30.7665	29.9644	31.9335	32.2049
		$FSIM_{AVE}$	0.9970	0.9968	0.9956	0.9947	**0.9971**	0.9906	0.9923	0.9945	0.9969
		$SSIM_{AVE}$	0.9371	**0.9386**	0.9330	0.9231	0.9370	0.9094	0.9011	0.9237	0.9337
TI4	4	$PSNR_{OPT}$	**25.0967**	25.0248	23.8145	23.5509	23.4942	24.6870	24.6783	24.8779	22.9124
		$FSIM_{OPT}$	0.9598	**0.9600**	0.9576	0.9512	0.9066	0.9409	0.9542	0.9508	0.8864
		$SSIM_{OPT}$	0.9198	0.9179	0.9085	0.9045	0.9046	0.9172	**0.9270**	0.9231	0.9040
		$PSNR_{AVE}$	**24.8931**	22.6990	21.9672	22.4045	22.4702	23.5840	23.9223	23.6128	21.7421
		$FSIM_{AVE}$	0.9410	0.9516	0.9554	0.9463	0.8992	0.9297	**0.9492**	0.9394	0.8738
		$SSIM_{AVE}$	0.8994	0.9071	0.8815	0.8757	0.8662	0.8706	**0.9190**	0.8989	0.8316
	8	$PSNR_{OPT}$	**30.2776**	29.9667	29.8125	28.7596	29.2583	29.2379	29.4146	29.6568	28.5423
		$FSIM_{OPT}$	0.9943	**0.9950**	0.9929	0.9912	0.9946	0.9923	0.9875	0.9944	0.9886
		$SSIM_{OPT}$	**0.9753**	0.9711	0.9711	0.9648	0.9653	0.9679	0.9713	0.9682	0.9633
		$PSNR_{AVE}$	**29.1131**	28.2197	29.0618	27.9243	27.4528	28.4622	26.9897	26.7425	26.4580
		$FSIM_{AVE}$	**0.9875**	0.9834	0.9907	0.9732	0.9771	0.9761	0.9824	0.9826	0.9881
		$SSIM_{AVE}$	0.9670	0.9650	**0.9680**	0.9613	0.9572	0.9661	0.9597	0.9591	0.9499
	12	$PSNR_{OPT}$	**32.6516**	32.2969	29.4568	31.8648	31.4973	32.6384	31.2034	32.2362	32.1106
		$FSIM_{OPT}$	**0.9985**	0.9983	0.9912	0.9973	0.9966	0.9971	0.9936	0.9968	0.9970
		$SSIM_{OPT}$	0.9828	0.9800	0.9694	0.9804	0.9808	**0.9847**	0.9800	0.9811	0.9802
		$PSNR_{AVE}$	**31.9112**	31.8803	27.6678	30.4305	30.0524	30.4779	28.7999	31.1073	29.9849
		$FSIM_{AVE}$	**0.9902**	0.9815	0.9747	0.9922	0.9844	0.9855	0.9829	0.9794	0.9917

Table 5
(*Continued*)

		$SSIM_{AVE}$	0.9766	**0.9777**	0.9511	0.9678	0.9714	0.9721	0.9694	0.9684	0.9696
TI5	4	$PSNR_{OPT}$	**26.3339**	25.2370	26.0969	25.6033	25.2370	25.6544	26.0024	25.6927	25.7392
		$FSIM_{OPT}$	0.9764	0.9581	0.9753	0.9638	0.9581	0.9641	**0.9782**	0.9644	0.9670
		$SSIM_{OPT}$	**0.9289**	0.9155	0.9284	0.9244	0.9155	0.9231	0.9238	0.9234	0.9248
		$PSNR_{AVE}$	**25.7522**	25.2161	25.1441	25.5437	25.2072	25.3377	24.4381	25.5263	25.2585
		$FSIM_{AVE}$	**0.9674**	0.9579	0.9611	0.9633	0.9579	0.9598	0.9512	0.9624	0.9605
		$SSIM_{AVE}$	**0.9249**	0.9154	0.9147	0.9240	0.9152	0.9174	0.9113	0.9226	0.9186
	8	$PSNR_{OPT}$	31.6015	**31.6272**	30.6433	30.6162	31.1169	31.1022	28.7858	30.6359	30.4560
		$FSIM_{OPT}$	**0.9941**	0.9938	0.9914	0.9930	0.9935	0.9943	0.9912	0.9902	0.9887
		$SSIM_{OPT}$	0.9740	**0.9747**	0.9687	0.9680	0.9721	0.9697	0.9583	0.9680	0.9703
		$PSNR_{AVE}$	31.3227	**31.3853**	30.0021	29.6498	31.0338	30.3693	27.5978	30.1483	30.1285
		$FSIM_{AVE}$	0.9934	**0.9936**	0.9893	0.9897	0.9917	0.9901	0.9854	0.9895	0.9895
		$SSIM_{AVE}$	0.9729	**0.9734**	0.9661	0.9602	0.9701	0.9692	0.9479	0.9676	0.9663
	12	$PSNR_{OPT}$	33.9156	33.8313	32.6933	32.4560	**34.3253**	33.4866	31.6368	33.5374	33.1658
		$FSIM_{OPT}$	0.9976	0.9966	0.9964	0.9961	**0.9982**	0.9958	0.9957	0.9968	0.9953
		$SSIM_{OPT}$	0.9844	**0.9846**	0.9804	0.9789	0.9841	0.9840	0.9740	**0.9846**	0.9798
		$PSNR_{AVE}$	32.8854	33.6961	31.7377	31.5215	**33.7379**	33.3778	30.2731	32.3157	32.2883
		$FSIM_{AVE}$	0.9953	0.9971	0.9927	0.9942	**0.9973**	0.9961	0.9895	0.9936	0.9945
		$SSIM_{AVE}$	0.9813	**0.9837**	0.9755	0.9740	0.9834	0.9829	0.9682	0.9794	0.9783
TI6	4	$PSNR_{OPT}$	**27.0952**	27.0571	26.5280	25.8064	27.0481	26.8089	26.4675	27.0168	26.8923
		$FSIM_{OPT}$	0.9416	0.9399	0.9158	0.9386	**0.9466**	**0.9466**	0.9375	0.9447	0.9326
		$SSIM_{OPT}$	**0.8127**	0.8120	0.7780	0.7631	0.7933	0.7989	0.7942	0.8088	0.8074
		$PSNR_{AVE}$	26.0380	26.7506	25.3058	25.1141	**26.8424**	26.6023	25.3038	26.7426	26.3512
		$FSIM_{AVE}$	0.9374	0.9408	0.9113	0.9091	**0.9437**	0.9409	0.9003	0.9366	0.9372
		$SSIM_{AVE}$	0.7767	**0.8004**	0.7392	0.7222	0.7899	0.7928	0.7378	0.7922	0.7837
	8	$PSNR_{OPT}$	**30.7683**	29.7804	28.5280	29.2569	29.6704	30.2685	29.0639	30.0731	29.1835
		$FSIM_{OPT}$	**0.9905**	0.9829	0.9796	0.9773	0.9859	0.9870	0.9658	0.9877	0.9838
		$SSIM_{OPT}$	**0.8986**	0.8771	0.8507	0.8780	0.8722	0.8820	0.8699	0.8819	0.8374
		$PSNR_{AVE}$	**30.0516**	29.4403	28.4357	28.7573	29.3790	29.4358	27.6929	29.1557	29.0021
		$FSIM_{AVE}$	**0.9871**	0.9839	0.9687	0.9777	0.9851	0.9811	0.9532	0.9830	0.9798
		$SSIM_{AVE}$	**0.8851**	0.8683	0.8438	0.8484	0.8671	0.8613	0.8278	0.8651	0.8503
	12	$PSNR_{OPT}$	**34.0682**	33.3724	31.6449	32.3395	32.4270	33.7192	32.5208	32.0305	32.1680
		$FSIM_{OPT}$	0.9966	0.9968	0.9887	0.9911	0.9940	**0.9974**	0.9921	0.9947	0.9887
		$SSIM_{OPT}$	**0.9481**	0.9403	0.9223	0.9270	0.9265	0.9452	0.9285	0.9153	0.9160
		$PSNR_{AVE}$	**33.0204**	32.9946	30.9151	31.4851	31.6649	33.0353	29.7240	31.2675	31.4242
		$FSIM_{AVE}$	0.9947	0.9963	0.9884	0.9885	0.9918	**0.9966**	0.9758	0.9907	0.9865
		$SSIM_{AVE}$	**0.9358**	0.9336	0.9042	0.9160	0.9137	0.9301	0.8564	0.9081	0.9109
TI7	4	$PSNR_{OPT}$	**25.8106**	25.5218	23.9090	25.2561	25.5107	24.9137	25.0154	25.4736	25.4562
		$FSIM_{OPT}$	0.9600	0.9575	0.9475	**0.9641**	0.9565	0.9519	0.9538	0.9560	0.9563
		$SSIM_{OPT}$	**0.8984**	0.8866	0.8560	0.8867	0.8872	0.8756	0.8749	0.8857	0.8850
		$PSNR_{AVE}$	**25.4929**	24.9973	23.5587	24.7786	25.4019	23.3312	24.3103	24.1016	24.6866
		$FSIM_{AVE}$	0.9504	0.9473	0.9391	**0.9617**	0.9471	0.9356	0.9371	0.9509	0.9523
		$SSIM_{AVE}$	**0.8883**	0.8752	0.8489	0.8831	0.8704	0.8741	0.8731	0.8832	0.8821
	8	$PSNR_{OPT}$	**30.2647**	29.5444	28.5365	27.6782	28.5677	29.1153	27.0458	28.6207	29.1583
		$FSIM_{OPT}$	**0.9917**	0.9910	0.9789	0.9843	0.9830	0.9870	0.9724	0.9847	0.9875
		$SSIM_{OPT}$	**0.9501**	0.9383	0.9297	0.9354	0.9270	0.9372	0.9286	0.9351	0.9357
		$PSNR_{AVE}$	**29.8134**	29.4759	27.8154	26.6244	27.6663	28.9844	26.9364	27.5084	27.8387
		$FSIM_{AVE}$	**0.9888**	0.9812	0.9628	0.9776	0.9772	0.9722	0.9722	0.9837	0.9743
		$SSIM_{AVE}$	**0.9387**	0.9284	0.9161	0.9221	0.9125	0.9318	0.9158	0.9247	0.9282
	12	$PSNR_{OPT}$	**32.7679**	32.5982	31.0779	31.2751	31.8878	31.3939	25.4264	31.4426	31.4026
		$FSIM_{OPT}$	0.9950	**0.9957**	0.9914	0.9953	0.9949	0.9930	0.9629	0.9915	0.9956
		$SSIM_{OPT}$	**0.9677**	0.9659	0.9599	0.9623	0.9610	0.9644	0.9090	0.9603	0.9613
		$PSNR_{AVE}$	**32.6180**	31.9376	30.9150	31.0995	30.6371	30.9362	24.6592	29.9264	30.7235
		$FSIM_{AVE}$	0.9812	0.9806	0.9828	0.9822	**0.9928**	0.9744	0.9593	0.9862	0.9797
		$SSIM_{AVE}$	0.9583	0.9510	0.9523	0.9570	**0.9603**	0.9515	0.9012	0.9516	0.9495
TI8	4	$PSNR_{OPT}$	**26.7213**	25.1606	26.2764	26.8710	25.9750	26.1720	26.3807	25.7760	26.2535
		$FSIM_{OPT}$	**0.9059**	0.8487	0.8951	0.8957	0.8684	0.8869	0.8880	0.8695	0.8764
		$SSIM_{OPT}$	0.9391	0.9378	0.9370	0.9404	0.9426	0.9404	0.9421	0.9393	**0.9438**
		$PSNR_{AVE}$	**24.7694**	24.2600	25.4162	25.8784	25.3554	25.6181	26.1118	25.4175	25.7831
		$FSIM_{AVE}$	**0.8928**	0.8015	0.8636	0.8773	0.8554	0.8683	0.8807	0.8632	0.8749
		$SSIM_{AVE}$	0.9170	0.9135	0.9394	0.9384	0.9426	0.9394	0.9401	0.9375	**0.9391**
	8	$PSNR_{OPT}$	**30.8445**	29.7758	28.8876	29.9425	29.1859	30.5104	29.0244	30.3842	29.9509
		$FSIM_{OPT}$	0.9665	0.9515	0.9611	0.9595	0.9420	0.9648	0.9446	0.9620	**0.9675**
		$SSIM_{OPT}$	**0.9700**	0.9648	0.9590	0.9629	0.9621	0.9674	0.9562	0.9664	0.9625
		$PSNR_{AVE}$	**30.0744**	29.2353	27.8208	29.1908	29.3948	29.8612	28.5531	28.9138	29.0853
		$FSIM_{AVE}$	**0.9628**	0.9442	0.9396	0.9481	0.9458	0.9556	0.9469	0.9537	0.9413
		$SSIM_{AVE}$	**0.9657**	0.9635	0.9526	0.9609	0.9637	0.9647	0.9539	0.9582	0.9599
	12	$PSNR_{OPT}$	**33.1673**	33.1434	31.1347	32.0253	33.0374	33.3131	30.4638	32.0626	32.7513
		$FSIM_{OPT}$	0.9780	0.9782	0.9583	0.9720	0.9773	0.9780	0.9606	0.9719	**0.9799**
		$SSIM_{OPT}$	**0.9811**	0.9803	0.9741	0.9742	0.9801	0.9802	0.9649	0.9778	0.9791
		$PSNR_{AVE}$	**32.5798**	32.1333	30.9431	30.2601	32.0377	32.1140	30.2490	31.0997	31.9087
		$FSIM_{AVE}$	**0.9789**	0.9723	0.9621	0.9639	0.9749	0.9721	0.9596	0.9742	0.9704
		$SSIM_{AVE}$	**0.9785**	0.9769	0.9717	0.9664	0.9762	0.9766	0.9667	0.9718	0.9768
TI9	4	$PSNR_{OPT}$	25.1286	24.8940	**25.5159**	25.3399	24.9301	25.0029	23.0198	24.7994	24.9412
		$FSIM_{OPT}$	0.9546	0.9517	**0.9588**	0.9534	0.9515	0.9536	0.9088	0.9549	0.9587
		$SSIM_{OPT}$	0.9359	0.9334	**0.9392**	0.9397	0.9343	0.9339	0.9114	0.9299	0.9337

Table 5
(*Continued*)

		$PSNR_{AVE}$	24.5015	24.1732	24.1433	24.3072	24.9011	**24.9399**	22.9863	24.6826	24.3894
		$FSIM_{AVE}$	**0.9456**	0.9203	0.9419	0.9390	0.9516	0.9514	0.9271	0.9535	0.9428
		$SSIM_{AVE}$	0.9290	0.9217	0.9211	0.9265	0.9336	**0.9338**	0.9042	0.9289	0.9275
	8	$PSNR_{OPT}$	30.2413	30.1749	29.2808	28.6627	**30.4116**	29.7491	27.7169	29.8082	29.5684
		$FSIM_{OPT}$	0.9879	0.9880	0.9839	0.9869	**0.9891**	0.9854	0.9753	0.9856	0.9862
		$SSIM_{OPT}$	0.9759	0.9754	0.9707	0.9662	**0.9768**	0.9737	0.9625	0.9740	0.9714
		$PSNR_{AVE}$	**30.0288**	29.7013	27.8510	28.2162	29.6948	29.0018	27.1644	29.3461	28.8566
		$FSIM_{AVE}$	**0.9878**	0.9856	0.9807	0.9801	0.9863	0.9811	0.9720	0.9850	0.9820
		$SSIM_{AVE}$	**0.9749**	0.9732	0.9603	0.9650	0.9731	0.9701	0.9579	0.9717	0.9688
	12	$PSNR_{OPT}$	**33.3181**	32.6910	32.1054	31.8795	32.4966	32.5028	31.1123	32.4794	32.7668
		$FSIM_{OPT}$	**0.9947**	0.9942	0.9928	0.9927	0.9938	0.9917	0.9909	0.9935	0.9934
		$SSIM_{OPT}$	**0.9867**	0.9855	0.9840	0.9829	0.9849	0.9856	0.9801	0.9849	0.9854
		$PSNR_{AVE}$	**32.6398**	32.4817	31.3471	30.0379	32.1159	31.4299	29.0111	31.7748	31.5425
		$FSIM_{AVE}$	**0.9935**	**0.9935**	0.9905	0.9852	0.9927	0.9892	0.9810	0.9917	0.9913
		$SSIM_{AVE}$	**0.9854**	0.9851	0.9809	0.9756	0.9838	0.9815	0.9695	0.9828	0.9813
TI10	4	$PSNR_{OPT}$	**24.9725**	22.8728	24.2190	23.6342	23.1077	22.8389	24.6778	24.2442	24.2683
		$FSIM_{OPT}$	**0.9416**	0.8699	0.9247	0.9013	0.8846	0.8946	0.9144	0.9078	0.8932
		$SSIM_{OPT}$	0.7362	0.6752	**0.7985**	0.7674	0.6846	0.7662	0.7817	0.7063	0.7447
		$PSNR_{AVE}$	**23.9164**	22.7516	22.8019	23.2465	22.8552	23.2187	23.1274	23.3012	23.3246
		$FSIM_{AVE}$	**0.9111**	0.8651	0.9043	0.9092	0.8719	0.9001	0.8990	0.8933	0.8881
		$SSIM_{AVE}$	**0.7393**	0.7092	0.6814	0.7035	0.6962	0.7284	0.6860	0.7004	0.7174
	8	$PSNR_{OPT}$	**29.4476**	28.1726	28.0241	28.1767	28.6990	29.4345	29.3118	28.9466	28.9818
		$FSIM_{OPT}$	0.9681	0.9602	0.9686	0.9720	0.9583	0.9698	**0.9767**	0.9752	**0.9767**
		$SSIM_{OPT}$	**0.8746**	0.8527	0.8258	0.8225	0.8648	0.8660	0.8587	0.8550	0.8472
		$PSNR_{AVE}$	**28.6454**	27.9537	27.3179	27.4278	28.1130	28.5336	28.5395	28.1281	28.3452
		$FSIM_{AVE}$	0.9665	0.9526	0.9643	0.9684	0.9526	0.9633	**0.9745**	0.9605	0.9698
		$SSIM_{AVE}$	**0.8480**	0.8464	0.8102	0.8095	0.8558	0.8470	0.8306	0.8361	0.8303
	12	$PSNR_{OPT}$	32.5725	**32.6196**	30.7879	30.8428	32.2991	32.5998	30.6684	32.1626	31.6591
		$FSIM_{OPT}$	0.9881	0.9837	0.9773	0.9775	0.9860	0.9862	0.9763	**0.9909**	0.9889
		$SSIM_{OPT}$	0.9180	**0.9251**	0.9020	0.9072	0.9185	0.9225	0.8936	0.9114	0.9077
		$PSNR_{AVE}$	32.0101	**32.0126**	30.0686	30.2244	31.8495	31.3295	29.4384	31.0302	31.1451
		$FSIM_{AVE}$	**0.9854**	0.9828	0.9790	0.9787	0.9819	0.9813	0.9799	0.9842	0.9834
		$SSIM_{AVE}$	0.9116	**0.9143**	0.8845	0.8809	0.9127	0.8954	0.8618	0.8938	0.9023
↑ / ↔			106 / 1	25 / 2	5 / 0	4 / 0	16 / 1	8 / 1	6 / 1	2 / 1	4 / 1
Friedman's mean rank			**7.8750**	6.2639	3.5000	3.9694	5.5750	5.7167	2.7444	4.8194	4.5361
Rank			**1**	2	8	7	4	3	9	5	6

triplet corresponding to red (I^R), green (I^G) and blue (I^B) colour plane. For an arbitrary colour plane $I^p(x,y)$, $\forall p \in (R,G,B)$, the energy curve $E^p = \{E_0^p, E_1^p, \cdots, E_L^p\}$ is generated using Eq. (8). The optimal threshold values $\tau^{p,*} = (\tau_1^{p,*}, \tau_2^{p,*}, \cdots, \tau_d^{p,*})$, $\forall p \in (R,G,B)$, using CSED based multilevel thresholding method for a colour image, are estimated as:

$$\begin{aligned}\tau^{p,*} &= \left(\tau_1^{p,*}, \tau_2^{p,*}, \cdots, \tau_d^{p,*}\right)\\ &= \arg \min_{0<\tau_1^{p,*}<\tau_2^{p,*}<\cdots<\tau_d^{p,*}<L-1} \left\{\psi_1^p(C_1^p) + \cdots + \psi_i^p(C_i^p) + \cdots + \psi_{d+1}^p(C_{d+1}^p)\right\},\\ &\forall p \in (R,G,B) \qquad (27)\end{aligned}$$

where entropic information ψ_i^p of the ith class C_i^p($for\ i = 1,2,\cdots,d+1$) of an arbitrary plane (p) is evaluated using Eq. (28).

$$\begin{aligned}\psi_1^p(C_1^p) &= \log_e\left(\sum_{i=0}^{\tau_1} e_i^p\right) - \frac{1}{\sum_{i=0}^{\tau_1} e_i^p}\left[\left(\sum_{i=0}^{\tau_1-1} e_i^p\right)\log_e\left(\sum_{i=0}^{\tau_1-1} e_i^p\right) + E_{\tau_1}^p \log_e e_{\tau_1}^p\right]\\ &\vdots\\ \psi_i^p(C_i^p) &= \log_e\left(\sum_{i=\tau_{i-1}}^{\tau_i} e_i^p\right) - \frac{1}{\sum_{i=\tau_{i-1}}^{\tau_i} e_i^p}\left[e_{\tau_{i-1}}^p \log_e e_{\tau_{i-1}}^p + \left(\sum_{i=\tau_{i-1}+1}^{\tau_i-1} e_i^p\right)\log_e\left(\sum_{i=\tau_{i-1}+1}^{\tau_i-1} e_i^p\right) + e_{\tau_i}^p \log_e e_{\tau_i}^p\right]\\ &\vdots\\ \psi_{d+1}^p(C_{d+1}^p) &= \log_e\left(\sum_{i=\tau_d}^{L} e_i^p\right) - \frac{1}{\sum_{i=\tau_d}^{L} e_i^p}\left[e_{\tau_d}^p \log_e e_{\tau_d}^p + \left(\sum_{i=\tau_d+1}^{L} e_i^p\right)\log_e\left(\sum_{i=\tau_d+1}^{L} e_i^p\right)\right]\end{aligned} \qquad (28)$$

The probability distribution of energy *ep=e0p,e1p,⋯,eLp* of all possible individual gray level in an arbitrary image plane *Ip* of dimension, *m×n* is described as:

$$e_l^p = \frac{E_l^p}{\sum_{i=0}^{L} E_i^p}, \ \forall l \in [0, L] \qquad (29)$$

where E_l^p is the energy value of the gray level l in the arbitrary image plane I^p, $\sum e_l = 1$ and $0 \le e_l \le 1$.

The optimal threshold values $\tau^{p,*} = (\tau_1^{p,*}, \tau_2^{p,*}, \cdots, \tau_d^{p,*})$, $\forall p \in (R,G,B)$ obtained using the CSED based multilevel thresholding method for a colour image has d threshold values for each plane, that classifies the image plane into $d+1$ different classes C_i^p for $i = 1,2,\cdots,d+1$. The thresholded image plane $I_T^p(x,y)$ consists of only $d+1$ gray levels,$\{\theta_1^p, \theta_2^p, \cdots, \theta_{d+1}^p\}$, which are mean gray level values calculated by averaging the intensity values of the corresponding classes as:

$$I_T^p(x,y) = \begin{cases} \theta_1^p, & 0 \le I^p(x,y) \le \tau_1^{p,*} \\ \theta_2^p, & \tau_1^{p,*} \le I^p(x,y) \le \tau_2^{p,*} \\ \cdots & \cdots \\ \theta_{d+1}^p, & \tau_{d+1}^{p,*} \le I^p(x,y) \le L \end{cases}, \ 1 \le x \le m \text{ and } 1 \le y \le n \qquad (30)$$

After getting the red, green, and blue thresholded image planes, we combine the individual thresholded plane to obtain the colour thresholding image $I_T(x,y)$ given as:

$$I_T(x,y) = \left[I_T^R(x,y), I_T^G(x,y), I_T^B(x,y)\right] \qquad (31)$$

It is needed to find 3 $\times d$ numbers of optimal threshold values for a colour image. Here, the computation complexity is $O(3L^d)$. It is noteworthy to mention here that finding the optimal solutions is an exhaustive search process. Therefore, there is a strong need to propose a soft computing approach. In this experiment, the suggested OEO is used as an optimizer. The proposed CSED-OEO based multilevel thresholding technique may attract readers for colour image thresholding applications, because of its inherent advantages of attaining contextual information along with the knowledge of the entropy interdependencies among different classes. An effort is made here to minimize the shred boundary between different classes, which improves the accuracy of the method. A detailed process of the proposal for colour image thresholding is displayed in Fig. 7.

Generally, there is 256 $\times$ 256 $\times$ 256 number of colour levels in an original RGB test image. If we use d thresholds to segment the original

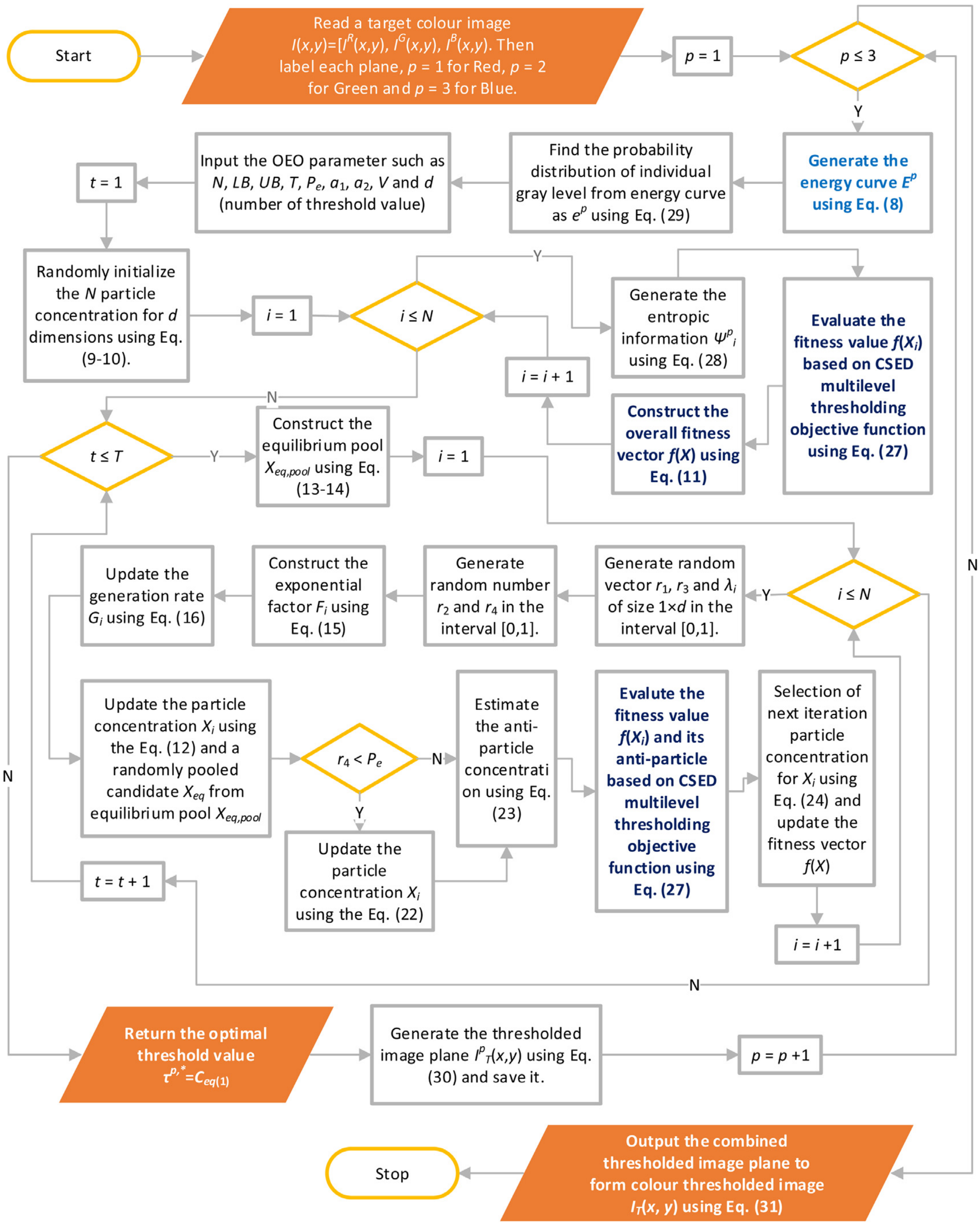

Fig. 7. Flowchart of the proposed CSED-OEO based multilevel thresholding for colour images.

test image, the number of colour levels is reduced to $(d+1)^3$, for the thresholded image. In our experiments, the segmented image is represented with 125 for d=4, 729 for d=8, and 2197 for d=12 colour levels. Thus, the proposed method reduced the distinct colour levels to such a large extent. Hence, it is well suited for simplified interpretation.

5. Results and discussions

In this section, we discuss the performance of the CSED-OEO based multilevel thresholding technique for remote sensing images. Its worthiness for the segmentation of multispectral images is highlighted. In these experiments, we use the high dimensional colour satellite images from the *Landsat image gallery* [44], which are captured by the Operational Land Imager (OLI) on the Landsat 8. The remote sensing images are taken well above the ground, so image features are rapidly changing their properties from one zone to another. This is the reason; the multilevel thresholding of high dimensional remote sensing images is more challenging. This demands us to use an efficient multilevel thresholding technique. A comparative study on the CSED based multilevel thresholding using recently developed and popular optimization algorithm are carried out. Here, the EO [29], HHO [36], SFO [37], WOA [38], GWO [39], PSO [35], DE [35] and L-SHADE [40] are also used for optimization.

Ten different test images (TI1 to TI10) from the *Landsat image gallery* [44] are considered for the experiments, which are displayed in Fig. 8. The visual information like test image, histogram, and energy curve of the corresponding RGB plane is also shown in Fig. 8. Along with this, Fig. 8 also provides information about the place and sensor of imaging,

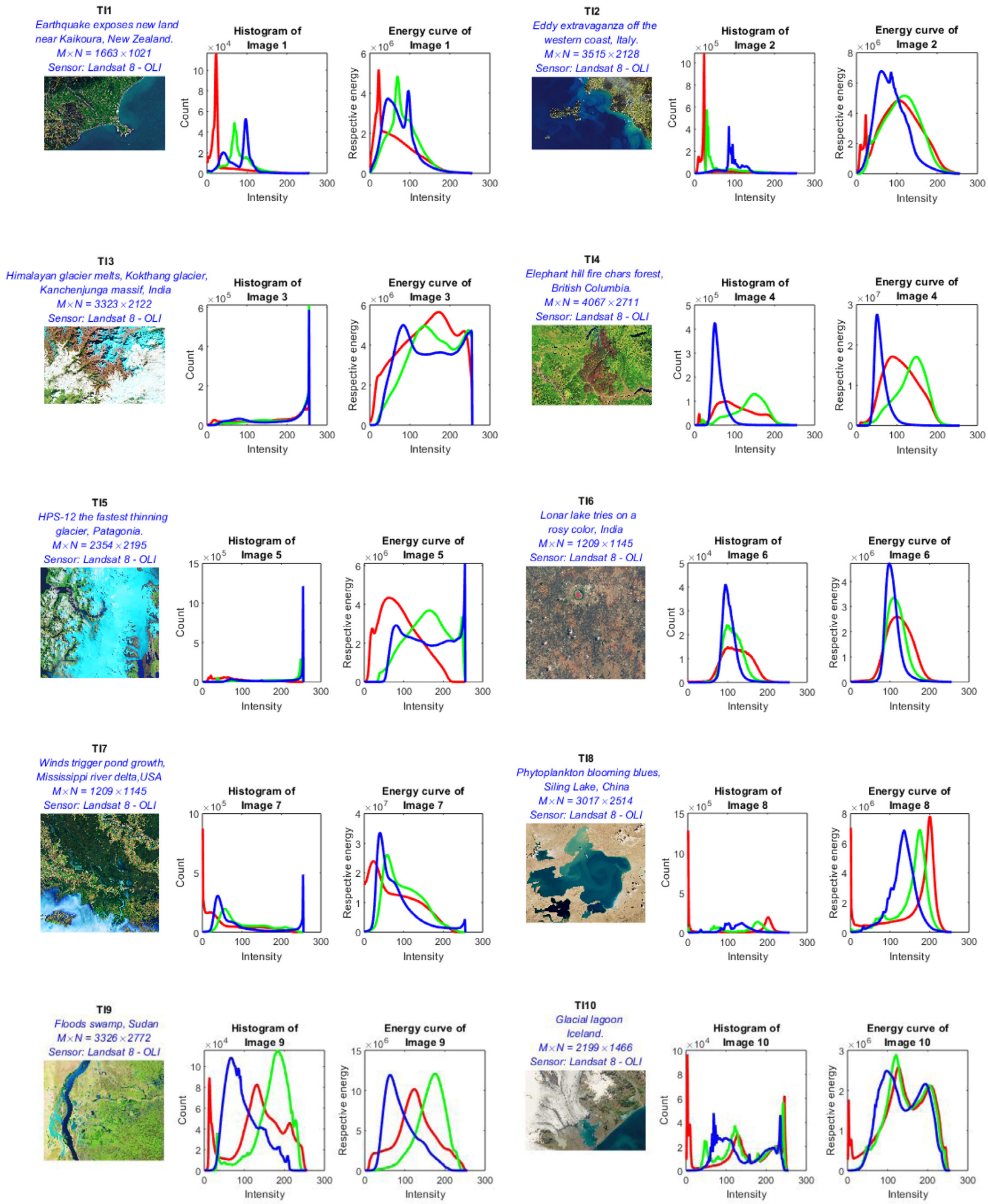

Fig. 8. Test images (TI1 to TI10) with their corresponding histograms.

dimensions of the images. In the experiments, all the algorithms are run independently 21 times for the threshold values $d = 4, 8, 12$, particle $N = 30$ and maximum number of iteration count $T = 100$, to maintain the consistency among the optimizer performances on the multilevel thresholding using the suggested CSED method. It is reiterated that the optimization parameters setting of the OEO, EO, HHO, SFO, WOA, GWO, PSO, DE, and L-SHADE are presented in Table 1.

For a numerical finding, the optimal threshold values of the test images are presented in Table A.1 of the Appendix. The mean gray level values of thresholded images using the optimal thresholds are displayed in Table A.2 of the Appendix. Tables A.1 and A.2 consists of numerical data to provide a practical understanding. Whereas the qualitative results on the OEO are presented in Fig. 9. The thresholded images provide a visual interpretation of the mean gray levels given in Table A.2. Fig. 9 shows the thresholded images of 10 test images (TI1 to TI10) for threshold values $d = 4, 8$ and 12. From Fig. 9, it is revealed that the CSED-OEO based multilevel thresholding method has the potential to obtain good quality threshold values. It is also evident that the quality of the thresholded images increases with an increase in the number of thresholds.

To conserve space, only two-sample test images TI8 and TI10 are displayed here for comparative analysis. The qualitative results using

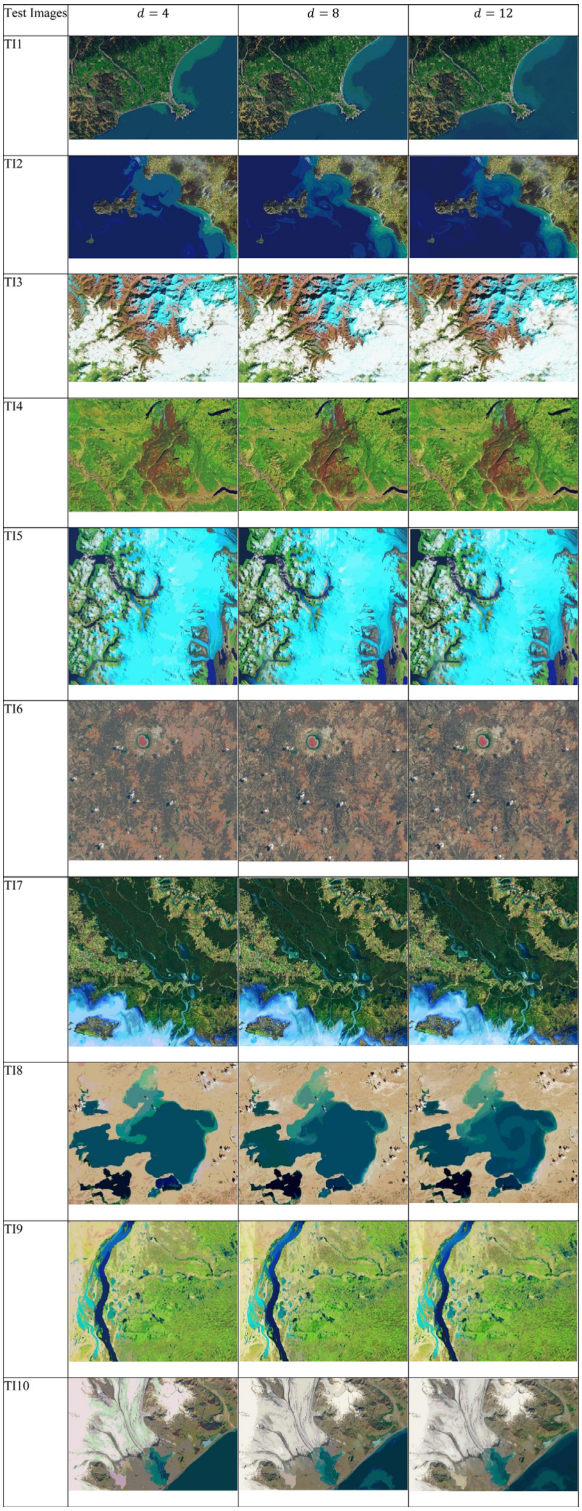

Fig. 9. Thresholded images using CSED-OEO multilevel colour image thresholding.

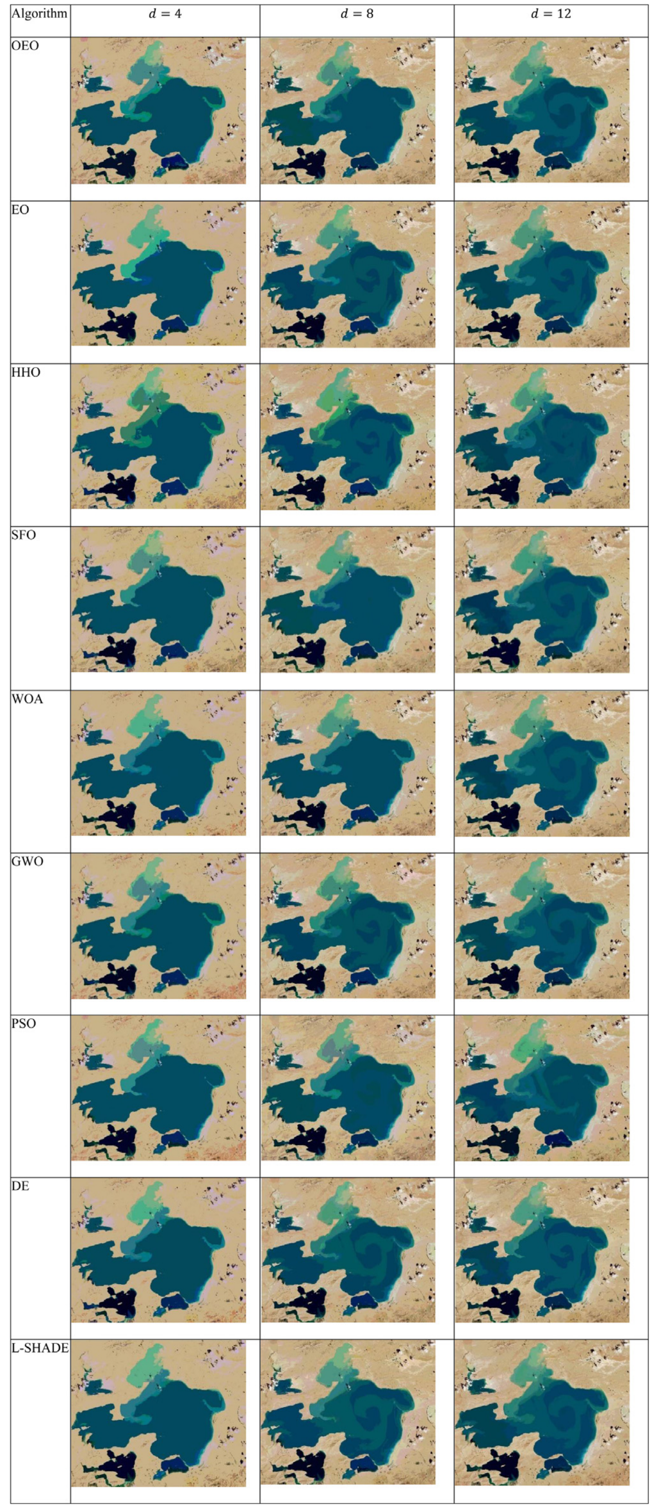

Fig. 10. Thresholded images using various optimization algorithms for multilevel colour image thresholding of test image TI8.

OEO, EO, HHO, SFO, WOA, GWO, PSO, DE, and L-SHADE are presented in Fig. 10 and Fig. 11, respectively. Fig. 10 and Fig. 11 shows that the overall visual quality of the OEO based thresholded images is more like the original images, the 2nd column is of 4-level, 3rd column is of 8-level and 4th column is of 12-level thresholded images. The 4-level thresholded images use 125 colour levels, 8-level thresholded images use 729 colour levels, and 12-level thresholded images use 2197 colour levels to represent, which are shown in Fig. 9-11.

The remote sensing images are high dimensional. The visual representation of thresholded images is not sufficient to ensure the superiority of a method. So, here some well-known quantitative metrics such as Peak Signal to Noise Ratio (PSNR) [45], Feature Similarity (FSIM) [46], and Structure Similarity (SSIM) [47] are used. The better is the PSNR, FSIM, and SSIM value, the better is the thresholding method. The results based on performance metric PSNR, FSIM, and SSIM are presented in Table 5. The first categories of metrics used in Table 5 are

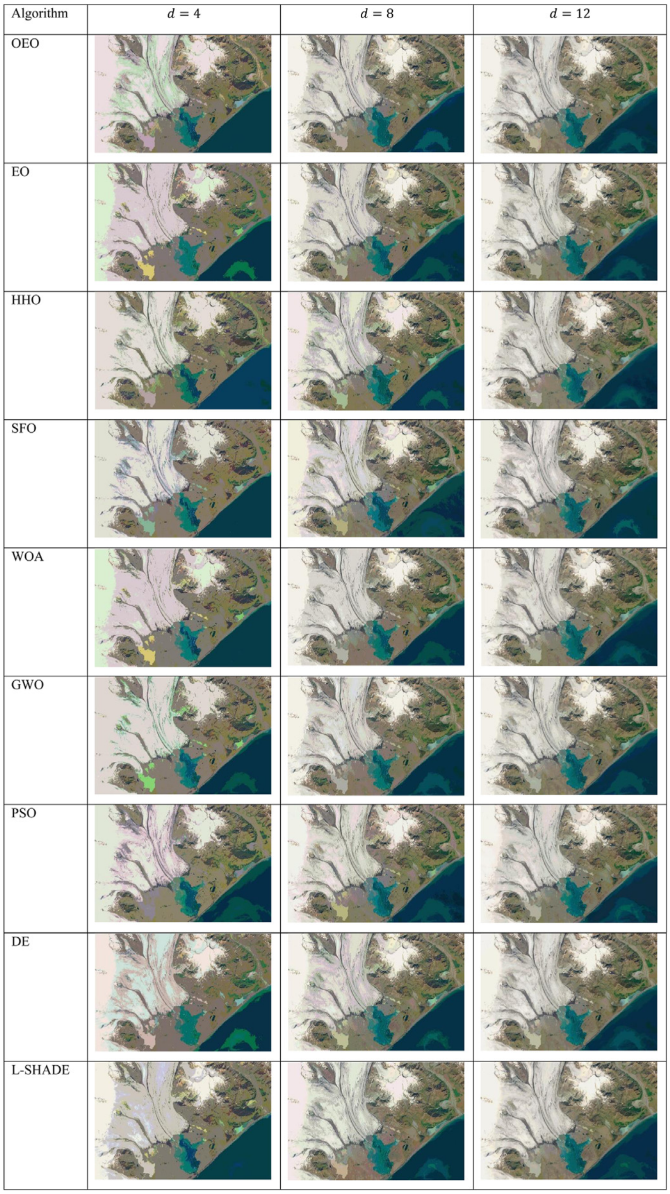

Fig. 11. Thresholded images using various optimization algorithms for multilevel colour image thresholding of test image TI10.

optimal PSNR (‘$PSNR_{OPT}$’), optimal FSIM (‘$FSIM_{OPT}$’), and optimal SSIM (‘$SSIM_{OPT}$’), which are obtained from the thresholded image using the optimal threshold value presented in Table A.1 and the corresponding mean gray level in Table A.2. The second categories of metric used in Table 5 to describe the performance of various optimizer in multilevel thresholding are average PSNR (‘$PSNR_{AVE}$’), average FSIM (‘$FSIM_{AVE}$’), and average SSIM (‘$SSIM_{AVE}$’), which are obtained from the thresholded image using independent threshold value obtained during the 21 independent runs of optimizer. These are estimated from the original test image, the corresponding thresholded image generated using the optimal threshold values presented in Table A.1 (see the Appendix), and the mean gray levels presented in Table A.2 (see the Appendix). Let us assign ‘↑’ for the superior results and ‘↔’ for the similar results of PSNR, FSIM, and SSIM using different optimization algorithms. The OEO has shown superior results for PSNR and SSIM metrics. However, it shows competitive results for FSIM metric. The performance on the quantitative metrics presented in Table 5 summarizes the following – OEO (‘↑’ 58.8%), EO (‘↑’ 13.8%), HHO (‘↑’ 2.8%), SFO (‘↑’ 2.2%), WOA (‘↑’ 8.9%), GWO (‘↑’ 4.4%), PSO (‘↑’ 3.3%), DE (‘↑’ 1.1%) and L-SHADE (‘↑’2.22). Friedman’s mean rank test is also performed on the data presented in Table 5. Interestingly, the OEO ranked first among other optimization algorithms. For instance, last row of Table 5 shows its superiority over others.

6. Conclusion

The paper highlighted the merits of the proposal covering all aspects of the multilevel colour image thresholding. As opposed to the previously published research work, mostly based on the maximization of entropy, the method proposed in this paper is based on the minimization of an entropic objective function. Another new contribution is the attainment of the contextual information in the thresholded output. The reason for attainment is the inherent mechanism using the energy curve. Interesting statistical results are achieved in connection with the newly introduced OEO because opposition particle concentration and escaping strategy are also utilized to enhance the exploration capability. Even more interesting is its scalability and stability performances because the search trajectory follows both directions. The search history, trajectory, and the average fitness history of the OEO explicitly discuss its effectiveness for optimization. Also, the Box plots and the convergence curves ensure its stability and faster convergence to obtain the optimal solutions based on the iteration count, respectively. The limitation of the OEO is it takes more number function evaluation as compared to its predecessors EO. The Friedman mean rank test, Bonferroni-Dunn test, Holm’s test, and p-value of Wilcoxon’s signed ranked test shows the commendable statistical performance of OEO over other optimizers such as EO, GWO, WOA, PSO, and DE. The OEO can be replaced in place of HHO, SFO, and L-SHADE optimization problem based on the posthoc analysis of Holm’s test. The OEO can be further explored to the multi-objective and constrained handling optimization problem. Nonetheless, the OEO has the potential to be used for the world of optimization

Moreover, the CSED-OEO method provides reduced complexity because the energy curve is used instead of the 2D histogram used in multilevel thresholding techniques. Nevertheless, its performance on the high dimensional application is encouraging. The reason may be due to its effective strategy to minimize the shred boundary between different classes by minimizing their entropy dependencies. An in-depth statistical analysis is provided to validate the method. Encouraging results are shown, which may attract readers for its future applications. Noteworthy differences are observed from the visual results displayed in Figs. 9-11. Quantitative metrics – PSNR, FSIM, and SSIM are used for validation. Friedman’s mean rank test is also carried out (Table 7) to justify the superiority of our method over others. Its performances are compared with state-of-the-art methods and found better than others. It is believed that the idea may attract other researchers to explore further. The paper may enrich the literature in the context of segmentation-based analysis of colour images. It would be useful for the segmentation of biomedical images like magnetic resonance images (MRI), thermogram images, etc.

Author statement

Manoj Kumar Naik: Methodology, implementation, data handling, programming, Writing original draft **Rutuparna Panda:** Conceptualization, methodology, guidance, data analysis, revision of draft **Ajith Abraham:** Supervision, analysis

Declaration of Competing Interest

The authors declare that they have no known competing financial interests or personal relationships that could have appeared to influence the work reported in this paper.

Appendix

Tables A1 and A2

Table A1
The optimal threshold values for each color component of the test images.

Test Images	*d*		OEO	EO	HHO	SFO	WOA	GWO	PSO	DE	L-SHADE
TI1	4	R	34 82 142 243	33 112 185 243	36 128 171 243	52 109 198 243	33 112 185 243	34 94 154 243	40 132 178 204	34 116 177 243	38 89 167 243
		G	49 86 155 245	46 89 146 245	44 94 137 245	43 93 146 245	47 113 187 245	46 89 146 245	46 98 159 219	46 129 189 245	45 90 178 247
		B	68 134 175 244	80 135 202 244	19 80 157 225	80 171 209 241	9 80 135 225	80 138 193 244	58 74 129 212	81 133 189 232	72 133 175 241
	8	R	8 32 67 105 145 185 215 243	10 33 67 105 140 185 215 243	8 33 70 101 109 148 185 243	8 36 70 98 119 182 216 243	8 35 66 108 141 183 216 243	5 17 40 81 118 147 188 243	3 50 64 105 152 174 198 226	30 63 93 123 151 192 212 233	39 58 89 117 144 174 208 242
		G	21 50 82 113 150 183 217 245	22 49 82 113 150 183 212 245	27 78 114 148 166 197 230 248	28 43 83 123 164 205 221 245	9 45 79 112 145 178 212 248	21 57 84 107 129 177 223 235	4 25 52 63 84 151 214 243	5 52 81 102 141 188 212 245	33 52 85 107 147 193 226 250
		B	19 56 81 107 131 171 209 244	12 54 81 107 135 171 209 244	28 67 107 133 162 190 220 244	9 42 61 82 146 165 202 244	25 51 80 110 135 162 193 244	9 47 78 116 146 178 209 240	5 39 55 82 121 145 169 206	10 49 69 105 141 165 225 240	13 78 102 134 173 195 216 244
	12	R	9 35 60 82 97 123 147 171 193 215 230 243	7 35 66 86 112 130 148 182 200 219 232 243	1 19 29 47 70 86 129 154 179 206 216 240	9 15 31 70 86 128 134 144 168 181 215 243	10 36 54 71 91 112 139 162 185 207 230 243	10 25 30 66 91 105 128 147 164 179 199 226	27 35 48 61 90 103 114 128 204 210 224 242	17 38 53 65 88 100 131 155 161 187 220 237	8 39 68 88 108 123 136 158 176 204 225 245
		G	1 24 48 64 82 109 128 150 169 192 217 245	6 26 55 74 89 110 128 147 166 200 226 250	9 39 50 78 94 127 156 168 192 197 230 250	26 39 54 90 117 143 158 170 183 205 240 245	5 23 42 58 81 113 130 153 174 196 226 248	13 26 38 64 83 109 130 153 170 190 209 248	23 40 82 93 111 129 155 161 172 180 236 252	5 17 41 83 91 112 133 145 174 197 214 236	25 51 65 86 117 133 142 156 185 206 229 252
		B	9 27 51 66 82 107 131 154 175 202 220 244	11 27 47 63 80 107 132 147 170 191 225 241	14 36 51 81 116 124 134 145 193 202 217 240	13 34 51 60 77 100 124 137 149 166 190 246	8 19 32 50 66 82 106 134 164 195 216 244	35 48 62 85 117 127 140 172 184 199 220 240	3 30 47 75 88 114 118 166 193 205 217 244	12 24 36 49 85 112 130 145 169 191 202 225	20 38 59 78 102 143 160 187 198 205 216 241
TI2	4	R	30 90 157 222	30 90 157 222	43 79 157 222	37 85 153 222	32 90 164 222	32 95 157 222	33 65 127 183	29 85 153 223	34 104 161 226
		G	58 118 168 232	58 118 168 232	58 110 156 232	66 118 171 232	57 118 171 232	60 117 162 216	50 79 156 209	56 110 154 216	50 105 153 226
		B	35 77 108 162	35 77 108 162	77 108 152 204	1 79 108 182	74 114 162 202	76 108 156 204	73 111 204 233	75 113 164 220	75 114 157 213
	8	R	14 32 67 93 125 154 182 220	16 30 65 99 136 175 213 244	13 43 74 95 118 158 183 238	44 80 102 141 166 214 228 247	16 30 65 99 136 175 213 244	1 13 28 67 110 160 207 244	15 32 111 121 146 168 233 251	30 61 94 122 150 179 213 244	29 55 90 119 157 180 205 238
		G	45 69 85 108 138 168 196 235	47 68 95 118 148 178 207 235	50 67 84 112 158 198 216 232	45 67 100 131 154 168 207 232	25 47 80 111 148 175 207 235	24 46 68 89 123 163 197 239	46 69 106 125 133 171 187 249	25 50 85 120 150 178 210 232	46 79 112 143 163 177 210 241
		B	11 41 79 108 148 182 205 235	1 36 77 108 151 180 212 247	4 11 71 93 108 173 196 245	48 67 73 93 112 148 194 240	1 31 54 79 108 162 204 240	38 76 99 123 147 174 200 226	12 78 103 130 153 169 215 245	1 36 75 108 133 163 203 240	9 52 79 111 154 185 217 254
	12	R	1 13 30 64 90 115 138 159 183 207 232 253	13 35 63 94 113 128 148 169 186 207 228 247	17 38 47 55 72 98 127 158 176 217 233 251	17 37 50 65 83 90 111 119 171 198 226 244	16 29 48 68 88 110 132 153 175 196 222 247	29 42 81 99 128 142 151 174 181 190 228 249	4 21 55 88 104 128 157 170 203 214 242 251	1 16 29 54 89 104 137 165 181 200 208 251	1 17 36 88 103 123 145 161 183 201 213 235
		G	7 25 44 60 80 99 120 143 163 187 211 232	3 24 50 73 92 111 130 149 172 193 216 237	26 35 46 70 88 137 145 167 197 211 221 241	9 15 25 46 52 89 104 119 144 189 205 241	1 25 46 67 87 109 128 149 168 187 211 239	4 16 50 71 95 108 128 146 163 184 204 226	22 43 62 69 77 102 125 134 168 183 187 215	1 25 38 73 94 116 137 152 173 193 233 248	24 41 62 86 99 117 147 166 197 214 220 245
		B	6 23 44 77 93 108 125 151 175 202 226 254	1 21 53 79 97 114 133 156 176 212 236 254	19 39 65 76 99 108 124 139 176 207 226 240	11 27 38 49 64 99 124 139 159 201 227 254	1 21 45 77 93 114 150 175 199 220 240 254	1 21 58 77 86 99 110 123 151 178 207 233	2 20 61 73 91 112 123 151 215 230 248 254	6 24 52 78 103 129 149 172 189 208 223 245	10 38 77 93 121 148 163 174 202 227 229 252
TI3	4	R	48 102 155 214	42 97 153 212	50 97 153 212	42 120 171 212	42 97 153 212	41 97 155 212	53 109 154 225	42 97 155 210	44 104 158 212
		G	65 117 172 219	60 112 167 219	62 120 165 219	72 126 165 213	60 112 167 219	60 112 167 219	81 112 167 225	60 110 167 219	57 111 164 219

(*continued on next page*)

Table A1 (*continued*)

		B	59 120 168 219	57 114 171 219	62 120 157 213	54 107 162 219	57 112 162 218	59 112 167 219	114 143 202 227	57 112 163 219	53 110 172 215
	8	R	31 59 90 116 143 172 201 229	31 58 87 115 143 172 201 228	41 58 87 115 134 166 196 228	34 56 95 125 152 181 203 237	29 58 87 117 149 177 207 237	24 47 84 118 152 178 210 237	3 48 64 79 109 142 171 208	36 66 94 114 149 180 205 237	27 52 106 127 158 190 221 239
		G	37 66 96 122 151 179 208 235	40 66 97 126 155 181 208 236	36 51 86 131 156 172 206 234	63 92 103 128 167 187 209 233	37 66 94 120 149 175 205 234	40 65 94 119 142 172 209 238	49 88 95 114 157 179 209 221	40 84 116 142 170 201 218 234	50 93 112 144 164 193 211 235
		B	47 74 99 125 151 179 207 234	1 51 81 112 142 171 203 233	22 50 76 107 145 169 203 234	1 47 75 107 137 172 206 233	45 72 97 122 149 177 207 233	24 48 78 105 133 167 201 233	55 119 129 150 173 195 210 240	1 54 78 110 139 172 207 241	52 89 107 143 164 198 224 240
	12	R	3 24 43 64 83 99 118 141 163 187 214 237	1 24 42 61 78 97 120 143 168 193 217 242	6 13 27 59 74 85 114 149 168 194 221 237	25 43 91 112 128 157 174 179 200 213 222 233	2 23 42 61 86 107 127 149 169 190 215 237	36 59 76 90 105 116 129 143 162 185 214 235	32 52 73 94 99 115 146 157 188 203 215 222	1 29 55 87 102 119 133 156 181 202 214 235	4 25 72 90 107 124 136 150 173 199 218 233
		G	36 58 77 96 117 135 152 167 185 201 220 241	33 53 71 92 112 130 149 167 185 203 222 241	34 50 59 87 104 112 132 173 185 207 222 241	27 46 67 84 93 112 137 152 185 203 223 242	31 48 68 87 107 126 144 162 181 201 222 241	8 19 38 62 84 104 122 140 163 185 215 237	26 64 74 80 94 124 145 169 188 206 214 222	25 36 55 76 100 108 131 157 167 186 221 241	37 63 87 98 114 136 160 189 199 226 237 246
		B	1 22 46 68 88 109 130 153 174 194 217 239	1 15 40 62 85 107 130 153 175 196 219 240	8 20 38 67 94 119 142 158 171 194 221 239	15 34 51 87 96 111 142 163 180 191 213 243	1 22 48 71 92 114 133 153 173 196 219 240	8 20 43 59 89 115 136 169 178 187 221 228	25 45 81 97 117 121 151 171 186 200 233 238	4 26 44 55 71 101 127 150 174 198 221 247	4 47 63 83 101 132 146 176 194 209 227 241
TI4	4	R	21 98 154 241	20 99 158 241	21 65 166 241	30 65 156 241	20 99 158 241	20 99 163 241	16 82 131 200	20 91 147 241	20 90 142 241
		G	6 32 102 161	6 32 102 161	38 82 116 167	6 32 99 162	6 32 108 217	6 38 101 134	37 81 142 225	6 30 95 169	6 29 99 213
		B	14 81 138 198	16 81 140 198	79 125 170 198	16 101 132 198	16 81 133 198	16 81 136 198	8 97 171 214	16 68 145 198	10 113 150 199
	8	R	20 54 82 109 139 170 203 241	20 59 89 119 149 174 206 241	34 52 83 111 130 149 194 241	2 21 58 91 132 172 202 241	2 20 65 104 138 170 206 241	3 21 38 63 108 134 167 241	20 57 88 104 123 153 202 246	1 20 62 92 112 156 194 242	25 77 98 112 137 161 206 242
		G	6 36 60 84 113 151 187 221	6 32 72 102 131 163 194 221	7 28 74 102 134 163 205 221	5 36 69 97 112 138 179 223	6 32 76 108 138 167 194 221	6 30 62 85 113 147 184 220	11 54 87 102 117 144 195 208	6 31 75 117 147 164 189 225	7 34 81 109 144 188 203 224
		B	16 41 59 79 106 133 166 198	16 67 93 121 146 170 198 216	19 65 86 118 137 170 220 234	21 68 113 131 167 189 201 234	7 16 21 69 102 133 170 203	10 21 59 82 121 140 177 213	11 41 62 80 93 165 187 214	20 60 91 125 162 195 213 230	16 76 95 119 146 166 177 203
	12	R	2 6 21 54 81 104 124 145 166 188 209 241	2 25 54 90 109 126 139 156 180 208 225 241	2 25 47 64 83 123 131 144 176 195 204 241	1 6 21 33 58 72 111 125 152 181 195 251	20 44 64 88 111 135 154 171 191 209 228 241	2 17 39 66 82 96 108 138 163 196 227 241	16 21 48 67 87 104 118 126 130 173 186 208	1 18 57 88 100 111 121 139 164 192 209 240	1 20 42 53 82 98 117 139 178 186 206 238
		G	7 12 32 59 82 102 122 142 163 184 205 224	6 30 53 83 104 130 148 161 176 189 202 224	6 13 24 82 117 121 136 170 195 200 219 243	8 39 59 76 96 119 125 127 152 170 193 224	1 6 29 45 63 85 107 132 166 195 222 243	8 29 37 54 67 83 96 110 135 156 177 217	4 49 56 70 90 102 128 143 173 175 228 238	4 29 52 76 88 127 149 162 175 198 207 243	4 31 79 114 124 135 151 164 178 197 212 225
		B	7 41 61 81 102 121 138 151 170 189 216 234	8 32 47 66 92 107 123 140 158 179 203 234	1 10 42 80 103 133 151 156 169 198 230 234	8 49 70 77 83 103 124 146 170 189 228 234	1 14 39 65 81 100 121 146 167 198 216 234	1 57 66 76 91 107 137 151 167 183 212 234	58 86 92 120 124 133 147 153 167 175 177 188	14 22 34 56 67 81 97 114 136 167 189 213	8 39 53 73 106 115 135 152 171 192 209 234
TI5	4	R	41 82 126 171	37 78 123 171	37 92 127 183	37 80 127 171	37 78 123 171	36 82 126 171	31 80 115 164	37 78 123 164	40 82 134 183
		G	55 129 177 227	9 55 133 225	57 99 163 225	7 62 143 199	9 55 133 225	9 55 133 209	65 111 180 218	7 56 141 208	20 65 142 209

(*continued on next page*)

Table A1 (*continued*)

		B	9 131 167 225	22 108 167 230	5 105 177 227	34 105 161 232	34 108 167 230	10 108 167 230	36 132 167 235	34 110 158 219	15 97 159 221
	8	R	28 51 78 102 123 146 164 197	26 51 78 102 123 148 171 195	37 60 83 102 122 153 181 200	1 26 51 78 104 133 155 193	25 58 82 111 140 168 194 230	38 57 70 90 104 142 162 180	2 46 62 80 121 162 187 207	29 49 70 90 109 150 166 188	37 62 94 112 147 161 180 205
		G	20 49 79 113 140 171 203 232	3 49 82 112 143 171 201 232	24 53 88 116 154 180 189 229	49 68 96 112 158 174 211 232	9 49 78 108 140 171 201 232	22 61 90 119 148 172 205 232	4 50 85 110 152 182 222 235	9 52 103 137 149 171 196 221	9 45 83 114 137 158 190 216
		B	10 80 108 137 160 186 216 242	12 81 108 137 159 186 216 242	3 10 91 119 165 186 205 241	34 46 96 126 154 186 206 241	22 81 108 137 159 186 216 243	14 44 67 99 133 169 207 241	2 78 90 118 177 185 204 210	5 69 103 145 160 188 206 244	15 81 95 131 157 200 220 243
	12	R	1 30 51 69 90 119 143 159 176 191 207 230	1 25 41 62 78 94 111 127 146 165 183 204	25 47 62 97 109 121 148 166 179 189 221 230	25 36 45 49 63 97 122 143 158 173 183 230	25 41 58 70 84 102 127 153 171 189 206 230	22 35 58 80 92 111 121 143 160 183 212 230	6 24 44 56 85 98 115 155 184 192 218 229	31 55 69 83 110 130 144 162 179 197 214 228	25 36 49 66 78 99 135 161 175 190 218 229
		G	7 30 48 73 95 112 131 149 170 190 208 230	7 29 46 68 88 112 136 161 186 209 232 254	46 56 68 82 110 119 136 168 180 205 229 239	20 58 73 98 108 130 151 176 186 202 224 241	7 46 62 82 104 126 150 171 190 209 225 240	45 57 77 97 116 130 144 162 182 201 222 238	24 28 53 61 66 91 108 148 181 208 220 232	25 44 57 83 112 129 141 172 185 203 218 239	24 44 54 100 113 129 150 172 192 204 214 232
		B	3 38 74 92 111 126 145 158 178 201 223 243	5 38 66 80 96 116 137 156 179 201 223 244	38 65 88 95 106 126 145 153 174 201 212 244	38 50 89 105 113 126 133 157 189 199 221 230	3 22 46 66 85 108 137 156 179 201 221 244	15 42 83 95 111 130 145 156 178 197 216 237	6 49 54 62 79 82 110 153 168 194 213 244	14 72 79 91 108 122 143 159 174 187 211 236	9 34 69 80 95 104 126 143 183 206 232 250
TI6	4	R	42 106 148 219	42 106 148 227	29 116 152 223	42 107 158 227	42 116 162 227	42 106 154 227	41 83 125 195	45 106 152 219	45 103 146 231
		G	50 111 167 208	62 111 170 208	50 122 177 206	59 116 170 225	62 110 156 208	59 111 167 208	127 153 185 211	64 110 168 211	51 120 177 211
		B	110 147 188 230	110 147 188 230	113 154 188 230	138 167 199 226	107 149 188 230	115 146 190 230	108 126 174 217	110 150 190 230	106 151 188 226
	8	R	17 43 79 107 134 158 197 227	17 45 75 106 138 170 202 233	19 33 82 105 157 193 213 247	19 69 86 107 139 177 219 233	17 48 80 116 148 185 219 247	38 60 101 137 162 195 220 252	39 97 116 134 145 203 232 243	17 48 86 109 143 165 189 228	15 44 80 134 148 183 218 240
		G	24 59 86 114 142 167 200 238	24 52 104 131 160 188 216 251	32 54 105 131 145 180 223 251	24 51 97 125 187 208 238 251	24 50 82 113 146 177 208 251	24 62 96 127 147 170 200 230	47 65 112 146 173 176 202 225	24 51 96 117 141 170 197 228	50 100 121 137 153 176 211 249
		B	44 69 102 127 147 177 203 230	44 73 108 140 172 199 221 246	44 51 103 143 161 176 209 230	74 112 124 147 189 216 234 246	44 73 104 131 159 188 215 238	48 87 106 131 160 196 236 252	40 67 84 113 148 185 213 225	51 76 116 143 164 194 229 252	54 104 124 138 150 172 200 230
	12	R	25 31 54 69 87 112 126 140 157 182 223 247	4 17 45 65 85 106 129 149 172 202 227 247	13 23 73 91 117 129 143 167 187 197 238 252	3 29 61 93 112 138 159 178 193 209 243 247	4 30 52 76 102 121 139 162 187 212 229 247	22 41 55 70 87 106 126 149 172 199 223 252	23 33 45 65 78 99 133 143 150 161 188 232	1 20 42 59 73 106 120 147 161 200 229 247	7 23 42 52 70 97 128 151 169 190 202 234
		G	24 40 56 83 93 111 125 147 171 206 223 251	24 39 62 75 94 113 134 155 177 200 223 242	24 52 62 91 105 121 161 185 215 219 238 251	45 63 99 120 140 157 184 196 206 225 244 251	24 50 62 86 108 131 162 180 198 211 230 251	24 39 59 77 92 111 130 150 170 198 220 238	40 64 66 83 106 127 134 173 185 208 237 252	24 51 80 99 119 126 147 161 182 195 216 241	41 49 69 106 117 129 144 160 173 213 237 251
		B	54 66 81 91 106 122 135 147 167 192 208 238	48 73 91 104 122 143 161 181 199 215 238 252	44 73 83 96 126 154 159 180 217 226 238 254	49 71 87 98 110 147 152 173 183 201 230 246	54 71 85 107 124 143 156 173 190 209 230 246	44 59 79 93 109 125 140 165 196 217 246 254	75 78 94 104 119 123 140 162 187 224 239 245	44 56 71 81 102 129 151 172 184 211 219 236	44 56 96 110 127 141 157 170 179 195 219 239
TI7	4	R	16 64 120 190	54 107 158 205	56 163 191 239	10 64 118 174	54 102 155 205	55 128 195 239	7 67 93 166	55 112 162 205	57 103 159 205
		G	22 81 135 186	22 81 135 186	81 123 185 219	23 75 134 185	22 81 126 185	22 84 132 186	90 125 153 192	22 83 130 187	21 80 130 179

(*continued on next page*)

Table A1 (*continued*)

		B	64 118 171 228	61 113 171 228	64 110 171 229	6 68 145 213	62 118 177 228	62 118 176 229	54 135 170 234	64 109 172 228	63 116 174 227
	8	R	18 51 79 107 135 166 202 239	16 59 94 124 152 179 205 239	28 54 87 108 136 166 200 239	13 26 64 96 110 138 209 239	13 56 96 129 165 205 236 250	31 52 93 118 145 162 205 239	16 57 124 154 164 174 213 237	16 53 82 100 164 197 239 250	12 58 105 133 155 181 202 240
		G	18 43 70 100 128 155 185 219	20 49 77 103 131 159 186 219	14 29 84 108 135 177 195 221	11 39 71 137 158 181 198 226	22 75 105 135 165 194 221 246	12 40 70 100 129 160 186 219	26 40 48 80 103 123 203 218	21 39 69 94 113 153 184 218	17 41 79 107 128 155 176 214
		B	11 48 73 102 135 166 200 239	11 59 93 118 150 184 214 240	59 99 118 133 158 194 212 239	10 38 61 84 114 187 220 237	9 60 92 121 153 184 213 240	8 21 60 90 110 159 180 222	19 36 73 97 135 196 200 226	9 62 94 113 135 154 187 233	10 51 70 98 122 143 191 233
	12	R	17 47 65 82 100 119 135 154 173 195 212 239	6 17 33 51 72 92 113 133 155 179 205 239	14 32 42 57 87 103 142 160 182 199 214 239	14 22 45 78 99 126 146 167 174 210 244 250	9 37 62 88 107 127 149 172 193 213 236 250	4 29 41 67 81 96 122 138 152 189 239 250	5 16 56 71 78 123 147 163 174 202 232 247	11 37 55 80 99 138 152 165 199 208 226 252	11 34 54 77 117 134 157 166 182 195 214 238
		G	10 30 51 71 90 112 136 155 177 198 225 246	11 28 48 66 84 103 122 140 159 179 199 222	1 11 24 54 83 98 138 153 167 190 223 246	22 37 60 80 99 141 149 185 203 218 234 246	2 23 46 75 98 122 146 165 185 203 225 246	1 13 24 38 61 77 102 127 171 196 225 246	10 49 51 54 63 67 161 176 214 226 236 243	12 22 32 69 86 111 136 147 169 190 213 233	10 29 50 73 96 118 129 159 196 215 226 248
		B	10 27 46 64 82 103 121 146 170 191 215 241	6 20 57 81 102 121 141 160 181 202 222 242	5 24 49 82 98 114 125 161 178 185 217 239	8 22 48 66 102 121 140 176 199 209 236 244	1 17 44 66 93 118 138 160 183 202 222 242	5 15 39 64 85 114 139 164 181 203 221 241	8 36 85 101 113 128 145 151 174 177 212 247	4 13 38 51 82 101 113 129 156 185 217 238	3 18 30 57 88 112 123 136 180 202 218 237
TI8	4	R	43 98 126 177	27 61 96 146	23 95 130 174	27 57 108 177	27 61 96 146	27 57 96 149	27 61 115 149	24 61 86 147	25 61 137 169
		G	46 98 159 219	10 52 115 229	15 53 94 152	19 52 118 156	10 52 99 140	10 52 99 153	10 52 115 156	15 51 98 140	9 50 98 143
		B	70 113 165 192	67 109 171 216	38 125 153 212	39 115 147 189	67 109 171 216	46 113 171 216	68 114 170 216	39 109 170 219	70 110 169 217
	8	R	15 63 88 116 146 174 189 221	24 61 88 115 138 162 185 225	9 29 57 117 146 165 220 242	12 38 64 95 108 130 187 225	10 27 61 88 115 146 180 226	10 27 45 88 115 146 178 223	13 29 45 58 144 158 182 195	13 29 61 83 111 124 180 225	13 29 61 93 147 183 202 225
		G	26 52 94 118 152 181 200 226	15 52 71 104 140 160 200 229	30 52 69 102 130 180 196 229	10 52 104 118 128 142 173 200	11 52 99 140 160 200 227 247	23 53 71 95 116 154 183 229	13 25 52 54 99 151 175 228	6 50 77 109 136 165 197 227	24 53 75 112 138 159 192 234
		B	7 49 89 110 139 168 190 220	1 21 39 69 109 146 180 216	39 69 125 146 154 168 187 216	23 67 90 107 137 174 198 225	7 39 68 109 147 181 216 253	7 39 56 109 131 149 177 209	24 38 51 96 112 150 177 230	18 37 67 109 127 152 179 209	7 17 37 73 117 146 209 228
	12	R	26 49 67 85 108 125 145 163 180 202 223 240	9 27 45 61 95 111 127 143 165 186 220 240	4 34 63 85 103 111 115 147 167 184 214 240	3 11 41 88 99 118 131 145 176 194 226 241	10 28 47 60 88 115 135 153 170 189 220 240	7 21 28 58 88 113 127 143 165 184 223 254	9 26 36 59 69 80 108 134 157 193 234 254	29 41 67 85 103 115 143 157 170 196 207 223	9 31 45 56 74 85 104 134 153 168 205 229
		G	6 24 36 51 76 97 112 128 156 180 209 227	10 28 52 71 99 119 140 157 178 196 210 229	10 26 36 52 66 90 121 134 152 194 220 226	15 24 61 73 103 114 132 141 165 177 211 229	10 32 50 61 77 98 118 140 156 183 206 229	6 21 39 52 74 95 118 138 158 182 201 216	48 52 61 83 109 132 140 145 192 221 222 236	10 25 51 71 117 139 165 181 195 213 241 251	16 28 48 77 98 123 140 164 188 208 224 253
		B	21 39 61 79 97 114 132 153 176 198 221 243	3 22 39 56 71 89 109 129 150 171 195 221	1 21 44 69 90 107 135 161 187 227 239 253	1 6 27 72 88 111 136 149 177 208 221 253	7 22 39 69 88 109 129 150 171 195 216 233	20 40 70 89 100 115 123 136 147 164 184 204	3 53 65 79 105 131 143 155 170 184 195 207	7 41 69 85 118 141 172 192 201 212 230 243	3 44 62 90 115 124 144 161 167 176 212 237
TI9	4	R	35 90 147 199	34 83 150 199	37 108 152 199	61 111 156 194	34 83 150 199	34 83 151 199	38 79 122 186	35 83 151 199	39 87 151 199
		G	21 68 119 187	21 69 118 189	14 72 143 195	16 65 115 186	16 69 118 189	14 67 121 189	10 39 50 176	16 69 115 168	21 69 122 186

(*continued on next page*)

Table A1 (*continued*)

		B	5 80 126 172	5 80 130 173	64 116 160 200	5 75 121 171	5 80 128 171	5 75 124 171	100 121 180 188	5 66 112 173	5 91 133 179
	8	R	31 60 85 111 143 173 200 229	1 34 69 104 137 165 195 228	35 57 91 120 142 175 193 229	16 49 80 108 141 182 201 228	29 56 83 111 143 171 199 228	6 34 66 100 129 159 195 226	34 78 112 127 140 176 192 222	1 26 61 101 127 155 189 222	2 32 69 94 116 149 186 221
		G	16 43 71 108 131 159 192 217	16 42 69 109 136 164 192 221	21 39 72 111 167 175 204 221	14 55 71 113 129 168 200 221	11 42 73 110 136 164 194 221	16 48 68 110 132 158 192 222	21 27 54 71 115 176 215 246	20 41 70 105 131 156 177 208	21 36 79 118 150 176 193 219
		B	5 26 56 81 105 133 163 200	1 48 74 100 130 155 175 200	47 74 92 102 118 146 203 230	1 32 55 97 133 158 203 214	1 49 78 103 130 155 175 200	1 16 58 83 114 137 168 200	5 40 83 92 131 170 188 201	6 41 79 104 129 153 168 203	5 45 68 108 143 158 185 199
	12	R	1 25 55 73 96 113 137 156 178 203 229 254	1 23 38 59 77 96 114 135 155 177 199 229	1 25 62 81 104 120 142 154 176 192 201 229	21 57 72 89 112 123 154 173 184 199 211 231	1 29 50 71 95 116 140 160 180 199 221 237	24 42 62 86 107 121 130 145 160 174 192 218	23 52 66 99 114 129 156 175 212 213 223 231	1 28 71 89 104 134 146 154 167 188 207 229	6 19 32 51 80 107 120 131 146 176 200 231
		G	16 38 68 87 102 119 139 162 180 195 210 223	3 21 41 55 77 100 118 137 157 178 201 222	21 36 45 69 75 109 114 135 169 188 202 222	19 28 39 74 85 122 132 154 175 194 208 221	14 42 65 89 112 138 159 181 201 221 242 254	1 23 37 57 70 101 117 149 175 201 221 254	3 14 59 71 91 98 116 139 159 193 212 222	10 43 69 89 100 120 129 138 160 178 199 216	19 35 53 64 85 114 127 141 167 185 200 219
		B	3 22 44 60 78 96 114 132 151 171 186 200	1 26 50 74 93 112 129 149 171 190 202 230	3 55 62 87 107 122 142 171 179 193 214 230	10 30 41 57 70 83 101 117 134 186 199 230	1 26 48 68 93 114 135 159 180 200 217 230	1 43 59 70 81 103 122 142 169 200 218 230	6 53 78 100 110 112 126 154 189 195 197 227	1 16 43 52 70 94 113 130 157 178 215 229	8 43 62 74 83 98 125 150 167 179 204 215
TI10	4	R	20 87 149 219	22 82 166 252	27 102 160 199	21 76 188 252	22 82 166 252	21 87 185 252	18 84 113 185	23 79 160 236	18 87 158 235
		G	90 140 187 251	71 159 231 251	94 140 186 251	89 159 198 251	89 159 231 251	66 99 159 251	52 103 181 211	64 147 207 251	96 151 229 251
		B	6 91 142 205	8 91 161 247	59 140 186 247	8 92 133 168	8 91 161 247	8 90 164 247	89 129 163 184	8 87 136 199	88 152 212 247
	8	R	20 56 86 111 146 173 199 236	18 49 80 107 160 195 236 252	43 81 115 147 185 216 235 252	51 87 112 145 172 190 226 252	16 49 80 107 158 195 236 252	19 91 108 124 154 190 234 253	21 32 77 113 139 160 202 226	24 75 96 138 171 208 239 252	15 63 80 120 173 213 235 252
		G	31 66 106 134 155 181 206 234	30 59 93 132 159 195 231 251	12 26 73 104 140 154 211 251	47 99 122 141 157 190 230 251	30 59 93 132 159 191 231 251	30 63 93 140 162 181 206 232	42 60 89 107 149 166 198 236	69 80 111 139 157 215 232 251	31 66 84 126 141 163 186 212
		B	6 27 75 110 146 175 223 247	8 30 59 91 135 170 225 247	6 59 106 133 162 182 226 247	15 55 84 107 163 184 196 247	6 51 90 120 147 182 225 247	1 59 80 101 130 151 178 216	22 63 93 108 164 195 213 224	4 36 87 107 139 163 186 226	5 31 81 104 128 159 200 227
	12	R	16 32 49 66 84 103 124 146 172 208 237 252	1 23 49 69 88 112 140 163 184 210 237 252	14 50 82 112 121 132 147 166 183 221 237 252	15 41 52 66 96 123 147 166 184 201 221 252	1 16 42 70 93 116 143 164 185 210 237 252	30 42 67 76 106 123 132 153 188 213 237 252	5 49 68 84 96 143 156 177 183 188 216 234	23 34 53 62 75 114 139 154 167 206 233 252	33 44 70 87 109 118 131 161 181 205 230 252
		G	30 51 66 93 122 142 163 177 198 218 234 251	7 12 30 54 66 89 116 140 159 181 206 232	19 44 59 66 77 96 113 155 180 219 236 251	3 27 77 109 116 123 147 180 211 217 224 251	7 31 54 71 89 116 140 168 189 214 235 251	27 60 88 98 112 123 138 150 168 180 209 232	7 25 55 79 106 112 133 144 160 188 230 240	28 52 71 88 105 121 139 159 171 205 223 235	28 55 84 112 126 139 150 172 186 202 219 233
		B	8 30 59 75 95 110 129 146 161 185 213 227	5 26 51 70 90 105 121 142 161 182 204 226	8 33 44 59 76 91 133 144 176 207 226 247	1 31 55 75 85 100 126 154 160 172 206 247	1 26 51 66 85 105 126 147 168 199 226 247	1 16 34 51 70 91 109 126 149 170 206 226	10 47 73 96 123 140 150 167 182 219 232 245	8 27 59 81 99 108 129 141 178 199 219 237	4 34 40 56 93 117 152 174 198 228 244 247

Table A2
Mean gray level for each color component of the thresholded images obtained using the optimal threshold values.

Test Images	d		OEO	EO	HHO	SFO	WOA	GWO	PSO	DE	L-SHADE
TI1	4	R	19 57 109 167 249	19 69 142 200 249	20 76 148 189 249	21 78 142 211 249	19 69 142 200 249	19 57 109 167 249	20 80 152 189 223	19 70 142 194 249	20 63 123 185 249
		G	32 69 109 173 254	30 70 109 165 254	29 71 110 157 254	29 70 112 165 254	31 77 134 207 254	32 69 109 173 254	30 73 118 174 242	30 80 148 209 254	30 70 114 199 255
		B	42 98 150 197 252	46 100 156 220 252	11 48 101 178 244	46 101 186 223 251	5 47 100 158 244	42 98 150 197 252	39 66 99 152 236	46 100 152 206 248	44 98 149 197 251
	8	R	5 21 49 85 124 162 197 226 249	6 21 50 85 122 159 197 226 249	5 21 51 85 105 128 164 200 249	5 21 53 84 109 145 195 227 249	5 21 51 86 124 159 195 227 249	3 13 24 60 98 132 164 203 249	2 21 57 83 127 163 184 208 243	19 46 78 108 137 168 201 221 246	20 49 73 103 130 158 187 220 249
		G	14 37 68 97 128 162 197 230 254	15 37 68 97 128 162 195 226 254	18 62 94 128 157 177 211 239 255	19 36 67 100 139 177 213 232 254	5 31 67 94 126 158 191 227 255	14 42 70 96 117 146 193 229 251	3 18 40 59 72 107 167 227 254	3 35 68 92 117 157 199 226 254	22 43 70 96 122 162 207 237 255
		B	11 40 68 96 115 147 186 225 252	6 39 66 96 116 150 186 225 252	19 46 94 116 146 174 203 231 252	5 32 51 71 101 155 180 220 252	16 40 64 97 118 147 175 213 252	5 35 61 98 126 159 191 223 251	3 30 47 67 99 130 156 184 232	5 36 59 94 115 152 185 233 251	7 47 95 111 150 183 205 229 252
	12	R	5 21 48 71 90 110 135 159 181 202 222 236 249	4 21 51 76 99 121 139 163 190 208 225 238 249	1 13 23 38 59 78 106 141 166 190 211 226 248	5 13 22 50 78 106 131 139 156 174 194 226 249	6 21 45 63 81 102 126 150 172 195 216 236 249	6 20 27 48 78 98 117 138 156 171 188 209 243	19 30 42 55 75 97 109 121 155 207 216 232 249	11 24 46 59 77 94 115 143 158 172 199 228 247	5 21 54 78 98 116 130 147 167 188 212 234 249
		G	1 16 37 59 72 95 118 138 159 178 203 230 254	4 19 43 67 81 99 119 137 156 177 212 237 255	5 28 45 67 86 108 139 162 177 195 211 240 255	18 33 48 71 102 128 150 164 176 193 220 243 254	3 17 34 52 70 96 121 140 162 183 209 236 255	8 21 33 55 72 96 119 140 161 178 199 225 255	16 33 67 88 102 120 140 158 166 176 199 244 255	3 13 31 67 87 101 122 139 157 183 205 224 251	17 39 60 74 100 125 138 149 167 194 217 240 255
		B	5 21 40 59 74 97 115 142 163 187 211 231 252	6 21 39 55 71 96 115 139 157 180 205 233 251	8 29 44 65 98 120 129 140 162 198 209 228 251	7 27 43 56 68 93 108 130 143 157 177 211 252	5 15 27 42 58 74 96 115 147 177 205 229 252	25 42 55 73 99 122 133 153 178 191 209 230 251	2 21 39 60 83 99 116 132 178 199 211 229 252	6 20 32 43 65 98 119 137 156 179 197 213 244	12 32 48 68 95 112 151 172 193 202 211 228 251
TI2	4	R	20 62 120 183 236	20 62 120 183 236	21 62 114 183 236	21 62 116 181 236	20 63 122 187 236	20 63 122 187 236	20 51 95 153 201	20 59 116 181 237	20 70 129 186 239
		G	36 87 141 185 243	36 87 141 185 243	36 84 131 177 243	38 91 142 187 243	36 87 142 187 243	36 87 142 187 243	35 64 112 175 224	36 83 131 174 230	35 77 127 174 239
		B	26 57 92 126 188	26 57 92 126 188	53 92 125 172 220	1 54 92 127 203	52 93 129 179 218	52 93 129 179 218	52 93 129 216 244	52 93 128 185 233	52 93 128 178 227
	8	R	10 23 51 80 109 139 168 196 234	11 23 50 82 117 155 191 224 252	10 23 59 85 107 137 171 199 248	21 63 91 120 153 187 220 236 253	11 23 50 82 117 155 191 224 252	1 10 22 50 89 133 182 219 252	11 23 73 116 133 157 190 241 255	20 47 78 108 136 164 193 224 252	20 44 73 105 137 169 192 216 248
		G	34 56 78 96 123 152 180 209 245	34 57 82 106 133 162 189 218 245	35 58 76 98 133 174 206 223 243	34 55 84 115 142 161 182 217 243	21 35 63 95 129 161 187 218 245	20 34 57 79 105 141 177 210 248	34 57 88 116 129 150 179 202 254	21 35 67 101 135 163 190 219 243	34 62 95 127 153 170 189 221 249

(continued on next page)

Table A2 (*continued*)

		B	6 32 60 92 125 161 193 217 245	1 27 58 92 125 163 194 224 254	2 9 51 87 100 126 184 212 252	37 58 70 87 101 127 165 210 249	1 24 45 66 92 126 180 217 249	29 58 90 110 132 158 186 211 238	7 54 91 117 137 161 187 226 252	1 27 57 92 121 141 180 216 249	5 40 65 93 127 167 199 228 255
	12	R	1 10 22 49 77 103 126 148 171 194 217 241 255	10 22 50 79 104 121 138 159 178 196 215 236 253	12 23 43 52 64 85 112 142 167 193 224 241 255	12 23 44 58 74 87 101 115 142 185 208 234 252	11 23 40 59 78 99 121 142 164 186 206 232 253	20 36 62 90 113 135 147 163 178 186 203 237 254	3 15 26 72 96 116 142 164 186 208 225 247 255	1 11 23 43 72 97 120 151 173 191 204 221 255	1 12 23 63 96 113 134 153 172 192 207 222 246
		G	5 21 34 52 70 90 109 132 153 174 196 220 243	2 20 35 61 83 101 121 139 160 182 202 225 247	22 32 40 57 80 110 141 156 180 203 216 230 249	7 13 22 34 49 70 97 112 132 163 196 217 249	1 21 34 56 78 98 119 138 159 177 196 222 248	3 14 35 60 84 102 118 137 155 173 192 213 239	19 34 52 66 74 90 113 130 150 176 185 197 230	1 21 33 51 84 105 127 145 162 182 206 240 253	20 33 50 75 93 108 132 157 179 204 217 230 252
		B	3 18 36 60 88 100 117 134 161 187 212 235 255	1 15 42 66 89 105 124 140 165 191 222 243 255	13 32 53 71 90 104 117 131 149 190 216 232 249	6 22 34 45 57 88 111 131 146 177 212 236 255	1 15 37 61 88 102 128 161 186 209 228 246 255	1 15 45 67 84 92 104 117 133 163 191 218 244	1 15 47 67 86 100 118 133 173 222 237 251 255	3 19 42 65 91 116 136 159 180 198 215 231 252	5 30 58 88 105 131 155 169 187 213 228 237 255
TI3	4	R	28 75 130 187 240	25 70 127 185 239	28 74 127 185 239	25 81 148 193 239	25 70 127 185 239	24 69 128 185 239	30 81 133 193 244	25 70 128 184 239	26 74 133 187 239
		G	43 95 145 197 245	40 90 140 195 245	41 96 143 194 245	46 103 146 190 243	40 90 140 195 245	40 90 140 195 245	52 98 140 199 246	40 89 139 195 245	39 88 138 193 245
		B	45 87 145 197 245	43 84 143 198 245	46 88 139 188 243	42 80 134 194 245	43 83 137 194 244	45 84 140 196 245	73 129 175 216 247	43 83 138 195 245	41 81 141 196 244
	8	R	20 45 75 104 130 159 187 217 245	20 45 73 102 130 159 187 216 245	24 50 73 102 125 151 182 214 245	21 45 76 111 140 168 193 223 248	19 44 73 103 134 164 193 225 248	17 36 66 102 136 166 195 226 248	2 28 56 72 94 127 158 190 238	22 51 81 105 133 166 193 224 248	18 40 79 117 144 175 207 231 249
		G	28 52 83 110 137 165 194 224 249	30 54 83 113 141 168 195 225 249	28 44 70 111 144 164 190 223 249	42 79 98 117 148 178 199 223 248	28 52 82 108 135 162 191 222 249	30 53 81 108 131 157 191 227 250	34 70 92 105 136 168 195 216 245	30 64 102 130 156 186 210 227 249	35 74 103 129 154 179 203 225 249
		B	38 62 86 111 138 166 194 223 249	1 40 68 95 127 157 188 221 248	19 40 64 91 126 158 187 222 249	1 38 63 90 122 155 190 222 248	37 60 85 109 136 164 193 222 248	21 39 65 91 119 151 185 220 248	42 85 124 140 162 185 203 228 251	1 42 67 93 124 156 191 228 251	41 72 98 125 154 182 213 233 251
	12	R	2 17 34 54 74 91 109 130 153 176 201 227 248	1 17 33 52 70 88 109 132 157 181 206 232 250	3 11 20 43 67 80 100 133 159 182 209 230 248	17 34 67 102 121 144 166 177 190 207 218 228 247	1 16 33 52 74 97 118 139 160 180 203 228 248	22 48 68 83 98 111 123 137 153 174 200 226 247	20 42 63 84 97 108 132 152 174 196 210 219 242	1 19 42 71 95 111 127 145 169 192 209 226 247	2 18 48 81 99 116 131 144 162 187 209 227 247
		G	28 48 68 87 108 127 144 160 177 194 212 233 251	26 44 63 83 103 122 140 158 177 195 214 233 251	27 43 55 74 96 109 123 152 180 197 215 233 251	23 37 57 76 89 103 125 145 169 195 214 234 251	25 40 59 79 98 117 136 153 172 192 213 233 251	7 18 29 51 74 95 114 132 152 174 201 228 250	22 46 70 78 88 111 135 157 179 198 211 219 245	22 31 46 66 89 105 120 144 162 177 205 233 251	28 51 76 93 107 126 148 175 195 214 232 242 253
		B	1 19 38 58 79 98 120 142 164 185 207 230 250	1 12 34 52 74 96 118 142 165 186 209 232 251	5 17 33 54 81 106 131 151 165 183 209 232 250	12 30 43 71 92 104 126 153 172 186 203 232 252	1 19 39 61 82 102 124 143 164 185 209 232 251	5 17 36 52 75 101 126 153 174 183 206 225 247	22 37 65 89 107 119 136 162 179 194 220 236 250	2 23 37 50 64 86 113 139 163 187 211 237 253	2 38 56 74 92 116 139 162 186 202 219 235 251
TI4	4	R	13 70 124 178 251	12 70 126 181 251	13 52 108 185 251	16 53 105 179 251	12 70 126 181 251	12 70 128 183 251	12 61 105 162 209	12 66 117 174 251	12 66 114 171 251
		G	2 22 78 137 180	2 22 78 137 180	23 66 101 144 184	2 22 76 136 180	2 22 82 153 227	2 23 78 120 164	23 66 118 167 232	2 22 73 139 185	2 21 76 151 224
		B	3 56 93 156 212	3 56 93 158 212	56 91 140 182 212	3 58 111 151 212	3 56 93 151 212	3 56 93 154 212	2 58 111 187 223	3 53 82 162 212	2 59 125 166 213
	8	R	12 45 69 95 124 154 185 211 251	12 48 75 104 134 162 187 213 251	19 45 68 97 121 140 171 203 251	1 13 48 75 111 151 185 210 251	1 12 52 84 121 154 185 213 251	2 13 33 53 85 121 150 185 251	12 47 73 96 114 138 175 210 253	1 12 50 77 102 133 175 203 251	13 59 88 105 125 149 180 213 251

(*continued on next page*)

Table A2 (*continued*)

		G	2 23 53 73 100 135 167 197 230	2 22 60 88 119 148 176 203 230	2 21 60 89 121 149 179 212 230	2 23 58 84 105 127 158 191 231	2 22 62 94 125 153 179 203 230	2 22 53 74 100 133 164 195 229	3 34 72 95 110 132 166 201 220	2 22 61 99 134 156 175 199 232	2 22 65 96 130 164 195 211 232
		B	3 39 51 67 89 116 146 179 212	3 53 77 102 131 156 182 207 224	4 52 74 96 126 150 188 226 239	4 53 81 121 144 177 195 213 239	2 12 20 53 80 112 147 183 215	2 17 50 68 93 129 154 192 222	3 39 52 70 86 106 175 199 223	4 50 71 101 138 175 204 221 234	3 55 84 103 129 155 172 188 215
	12	R	1 5 13 45 68 93 114 135 156 177 196 215 251	1 13 45 73 100 118 133 148 168 191 214 229 251	1 13 40 57 74 102 127 138 160 185 199 212 251	1 5 13 29 49 66 91 118 138 167 188 204 255	12 37 55 77 100 123 145 163 181 198 215 232 251	1 12 33 55 75 89 102 123 150 179 205 231 251	12 19 40 59 78 96 111 122 128 151 180 195 216	1 12 47 73 94 106 116 130 151 178 199 215 251	1 12 36 49 68 90 108 128 158 182 194 213 250
		G	2 11 22 51 71 93 113 133 153 173 192 212 232	2 22 46 70 94 119 140 155 169 182 195 210 232	2 13 20 64 101 120 130 153 181 198 207 228 245	2 24 52 68 87 109 123 127 141 161 180 202 232	1 3 21 39 56 75 97 121 150 178 204 230 245	2 21 34 48 61 76 90 104 124 146 166 189 227	1 29 53 64 81 97 117 136 158 174 188 233 241	1 21 44 66 83 110 139 156 169 185 202 218 245	1 22 64 98 120 130 144 158 171 186 203 218 232
		B	2 39 52 69 89 110 128 144 159 179 201 223 239	2 31 43 56 76 98 114 131 148 167 190 215 239	1 4 40 57 89 113 141 154 162 181 211 232 239	2 45 58 74 80 91 111 133 156 179 205 231 239	1 5 37 53 72 89 108 131 155 180 207 223 239	1 49 62 71 83 98 117 144 158 175 196 220 239	50 69 89 101 122 129 140 150 160 171 176 183 206	3 19 33 49 61 74 88 104 123 148 177 200 222	2 37 48 61 84 110 123 143 160 180 200 218
TI5	4	R	26 61 101 148 193	24 58 97 146 193	24 63 107 154 199	24 59 100 149 193	24 58 97 146 193	24 59 101 148 193	21 56 96 138 190	24 58 97 143 190	25 61 103 158 199
		G	42 95 156 203 246	3 42 97 185 245	42 80 135 196 245	2 44 105 174 239	3 42 97 185 245	3 42 97 175 241	45 89 151 200 244	2 42 102 178 241	3 45 106 178 241
		B	2 88 148 202 251	4 81 135 205 251	1 80 137 207 251	5 80 132 205 252	5 81 135 205 251	3 81 135 205 251	8 88 149 209 252	5 82 133 194 249	4 77 125 196 250
	8	R	20 41 64 90 112 135 155 181 207	19 40 64 90 112 136 160 184 206	24 50 71 93 112 137 167 191 209	1 19 40 64 91 117 144 174 205	19 43 69 96 124 154 182 205 232	24 49 64 80 97 121 152 171 198	1 28 55 71 98 141 175 197 213	21 40 60 80 99 127 158 178 202	24 51 76 103 128 154 171 193 212
		G	3 40 66 96 127 157 188 219 247	2 40 68 97 129 159 187 218 247	4 41 73 102 137 168 185 210 246	40 59 83 104 138 167 193 222 247	3 40 65 94 125 157 187 218 247	3 43 77 105 135 161 189 220 247	2 40 70 98 133 168 203 229 247	3 41 80 121 144 161 184 209 244	3 39 66 99 126 149 175 204 243
		B	3 70 93 122 149 174 203 231 254	3 70 94 122 148 173 203 231 254	1 7 75 104 141 176 197 226 253	5 44 77 110 141 171 197 226 253	4 70 94 122 148 173 203 232 254	3 42 62 82 115 150 191 227 253	1 69 84 103 145 182 196 208 248	1 63 84 123 152 175 198 229 254	4 70 88 112 145 181 211 233 254
	12	R	1 21 41 60 79 103 131 151 168 184 199 213 232	1 19 34 53 70 86 102 119 137 156 175 194 211	19 37 55 78 103 115 134 157 173 184 202 223 232	19 31 41 48 57 78 108 133 151 166 179 199 232	19 34 51 64 77 93 114 140 162 181 198 212 232	18 29 48 69 86 101 116 132 152 172 197 216 232	5 19 35 51 69 92 106 134 170 188 203 221 231	21 44 62 76 96 120 137 153 171 189 205 218 231	19 31 43 58 72 89 114 148 168 183 202 221 231
		G	2 29 40 62 85 104 122 141 161 181 200 220 246	2 27 39 58 79 100 125 150 174 198 221 246 255	39 51 63 76 96 115 128 154 175 193 218 235 248	3 42 67 86 103 120 142 165 182 194 214 234 248	2 39 54 73 94 116 139 162 181 200 218 234 248	39 51 68 88 107 124 138 154 173 192 212 231 248	4 27 41 58 64 79 100 130 166 195 215 227 247	5 39 51 72 98 121 136 158 179 194 211 230 248	4 39 49 80 107 122 141 162 183 199 210 224 247
		B	1 20 67 83 101 119 136 151 169 191 213 235 254	1 22 62 73 88 106 127 147 168 191 213 235 254	11 61 77 92 101 116 136 150 164 189 207 231 254	11 48 74 97 109 120 130 146 174 195 211 226 251	1 10 44 62 76 96 122 147 168 191 212 234 254	4 39 71 89 103 121 138 151 168 189 208 228 253	2 47 53 59 72 81 95 132 161 182 205 231 254	3 66 76 85 99 115 133 151 167 181 201 225 253	2 16 63 75 88 100 115 135 161 196 221 243 255
TI6	4	R	23 88 127 167 234	23 88 127 167 240	15 93 134 169 237	23 89 132 174 240	23 94 139 176 240	23 88 130 171 240	22 73 105 152 211	25 88 129 169 234	25 86 125 166 243

(*continued on next page*)

Table A2 (*continued*)

		G	43 95 130 180 226	51 96 131 183 226	43 101 138 188 224	49 98 134 185 238	51 95 128 170 226	49 95 130 180 226	103 138 164 195 228	52 95 130 181 228	43 100 137 189 228
		B	96 121 161 205 240	96 121 161 205 240	97 124 167 205 240	102 149 180 211 237	94 119 162 205 240	97 125 160 207 240	95 116 138 191 231	96 121 164 207 240	94 119 164 204 237
	8	R	8 32 70 95 121 146 172 207 240	8 33 67 93 122 153 181 213 244	9 27 71 95 131 171 201 226 253	9 58 79 97 123 156 188 226 244	8 35 71 99 132 164 195 231 253	20 53 86 119 150 174 204 233 255	21 82 107 125 140 164 213 238 250	8 35 75 98 126 154 175 200 241	7 32 71 108 141 163 193 228 248
		G	24 49 80 101 127 151 179 215 247	24 44 92 117 142 170 199 230 255	30 46 92 118 138 156 194 234 255	24 43 87 111 141 196 221 244 255	24 43 76 99 128 157 188 224 255	24 51 87 111 136 156 181 213 241	41 58 96 127 156 175 186 212 238	24 43 87 107 128 151 180 210 240	43 89 111 129 144 162 188 226 254
		B	42 65 92 112 135 158 188 215 240	42 69 95 119 152 183 209 231 251	42 49 92 116 151 168 190 219 240	69 97 118 132 161 201 224 240 251	42 69 93 115 141 170 200 225 246	46 82 97 116 141 173 212 243 255	37 64 80 99 124 161 198 219 237	48 71 98 125 152 176 209 238 255	51 93 113 130 144 159 184 213 240
	12	R	12 28 45 64 80 100 119 133 149 168 193 234 253	2 11 33 59 77 96 118 139 160 182 211 236 253	6 19 63 84 105 123 136 155 176 192 209 245 255	2 18 51 82 103 125 149 168 185 200 222 245 253	2 19 43 69 91 112 130 151 173 196 220 237 253	11 33 50 65 80 97 116 138 160 182 208 235 255	11 28 40 59 73 90 116 139 147 156 172 199 243	1 11 32 53 68 92 113 134 154 174 210 237 253	3 15 34 48 64 86 113 140 160 178 195 213 245
		G	24 36 49 77 89 102 118 135 156 183 214 234 255	24 36 53 72 87 104 123 143 164 186 210 232 249	24 44 58 84 99 113 136 170 196 217 228 244 255	40 56 89 110 130 147 167 190 201 215 234 248 255	24 43 57 80 98 120 143 170 188 204 220 239 255	24 36 51 73 86 102 121 139 158 181 208 229 247	36 55 66 78 96 117 131 146 179 194 221 244 255	24 43 75 91 109 123 136 153 170 188 204 227 249	37 46 63 93 112 123 136 151 166 186 224 243 255
		B	51 63 77 87 99 113 128 140 156 177 200 221 246	46 69 86 98 112 130 151 170 190 207 225 245 255	42 69 80 91 108 135 157 168 196 222 232 245 255	46 67 83 93 104 121 150 161 178 192 214 237 251	51 67 81 97 115 131 149 164 181 199 219 237 251	42 56 74 88 101 116 131 150 177 206 229 250 255	70 77 89 99 111 121 130 149 172 203 231 242 250	42 53 67 78 93 113 137 160 178 196 215 227 244	42 53 89 103 117 133 148 163 175 187 206 228 246
TI7	4	R	7 35 90 154 207	21 79 134 179 216	21 108 177 207 246	4 32 90 147 196	21 77 130 177 216	21 89 160 209 246	3 31 80 131 191	21 82 138 181 216	22 79 133 180 216
		G	14 57 106 159 212	14 57 106 159 212	56 101 153 203 230	15 55 102 158 211	14 57 102 154 211	14 58 107 157 212	59 107 140 171 215	14 58 105 157 212	13 57 103 154 208
		B	42 85 141 203 249	41 82 138 203 249	42 83 135 204 249	3 43 95 180 245	41 84 143 206 249	41 84 143 206 249	39 82 152 207 251	42 83 135 204 249	42 84 141 204 249
	8	R	7 33 65 93 122 151 182 214 246	7 34 76 109 139 166 191 215 246	12 39 70 98 123 151 182 212 246	5 20 41 80 103 125 169 217 246	5 31 76 113 147 183 215 242 254	13 41 72 106 133 154 181 215 246	7 33 88 140 159 169 191 220 245	7 32 67 91 133 180 210 244 254	5 31 81 120 145 168 191 214 247
		G	11 37 57 83 114 142 169 203 230	12 41 62 89 117 146 172 204 230	8 24 59 96 122 156 186 209 231	7 32 56 100 148 169 190 212 234	14 55 89 120 150 179 208 230 250	7 33 56 83 115 145 172 204 230	17 35 45 63 91 113 160 211 229	13 34 55 80 104 134 168 202 229	10 35 59 92 118 142 165 196 227
		B	6 37 59 86 117 150 184 222 252	6 41 75 105 133 167 200 229 252	41 77 108 126 145 176 204 227 252	5 32 48 72 97 144 205 230 251	4 41 75 105 136 168 200 228 252	4 17 41 74 99 131 170 203 248	12 31 50 84 114 164 199 214 249	4 42 77 103 124 145 170 213 250	5 38 60 83 109 132 166 215 250
	12	R	7 31 56 74 91 110 128 145 164 184 203 219 246	3 12 25 41 61 82 103 124 145 167 191 215 246	6 23 37 49 72 95 124 151 171 190 207 220 246	6 19 33 60 88 113 137 157 171 190 218 247 254	4 23 48 75 98 118 139 161 182 203 220 242 254	2 17 35 53 74 89 109 131 146 170 205 244 254	2 11 33 64 75 100 136 155 169 187 213 237 252	4 24 45 68 90 119 146 159 181 204 216 230 255	4 23 43 66 96 126 146 162 174 189 204 220 245
		G	6 23 44 61 80 101 124 146 166 188 212 233 250	7 22 42 57 74 93 113 132 150 169 190 211 231	1 7 19 45 67 91 118 146 160 178 207 231 250	14 32 51 69 89 120 146 166 195 211 226 238 250	1 15 40 60 86 110 135 156 175 195 214 233 250	1 8 20 34 51 69 89 115 149 184 211 233 250	6 41 51 53 59 65 107 169 196 220 231 239 247	7 18 29 54 77 98 124 142 158 179 202 223 239	6 22 43 61 84 107 124 145 176 206 221 233 252
		B	5 24 38 54 73 92 112 133 158 181 204 230 252	3 16 41 69 91 111 131 151 171 193 213 233 252	2 20 38 63 90 106 120 142 170 182 203 229 252	4 18 38 56 82 111 130 157 189 205 224 241 253	1 11 36 53 79 105 128 149 172 193 213 233 252	2 11 33 49 75 98 126 151 173 193 213 232 252	4 31 54 93 107 121 137 148 162 176 196 233 254	2 9 32 44 65 91 107 121 142 171 203 229 251	2 13 27 43 72 99 118 130 156 192 211 229 251

(*continued on next page*)

Table A2 (*continued*)

TI8	4	R	5 69 112 160 203	3 43 78 120 200	3 57 113 159 202	3 42 82 152 203	3 43 78 120 200	3 42 77 121 201	3 43 86 132 201	3 42 75 115 201	3 42 95 157 202
		G	17 75 137 180 230	3 37 78 174 238	3 39 74 128 180	4 40 78 142 180	3 37 75 122 177	3 37 75 132 180	3 37 78 141 180	3 38 75 121 177	2 36 75 123 178
		B	42 97 137 176 209	41 96 137 185 230	32 101 138 169 228	32 96 132 161 207	41 96 137 185 230	34 95 138 185 230	41 97 138 185 230	32 93 137 185 232	42 96 137 184 231
	8	R	3 36 76 103 131 164 184 203 230	3 42 75 102 127 152 177 203 233	2 17 43 86 131 157 200 227 247	2 24 50 79 102 119 172 203 233	2 17 43 75 102 130 169 202 234	2 17 37 67 102 130 167 202 232	2 20 37 52 97 152 174 191 207	2 20 44 73 98 118 163 202 233	2 20 44 77 119 172 196 209 233
		G	5 42 74 105 139 170 189 209 236	3 39 64 84 124 152 178 209 238	6 43 63 82 117 166 187 206 238	3 37 76 111 124 136 163 184 212	3 38 75 122 152 178 209 235 251	5 41 64 82 105 140 172 194 238	3 20 42 54 75 130 167 188 238	2 35 67 88 125 155 179 206 237	5 42 66 88 127 151 176 203 242
		B	4 35 79 100 127 151 177 201 233	1 17 33 55 96 130 159 193 230	32 55 103 136 150 161 176 198 230	18 41 83 100 125 151 184 208 235	4 32 54 96 130 160 193 230 255	4 32 49 95 122 140 160 189 225	19 33 46 86 103 132 161 192 239	15 32 53 96 120 139 163 191 225	4 15 32 56 99 132 163 218 237
	12	R	3 38 57 76 97 117 135 156 174 195 209 230 246	2 17 37 53 78 104 119 135 156 179 202 227 246	1 14 47 75 94 108 113 131 159 178 201 222 246	1 6 24 65 94 109 125 138 165 188 205 232 246	2 18 38 53 75 102 125 145 163 182 203 227 246	2 13 25 43 74 101 120 135 156 177 202 231 255	2 16 32 47 65 75 94 121 147 184 205 240 255	4 36 53 76 94 109 129 151 165 189 202 213 232	2 18 38 51 67 79 95 119 145 162 196 212 237
		G	2 16 31 44 67 85 105 122 145 171 190 216 237	3 20 42 64 83 109 131 150 170 186 202 217 238	3 19 32 44 62 78 103 128 145 175 203 223 236	3 20 53 67 84 109 125 137 156 172 188 218 238	3 22 43 59 69 85 108 131 150 172 192 214 238	2 14 32 45 66 83 106 130 150 172 190 207 227	18 50 59 73 92 122 136 143 173 201 222 228 243	3 19 41 64 86 130 156 174 188 202 222 245 253	3 22 41 67 85 110 132 155 176 196 215 234 255
		B	17 33 51 73 90 105 124 142 162 186 207 231 248	2 18 33 49 64 83 100 121 139 159 181 205 233	1 17 33 57 83 100 124 146 171 200 233 244 255	1 4 23 44 83 100 126 142 160 189 214 233 255	4 18 33 55 82 100 121 139 159 181 203 225 240	16 33 56 83 96 107 120 130 142 155 173 193 221	2 36 59 75 95 120 137 149 162 177 189 201 224	4 33 56 81 102 131 153 181 197 206 221 236 248	2 33 54 82 102 120 134 152 164 172 189 224 243
TI9	4	R	19 66 123 171 221	18 60 123 173 221	19 84 131 174 221	26 94 133 174 219	18 60 123 173 221	18 60 123 174 221	19 60 106 150 215	19 61 123 174 221	20 66 124 174 221
		G	5 44 99 163 208	5 45 99 164 209	4 46 120 173 213	4 43 96 161 207	4 45 99 164 209	4 44 100 164 209	3 34 45 145 201	4 45 97 149 197	5 45 102 163 207
		B	2 60 100 147 190	2 60 102 150 191	52 87 137 178 207	2 58 95 144 189	2 60 101 148 189	2 58 96 146 189	69 110 147 185 200	2 53 87 139 191	2 66 110 153 194
	8	R	18 45 74 101 128 158 186 214 239	1 18 52 91 123 150 180 212 238	19 46 77 108 131 158 184 211 239	13 28 66 97 126 160 192 214 238	17 42 71 100 128 157 185 214 238	4 18 50 87 117 143 176 211 237	18 57 99 120 134 157 184 208 235	1 16 43 86 116 140 172 206 235	1 18 50 84 107 133 167 205 234
		G	4 35 57 93 122 147 177 204 227	4 35 55 93 125 152 179 205 230	5 34 55 95 147 172 190 212 230	4 39 63 96 122 152 185 210 230	4 35 57 95 126 152 180 206 230	4 37 58 94 123 147 177 205 230	5 26 39 63 97 155 194 225 250	5 34 55 91 120 146 168 192 221	5 33 57 102 138 165 185 205 229
		B	2 23 47 69 92 119 148 180 207	1 41 62 87 114 143 165 187 207	41 62 83 97 110 132 169 208 234	1 29 47 75 114 146 178 208 219	1 42 65 90 116 143 165 187 207	1 13 48 71 97 125 151 183 207	2 35 64 88 110 149 180 194 208	2 36 62 91 116 141 160 184 209	2 39 58 86 125 151 171 192 207

(*continued on next page*)

Table A2 (*continued*)

	12	R	1 16 39 65 87 106 126 146 167 191 216 238 255	1 16 30 49 69 88 106 125 145 166 188 214 239	1 16 42 73 95 113 131 148 165 184 197 215 239	15 37 65 82 103 118 138 164 179 192 206 221 240	1 17 39 61 85 107 129 150 170 190 211 229 244	16 32 52 76 99 115 126 138 153 167 183 206 233	16 36 59 87 108 122 142 166 194 213 218 227 240	1 17 49 82 98 121 140 150 161 178 198 218 239	4 14 25 42 67 97 114 126 139 161 188 215 240
		G	4 34 53 79 95 111 131 152 172 188 203 216 231	1 9 34 49 66 91 110 129 148 169 190 211 230	5 33 41 57 73 95 112 127 155 179 195 211 230	4 27 34 56 80 106 128 145 166 185 201 214 230	4 35 54 79 102 128 150 171 191 210 229 245 255	1 8 33 47 64 89 110 137 164 188 210 229 255	1 7 41 65 83 95 108 130 150 177 202 217 230	3 35 56 81 95 111 125 134 151 170 189 207 227	4 33 44 59 76 101 122 135 156 177 193 209 229
		B	1 19 39 53 69 87 105 123 142 160 179 193 207	1 23 43 63 84 103 121 139 159 181 196 208 234	1 46 59 75 97 115 132 155 175 186 203 218 234	4 27 37 50 64 77 92 109 126 157 192 207 234	1 23 42 59 80 103 124 147 169 189 207 221 234	1 38 52 65 76 92 113 132 154 183 207 222 234	2 45 66 89 105 111 119 140 171 192 196 205 231	1 13 38 48 62 82 104 122 144 167 193 219 233	3 38 54 68 79 90 111 138 158 173 190 208 220
TI10	4	R	6 61 124 189 237	7 58 128 218 254	7 75 131 181 229	7 54 134 225 254	7 58 128 218 254	7 61 135 224 254	6 58 101 141 225	7 56 126 206 244	6 60 127 204 244
		G	61 118 163 222 253	52 118 202 240 253	63 119 163 222 253	60 123 181 226 253	60 123 202 240 253	51 84 125 214 253	46 79 133 199 232	50 113 181 229 253	64 123 198 240 252
		B	2 73 111 180 225	3 73 117 209 249	51 95 165 216 249	3 74 110 151 211	3 73 117 209 249	3 73 117 210 249	72 107 146 175 216	3 71 108 173 222	72 112 188 228 249
	8	R	6 40 73 101 129 158 187 219 244	6 35 66 96 132 179 218 244 254	9 65 102 131 165 203 226 244 254	10 71 102 129 157 181 211 240 254	6 34 66 96 132 178 218 244 254	6 63 101 118 137 173 215 244 255	7 27 58 99 127 149 183 215 240	7 54 87 122 152 192 224 245 254	6 42 72 106 140 196 224 244 254
		G	25 51 89 121 143 170 196 220 242	24 49 77 116 143 179 215 240 253	10 22 53 90 122 147 188 231 253	43 72 113 130 149 175 212 240 253	24 49 77 116 143 177 213 240 253	24 50 79 119 150 173 196 220 241	38 50 76 100 125 157 184 218 242	51 75 99 124 147 192 224 241 253	25 51 76 111 133 151 176 201 232
		B	2 22 65 93 124 161 202 233 249	3 25 51 76 110 153 202 234 249	2 51 83 118 148 173 206 234 249	9 47 72 96 128 175 191 220 249	2 44 74 105 131 166 206 234 249	1 51 71 91 114 140 165 200 230	17 55 78 101 129 182 205 219 234	2 31 72 98 120 152 176 207 234	2 26 68 93 115 144 184 214 235
	12	R	6 24 42 58 76 95 116 134 158 192 223 244 254	1 7 38 60 80 102 127 150 175 199 224 244 254	6 33 68 100 117 127 139 156 176 206 229 244 254	6 28 47 60 83 113 134 156 176 194 212 238 254	1 6 30 58 83 107 130 153 176 200 224 244 254	7 37 56 72 94 116 128 141 171 203 225 244 254	3 15 60 77 91 124 150 167 181 186 204 225 244	7 29 45 58 69 99 128 146 160 189 221 243 254	7 39 59 79 100 114 125 143 172 195 219 242 254
		G	24 46 58 81 111 131 152 171 188 209 226 241 253	6 11 25 47 60 79 106 127 149 172 196 220 241	16 40 51 63 72 87 106 129 169 203 228 242 253	2 22 55 96 113 120 133 165 198 215 221 237 253	6 25 47 62 81 106 127 153 179 203 225 242 253	22 49 75 94 106 118 130 144 159 175 197 221 241	6 21 47 67 94 110 123 138 152 175 212 236 244	23 46 61 80 98 114 129 148 166 190 215 229 242	23 47 70 101 120 132 145 161 179 195 211 226 241
		B	3 25 51 69 85 103 119 137 155 175 201 220 235	2 21 44 64 80 98 113 130 153 173 194 215 234	3 28 40 54 69 84 109 139 161 194 217 234 249	1 26 48 68 81 93 112 139 158 167 192 225 249	1 21 44 61 76 96 115 135 158 186 213 234 249	1 11 29 45 64 81 100 117 136 160 191 216 234	4 41 65 85 109 131 146 159 176 203 226 236 247	3 22 51 71 91 104 118 135 161 190 210 230 241	2 29 38 50 76 105 131 163 188 213 235 245 249

References

[1] M. Haindl, S. Mikeš, A competition in unsupervised color image segmentation, Pattern Recognit. 57 (2016) 136–151, doi:10.1016/j.patcog.2016.03.003.
[2] GIS (Geographic Information System) | National Geographic Society, (n.d.). https://www.nationalgeographic.org/encyclopedia/geographic-information-system-gis/ (accessed August 9, 2020).
[3] A.K. Bhandari, V.K. Singh, A. Kumar, G.K. Singh, Cuckoo search algorithm and wind driven optimization based study of satellite image segmentation for multilevel thresholding using Kapur's entropy, Expert Syst. Appl. 41 (2014) 3538–3560, doi:10.1016/j.eswa.2013.10.059.
[4] A.K. Bhandari, A. Kumar, S. Chaudhary, G.K. Singh, A novel color image multilevel thresholding based segmentation using nature inspired optimization algorithms, Expert Syst. Appl. 63 (2016) 112–133, doi:10.1016/j.eswa.2016.06.044.
[5] A. Bhandari, Tsallis entropy based multilevel thresholding for colored satellite image segmentation using evolutionary algorithms, Expert Syst. Appl. (2015) https://doi.org/, doi:10.1016/j.eswa.2015.07.025.
[6] H. Jia, X. Peng, W. Song, D. Oliva, C. Lang, Y. Li, Y. Yao, Masi Entropy for satellite color image segmentation using tournament-based lévy multiverse optimization algorithm, Remote Sens. 11 (2019) 942 https://doi.org/, doi:10.3390/rs11080942.
[7] B. Sankur, M. Sezgin, Image thresholding techniques: a survey over categories, Pattern Recognit. 34 (2001) 1573–1583.
[8] N.M. Zaitoun, M.J. Aqel, Survey on image segmentation techniques, Procedia Comput. Sci. 65 (2015) 797–806, doi:10.1016/j.procs.2015.09.027.
[9] M. Sezgin, B. Sankur, Survey over image thresholding techniques and quantitative performance evaluation, J. Electron. Imaging 13 (2004) 146–168 https://doi.org/, doi:10.1117/1.1631315.
[10] Otsu_1979_otsu_method Otsu, IEEE Trans. Syst. Man. Cybern. C (1979) 62–66 https://doi.org/, doi:10.1109/TSMC.1979.4310076.
[11] M. Portes de Albuquerque, I.A. Esquef, A.R. Gesualdi Mello, M. Portes de Albuquerque, Image thresholding using Tsallis entropy, Pattern Recognit. Lett. 25 (2004) 1059–1065, doi:10.1016/j.patrec.2004.03.003.
[12] J.N.N. Kapur, P.K.K. Sahoo, A.K.C.K.C. Wong, A new method for gray-level picture thresholding using the entropy of the histogram, Comput. Vision, Graph. Image Process. 29 (1985) 273–285, doi:10.1016/0734-189X(85)90125-2.
[13] M. Masi, A step beyond Tsallis and Rényi entropies, Phys. Lett. Sect. A Gen. At. Solid State Phys. 338 (2005) 217–224 https://doi.org/, doi:10.1016/j.physleta.2005.01.094.
[14] A. Renyi, On Measures of Entropy and Information, in: Proc. Fourth Berkeley Symp. Math. Stat. Probab. Vol. 1 Contrib. to Theory Stat., University of California Press, Berkeley, Calif., 1961: pp. 547–561. https://projecteuclid.org/euclid.bsmsp/1200512181.
[15] N.R. Pal, On minimum cross-entropy thresholding, Pattern Recognit. 29 (1996) 575–580, doi:10.1016/0031-3203(95)00111-5.
[16] A. Wunnava, M.K. Naik, R. Panda, B. Jena, A. Abraham, A novel interdependence based multilevel thresholding technique using adaptive equilibrium optimizer, Eng. Appl. Artif. Intell. 94 (2020) 103836 https://doi.org/, doi:10.1016/j.engappai.2020.103836.
[17] A.S. Abutaleb, Automatic thresholding of gray-level pictures using two-dimensional entropy, Comput. Vision, Graph. Image Process. 47 (1989) 22–32, doi:10.1016/0734-189X(89)90051-0.
[18] J. Liu, W. Li, Y. Tian, Automatic thresholding of gray-level pictures using two-dimensional Otsu method, (1991) 325–327.
[19] P.K. Sahoo, G. Arora, A thresholding method based on two-dimensional Renyi's entropy, Pattern Recognit. 37 (2004) 1149–1161, doi:10.1016/j.patcog.2003.10.008.
[20] P.K. Sahoo, G. Arora, Image thresholding using two-dimensional Tsallis–Havrda–Charvát entropy, Pattern Recognit. Lett. 27 (2006) 520–528, doi:10.1016/j.patrec.2005.09.017.
[21] A. Wunnava, M. Kumar Naik, R. Panda, B. Jena, A. Abraham, A differential evolutionary adaptive Harris hawks optimization for two dimensional practical Masi entropy-based multilevel image thresholding, J. King Saud Univ. - Comput. Inf. Sci. (2020) https://doi.org/, doi:10.1016/j.jksuci.2020.05.001.
[22] R. Panda, S. Agrawal, L. Samantaray, A. Abraham, An evolutionary gray gradient algorithm for multilevel thresholding of brain MR images using soft computing techniques, Appl. Soft Comput. 50 (2017) 94–108, doi:10.1016/j.asoc.2016.11.011.
[23] A. Wunnava, M.K. Naik, R. Panda, B. Jena, A. Abraham, An adaptive Harris hawks optimization technique for two dimensional grey gradient based multilevel image thresholding, Appl. Soft Comput. 95 (2020) 106526 https://doi.org/, doi:10.1016/j.asoc.2020.106526.
[24] S. Patra, R. Gautam, A. Singla, A novel context sensitive multilevel thresholding for image segmentation, Appl. Soft Comput. 23 (2014) 122–127, doi:10.1016/j.asoc.2014.06.016.
[25] S. Pare, A. Kumar, V. Bajaj, G.K. Singh, A multilevel color image segmentation technique based on cuckoo search algorithm and energy curve, Appl. Soft Comput. 47 (2016) 76–102, doi:10.1016/j.asoc.2016.05.040.
[26] S. Pare, A.K. Bhandari, A. Kumar, G.K. Singh, An optimal color image multilevel thresholding technique using grey-level co-occurrence matrix, Expert Syst. Appl. 87 (2017) 335–362, doi:10.1016/j.eswa.2017.06.021.
[27] M.-A. Díaz-Cortés, N. Ortega-Sánchez, S. Hinojosa, D. Oliva, E. Cuevas, R. Rojas, A. Demin, A multi-level thresholding method for breast thermograms analysis using Dragonfly algorithm, Infrared Phys. Technol. 93 (2018) 346–361, doi:10.1016/j.infrared.2018.08.007.
[28] P. Kandhway, A.K. Bhandari, Spatial context-based optimal multilevel energy curve thresholding for image segmentation using soft computing techniques, Neural Comput. Appl. 32 (2020) 8901–8937 https://doi.org/, doi:10.1007/s00521-019-04381-9.
[29] A. Faramarzi, M. Heidarinejad, B. Stephens, S. Mirjalili, Equilibrium optimizer: A novel optimization algorithm, Knowledge-Based Syst. 191 (2020) 105190. https://doi.org/https://doi.org/ 10.1016/j.knosys.2019.105190.
[30] H.R. Tizhoosh, Opposition-Based Learning: A New Scheme for Machine Intelligence, Int. Conf. Comput. Intell. Model. Control Autom. Int. Conf. Intell. Agents, Web Technol. Internet Commer. (2005) 695–701 https://doi.org/, doi:10.1109/CIMCA.2005.1631345.
[31] S. Dhargupta, M. Ghosh, S. Mirjalili, R. Sarkar, Selective Opposition based Grey Wolf Optimization, Expert Syst. Appl. 151 (2020) 113389, doi:10.1016/j.eswa.2020.113389.
[32] X. Yao, L. Yong, L. Guangming, Evolutionary programming made faster, Evol. Comput. IEEE Trans. 3 (1999) 82–102 https://doi.org/, doi:10.1109/4235.771163.
[33] M.K. Naik, R. Panda, A novel adaptive cuckoo search algorithm for intrinsic discriminant analysis based face recognition, Appl. Soft Comput. 38 (2016) 661–675 https://doi.org/, doi:10.1016/j.asoc.2015.10.039.
[34] J.J. Liang, B.Y. Qu, P.N. Suganthan, Problem Definitions and Evaluation Criteria for the CEC 2014 Special Session and Competition on Single Objective Real-Parameter Numerical Optimization, in: 2013.
[35] D. Simon, Biogeography-Based Optimization, Evol. Comput. IEEE Trans. 12 (2009) 702–713 https://doi.org/, doi:10.1109/TEVC.2008.919004.
[36] A.A. Heidari, S. Mirjalili, H. Faris, I. Aljarah, M. Mafarja, H. Chen, Harris hawks optimization: Algorithm and applications, Futur. Gener. Comput. Syst. 97 (2019) 849–872, doi:10.1016/j.future.2019.02.028.
[37] S. Shadravan, H.R. Naji, V.K. Bardsiri, The Sailfish Optimizer: A novel nature-inspired metaheuristic algorithm for solving constrained engineering optimization problems, Eng. Appl. Artif. Intell. 80 (2019) 20–34, doi:10.1016/j.engappai.2019.01.001.
[38] S. Mirjalili, A. Lewis, The Whale Optimization Algorithm, Adv. Eng. Softw. 95 (2016) 51–67, doi:10.1016/j.advengsoft.2016.01.008.
[39] S. Mirjalili, S.M. Mirjalili, A. Lewis, Grey Wolf Optimizer, Adv. Eng. Softw. 69 (2014) 46–61 https://doi.org/http://dx.doi.org/, doi:10.1016/j.advengsoft.2013.12.007.
[40] R. Tanabe, A.S. Fukunaga, Improving the search performance of SHADE using linear population size reduction, in: 2014 IEEE Congr. Evol. Comput., 2014, pp. 1658–1665, doi:10.1109/CEC.2014.6900380. https://doi.org/.
[41] J. Carrasco, S. García, M.M. Rueda, S. Das, F. Herrera, Recent trends in the use of statistical tests for comparing swarm and evolutionary computing algorithms: Practical guidelines and a critical review, Swarm Evol. Comput. 54 (2020) 100665, doi:10.1016/j.swevo.2020.100665.
[42] J.H. Zar, Biostatistical Analysis, Prentice-Hall, Inc., USA, 1999.
[43] S. Holm, A Simple Sequentially Rejective Multiple Test Procedure, Scand, J. Stat. 6 (1979) 65–70 http://www.jstor.org/stable/4615733.
[44] Landsat Image Gallery, (n.d.). https://landsat.visibleearth.nasa.gov/ (accessed June 12, 2020).
[45] S. Agrawal, R. Panda, S. Bhuyan, B.K. Panigrahi, Tsallis entropy based optimal multilevel thresholding using cuckoo search algorithm, Swarm Evol. Comput. 11 (2013) 16–30, doi:10.1016/j.swevo.2013.02.001.
[46] L.Z. Lin Zhang, FSIM: A Feature Similarity Index for Image Quality Assessment, IEEE Trans. Image Process. 20 (2011) 2378 https://doi.org/, doi:10.1109/TIP.2011.2109730.
[47] W. Zhou, A.C. Bovik, H.R. Sheikh, E.P. Simoncelli, Image quality assessment: from error visibility to structural similarity, IEEE Trans. Image Process. 13 (2004) 600–612 https://doi.org/, doi:10.1109/TIP.2003.819861.
[48] S. Ghosh, L. Bruzzone, S. Patra, F. Bovolo, A. Ghosh, A Context-Sensitive Technique for Unsupervised Change Detection Based on Hopfield-Type Neural Networks, IEEE Trans. Geosci. Remote Sens. 45 (2007) 778–789 https://doi.org/, doi:10.1109/TGRS.2006.888861.
[49] A.H. Halim, I. Ismail, S. Das, Performance assessment of the metaheuristic optimization algorithms: an exhaustive review, Artif. Intell. Rev. (2020) https://doi.org/, doi:10.1007/s10462-020-09906-6.
[50] S.-H. Liu, M. Mernik, D. Hrnčič, M. Črepinšek, A parameter control method of evolutionary algorithms using exploration and exploitation measures with a practical application for fitting Sovova's mass transfer model, Appl. Soft Comput. 13 (2013) 3792–3805, doi:10.1016/j.asoc.2013.05.010.